NUCLEOSYNTHESIS

N. Langer

Bonn University

SS 2012

Contents

Preface **v**

Physical and astronomical constants **vi**

1 Introduction **1**

2 Thermonuclear reactions **9**

3 Big Bang nucleosynthesis **23**

4 Hydrostatic nucleosynthesis in stars (A < 56) **35**
4.1 Stellar evolution and nuclear burning 35
4.2 Hydrogen burning 42
4.3 Advanced nuclear burning phases 61

5 Neutron-capture nucleosynthesis **71**
5.1 The s-process 71
5.2 The r- and p-process: explosive production 83

6 Thermonuclear supernovae **91**

7 The origin of Li, Be and B **99**

8 Galactic chemical evolution **103**

References **111**

Preface

These lecture notes are intended for an advanced astrophysics course on Nucleosynthesis given at Bonn University. It is based on a course developed at Utrecht University in collaboration with Dr. Onno Pols. These Notes provide a schematic but more or less complete overview of the subject, and as such are sufficient material to follow the course. However, consultation of books that provide more detailed information and/or of review articles is recommended. Suggested literature is indicated at the end of each chapter or section. In particular, we recommend the following book alongside these notes:

- B.E.J. Pagel, *Nucleosynthesis and Chemical Evolution of Galaxies*, 1997, Cambridge University Press, ISBN 0 521 55958 8.

Pagel's book (referred to as PAGEL hereafter) covers all the topics in these notes, although it puts more emphasis on galactic chemical evolution and somewhat less on the (stellar) nucleosynthesis processes than we do. A good supplement is the older but still excellent book by Donald Clayton:

- D.D. Clayton, *Principles of Stellar Evolution and Nucleosynthesis*, 1968, University of Chicago Press, ISBN 0 226 10953 4. (CLAYTON)

It provides a very detailed but well-written account of thermonuclear reactions and nuclear burning processes in stars.

The lecture notes still evolve and we try to keep them up to date. If you find any errors, we would be grateful if you notify us by email `nlanger@astro.uni-bonn.de`).

Norbert Langer

April 2009

Physical and astronomical constants

Table 1: Physical constants

gravitational constant	G	6.674×10^{-8} cm^3 g^{-1} s^{-2}
speed of light in vacuum	c	$2.997\,92 \times 10^{10}$ cm s^{-1}
Planck constant over 2π	$\hbar$	$1.054\,57 \times 10^{-27}$ erg s
radiation density constant	a	$7.565\,78 \times 10^{-15}$ erg cm^{-3} K^{-4}
Boltzmann constant	k	$1.380\,65 \times 10^{-16}$ erg K^{-1}
electron volt	eV	$1.602\,18 \times 10^{-12}$ erg
electron charge	e	4.803×10^{-10} esu
	e^2	1.440×10^{-7} eV cm
electron mass	m_e	$9.109\,38 \times 10^{-28}$ g
atomic mass unit	m_u	$1.660\,538 \times 10^{-24}$ g
proton mass	m_p	$1.672\,621 \times 10^{-24}$ g
neutron mass	m_n	$1.674\,927 \times 10^{-24}$ g
α-particle mass	m_α	$6.644\,656 \times 10^{-24}$ g

Table 2: Astronomical constants

Solar mass	$\mathrm{M}_\odot$	1.9891×10^{33} g
Solar radius	$\mathrm{R}_\odot$	6.9598×10^{11} cm
Solar luminosity	$\mathrm{L}_\odot$	3.844×10^{33} erg s^{-1}
year	yr	3.1558×10^7 s
astronomical unit	AU	1.4960×10^{13} cm
parsec	pc	3.0857×10^{18} cm
Hubble constant	H_0	$100h$ km s^{-1} Mpc^{-1}
		72 ± 7 km s^{-1} Mpc^{-1}

Chapter 1

Introduction

A. Goal: understand the distribution of isotopic abundances in the universe

Solar system abundances: two types of data sources:

1. Spectral analysis of the Sun

   - photospheric absorption lines $\longrightarrow$ abundance ratios **element:hydrogen**
     – exceptions: He, Ne, Ar, rare heavy elements
     – *no* information on isotopic abundances, except from some molecules (e.g. CO, CN, MgH)
   - emission lines from chromosphere, corona (far-UV) $\longrightarrow$ He, Ne, Ar, but less accurate

1.	H	0.70	X	
2.	He	0.28	Y	(indirect)
3.	O	0.0096		
4.	C	0.0030	Z	
5.	Ne	0.0015	$\downarrow$	
6.	Fe	0.0012	("metals")	
.				
.				

2. Direct measurements (chemical analysis, mass spectrometry)

   - Earth (crust, oceans, atmosphere): very inhomogeneous
     Moon rocks: same problem
     $\longrightarrow$ little information on elemental abundances
     $\longrightarrow$ but provides **isotope ratios**
   - meteorites (esp. chondrites): uniform atomic composition
     corresponds to solar photosphere
     $\longrightarrow$ represents **Solar System abundances**
     $\longrightarrow$ also **isotope ratios** (with interesting anomalies)
   - solar wind (ion counters on space probes) $\longrightarrow$ e.g. ^{3}He

Abundances outside the Solar system:

- chemical analysis of spectra of other stars, gaseous nebulae and external galaxies
- nearby stars, local ISM: similar abundance distribution to Solar system
  $\longrightarrow$ same *relative* distribution (but variations in Z/X)
  $\longrightarrow$ **local abundance distribution** (see Fig. 1.1, Table 1.1)
- assumption: **cosmic abundances** $\approx$ local abundances
  with interesting exceptions, and variations among stars and between/across galaxies
  $\longrightarrow$ nucleosynthesis sites; chemical evolution
- isotopic abundances: hardly testable outside Solar system
  (except for very light, some very heavy elements)

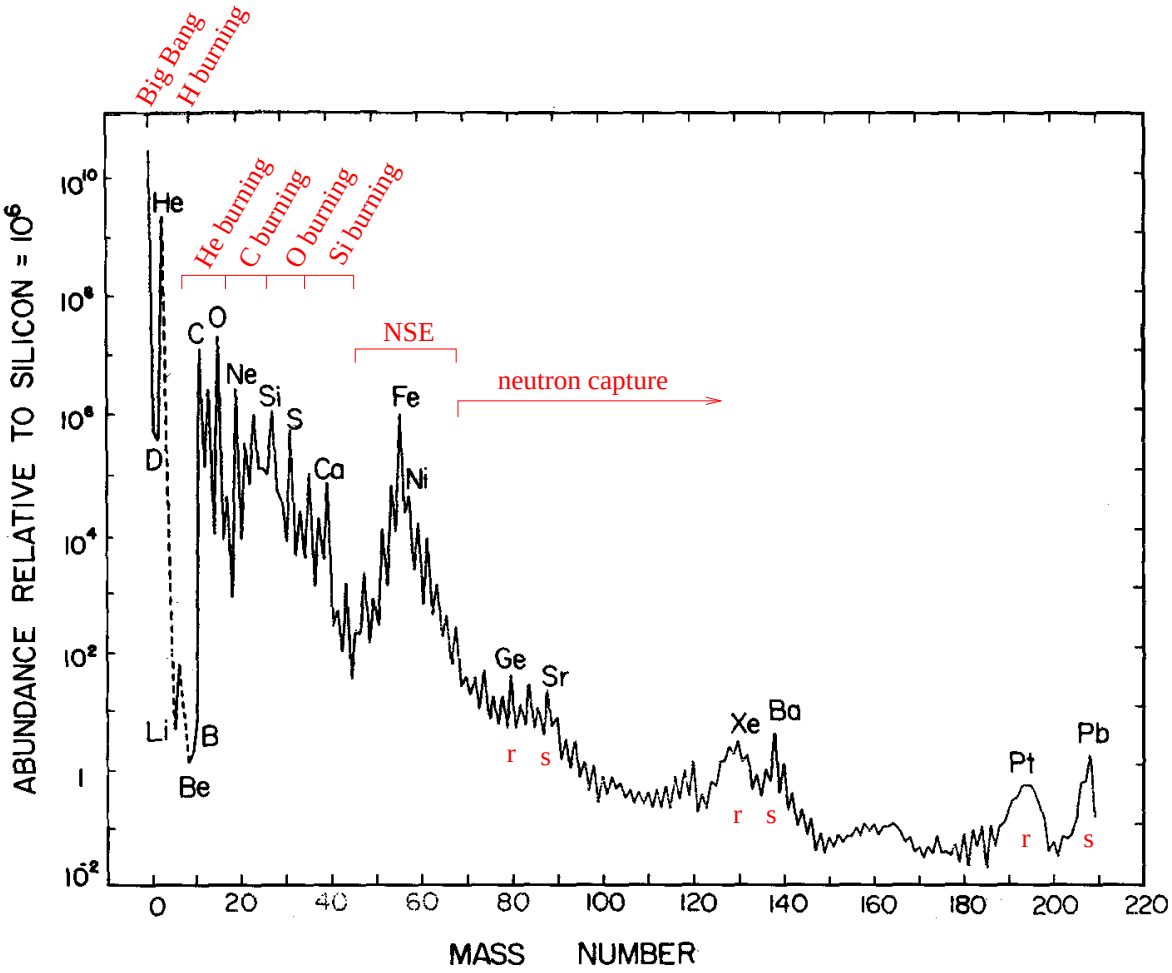

Figure 1.1: The 'local galactic' abundance distribution of nuclear species, as a function of mass number A. The abundances are given relative to the Si abundance which is set to 10^6. Peaks due to the r- and s-process are indicated. It is the main aim of this course to provide an understanding of this figure. Adapted from Cameron (1982).

Table 1.1: The 25 most abundant nuclei. Symbols in the last column indicate the nuclear burning stage, also 'BB': Big Bang, 'NSE': nuclear statistical equilibrium.

rank	Z	element	A	nucleon fraction	source (process)
1	1	H	1	7.057(−1)	BB
2	2	He	4	2.752(−1)	BB, H(CNO, pp)
3	8	O	16	9.592(−3)	He
4	6	C	12	3.032(−3)	He
5	10	Ne	20	1.548(−3)	C
6	26	Fe	56	1.169(−3)	NSE
7	7	N	14	1.105(−3)	H(CNO)
8	14	Si	28	6.530(−4)	O
9	12	Mg	24	5.130(−4)	C, Ne
10	16	S	32	3.958(−4)	O
11	10	Ne	22	2.076(−4)	He
12	12	Mg	26	7.892(−5)	C, Ne
13	18	Ar	36	7.740(−5)	Si, O
14	26	Fe	54	7.158(−5)	NSE, Si
15	12	Mg	25	6.893(−5)	C, Ne
16	20	Ca	40	5.990(−5)	Si, O
17	13	Al	27	5.798(−5)	C, Ne
18	28	Ni	58	4.915(−5)	Si, NSE
19	6	C	13	3.683(−5)	H(CNO)
20	2	He	3	3.453(−5)	BB, H(pp)
21	14	Si	29	3.445(−5)	C, Ne
22	11	Na	23	3.339(−5)	C, H(NeNa)[1]
23	26	Fe	57	2.840(−5)	NSE
24	14	Si	30	2.345(−5)	C, Ne
25	1	H	2	2.317(−5)	BB

[1]H-burning via the NeNa-chain.

B. Aspects of nuclear physics

- Atomic nucleus consists of Z protons and N neutrons; $A = Z + N$ = mass number (Z = constant: *isotopes*; A = constant: *isobars*)
- Stable nuclei → **valley of stability** in the (N, Z) plane (Fig. 1.2).
  Outside the valley: spontaneous, radioactive decay
  $\beta^-: (Z, A) \to (Z+1, A) + \mathrm{e}^- + \nu$
  $\beta^+: (Z, A) \to (Z-1, A) + \mathrm{e}^+ + \bar{\nu}$
  $\alpha: \ (Z, A) \to (Z-2, A-4) + {}^4\mathrm{He}$

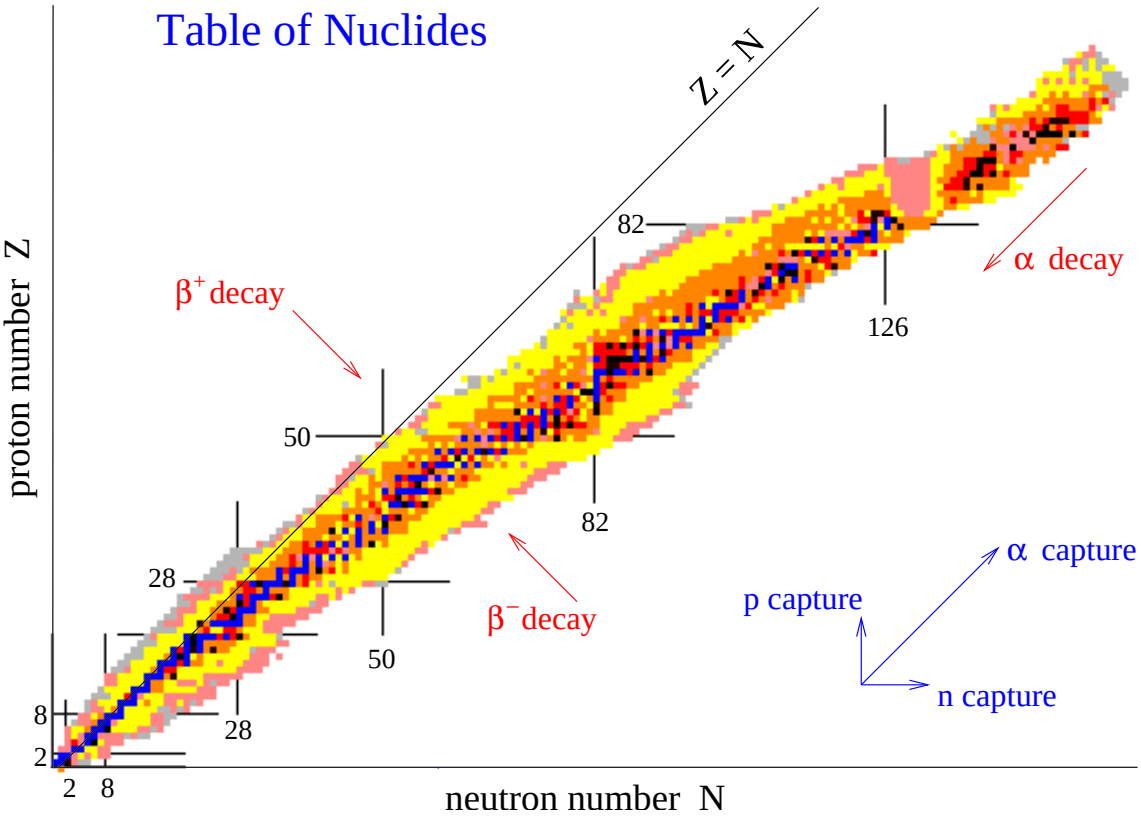

Figure 1.2: Chart of the nuclides, showing proton number Z vs neutron number N. Stable nuclei are in blue, and long-lived ($> 10^5$ years) radioactive isotopes are in black. Other (lighter) colours show isotopes with shorter decay times. The arrows show the directions of some simple nuclear transformations. Source: Korea Atomic Energy Research Institute (`http://atom.kaeri.re.kr/`; clickable map with information on each nuclide).

C. Why isotopic abundances?

Example: carbon 2 stable isotopes ^{12}C (99%); ^{13}C (1%)

Origin of ^{12}C:	nuclear fusion in stars (cf. Chapter 4)	
	first: H-burning	$4\ ^1\mathrm{H} \rightarrow\ ^4\mathrm{He}$
	second:	$3\ ^4\mathrm{He} \rightarrow\ ^{12}\mathrm{C}$
	(third:	$2\ ^{12}\mathrm{C} \rightarrow\ ^{20}\mathrm{Ne} + \alpha$)
		(but not all carbon is burnt)
	3α-process: $\alpha + \alpha \leftrightarrow\ ^8\mathrm{Be} + \alpha \rightarrow\ ^{12}\mathrm{C}$	
	this process can *not* make ^{13}C!	
Origin of ^{13}C:	only way is: make it from ^{12}C:	$^{12}\mathrm{C}$ (p, γ) $^{13}\mathrm{N}$ (β^+) $^{13}\mathrm{C}$
	(part of CNO cycle, Chapter 4)	
	can also be destroyed later:	$^{13}\mathrm{C} + \mathrm{p}$
		$^{13}\mathrm{C} + \alpha$
	but not all is destroyed	

$\Rightarrow$ ^{12}C and ^{13}C are made by completely different processes

Imagine: first generation of stars $\rightarrow$ no metals initially
$\Rightarrow 3\alpha \rightarrow\ ^{12}$C works, ^{12}C is formed
but $^{12}\mathrm{C} + \mathrm{p}$ does *not* work: ^{12}C is *absent* in H-burning layers

first stars produce as much ^{12}C as stars today
$\Rightarrow\quad \dot{X}(^{12}\mathrm{C}) = \text{const.}$
$\Rightarrow\quad X(^{12}\mathrm{C}) \propto t$

first stars produce no ^{13}C
$\Rightarrow\quad \dot{X}(^{13}\mathrm{C}) \propto X(^{12}\mathrm{C}) \propto t$
$\Rightarrow\quad X(^{13}\mathrm{C}) \propto t^2$

See figure 1.3;
assumptions like above and $X(^{13}\mathrm{C}) \ll X(^{12}\mathrm{C})$

Definition: **primary** isotopes: can be made in first stars
secondary isotopes: can **not** be made in first stars

Second example: nitrogen

^{14}N: formed in CNO cycle from ^{12}C, ^{16}O
$\Rightarrow$ ^{14}N *is secondary isotope*
but observations of metal-poor stars and galaxies indicate: ^{14}N **exists in first stars**

$\Rightarrow$ ^{14}N must have a primary component
origin still unclear
(mixing of protons into He-burning?)

^{15}N : abundance = 0.0037 of ^{14}N
$\rightarrow$ destroyed in CNO-cycle
exotic speculations about origin
- explosive H-burning in novae?
- neutrino-induced nucleosynthesis in supernovae?
  ^{16}O (ν,n) ^{15}O (β^+) ^{15}N

$\Rightarrow$ Many essential questions are still open

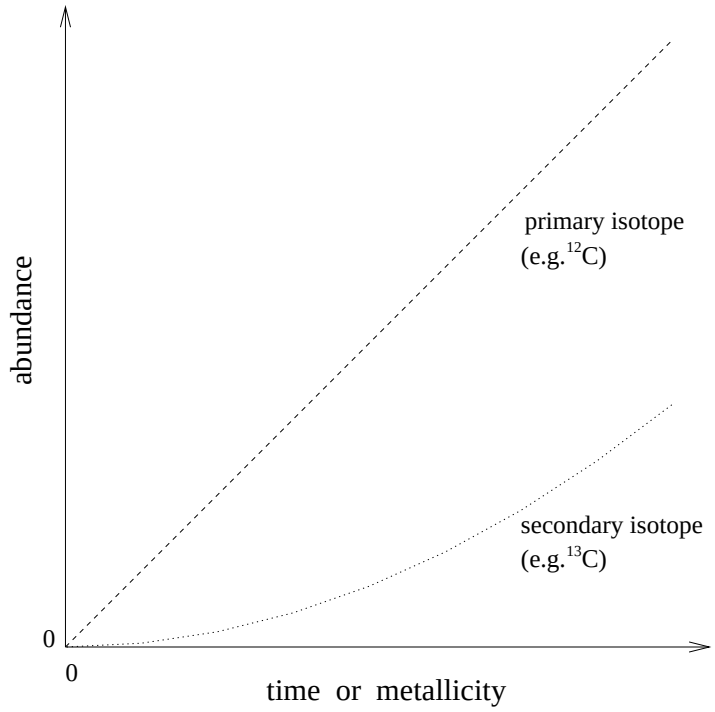

Figure 1.3: Schematic time or metallicity dependence of the abundances of primary and secondary nuclei in the course of chemical evolution (assuming constant production conditions).

D. Nucleosynthesis goes on

Cosmic recycling

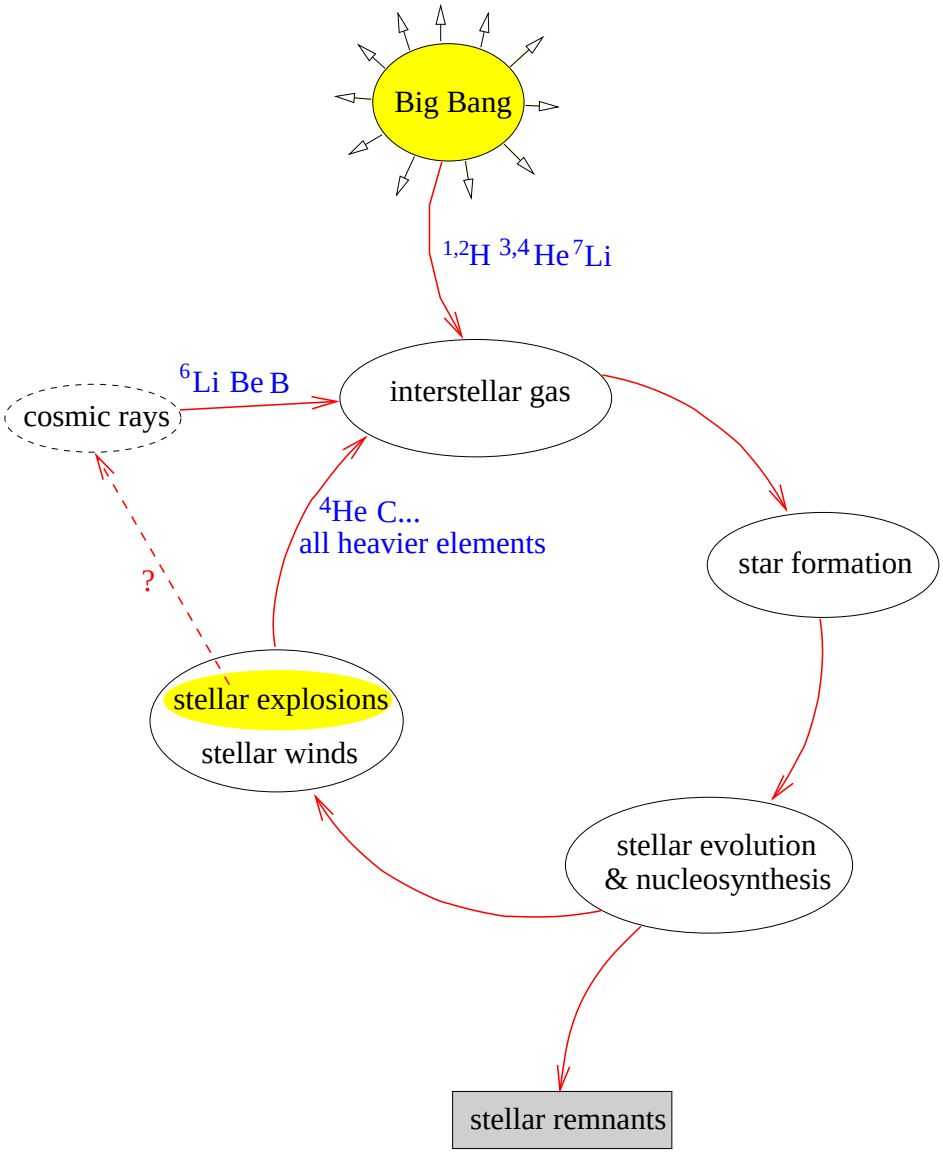

Figure 1.4: Schematic depiction of cosmic chemical evolution and recycling of the elements.

Evidence for ongoing nucleosynthesis:

- radioactive material:
  supernova light curves (esp. SNe Ia)
  Tc in AGB stars ($\tau_{1/2} \leq 4 \times 10^6$ yr)
  ^{26}Al decay $\rightarrow \gamma$-rays in Milky Way ($\tau_{1/2} = 7 \times 10^5$ yr)
- strong local enrichments:
  SNRs: C ... Fe in X-ray spectra (XMM, ASCA)
  carbon stars
  Wolf-Rayet stars

$\Rightarrow$ chemical evolution

Suggestion for further reading

– Chapter 1 of PAGEL, as well as Table 3.1 and Sect. 3.5 of Chapter 3.

Chapter 2

Thermonuclear reactions

A. Nuclear energy generation

• Hypotheses about solar energy production before $\sim$ 1930
- chemical burning, e.g. of coal ($\rightarrow$ dark sunspots)
- radioactive decay of heavy elements
- capture of meteorites/comets
- gravitational contraction

• Since $\sim$ 1930 clear:
thermonuclear fusion "makes the stars shine"

• notation: isotope ${}^{A}_{Z}\mathrm{X}$, or more commonly: ${}^{A}\mathrm{X}$
X designates chemical element, with proton number Z, mass number A
$\Rightarrow$ neutron number $N = A - Z$

• nuclear binding energy E_B of nuclei A_Z defined by

$$E_B(A_Z) := [(A-Z)m_n + Z \cdot m_p - M(A_Z)] \cdot c^2$$

m_n = neutron mass $\quad$ m_p = proton mass $\quad$ $M(A_Z)$ = mass of A_Z

$$\Delta M = (A-Z)m_n + Zm_p - M(A_Z) = \text{"mass defect"}$$

Note: electron mass is not considered
binding energy of electrons is not considered

• notation of nuclear reactions:
$X + a \rightarrow Y + b \quad$ or $\quad X(a,b)Y$

• energy generation by nuclear reaction $\rightarrow$ Q-value defined as

$$Q = (M_X + M_a - M_Y - M_b)c^2$$

$Q > 0 \rightarrow$ reaction is exothermic
$Q < 0 \rightarrow$ reaction is endothermic

Table 2.1: Binding energies for several nuclei.

nucleus	total BE E_B (MeV)	BE per nucleus E_B/A (MeV)
^{2}H	2.22	1.11
^{4}He	28.30	7.07
^{12}C	92.16	7.68
^{16}O	127.62	7.98
^{40}Ca	342.05	8.55
^{56}Fe	492.26	8.79
^{238}U	1801.70	7.57

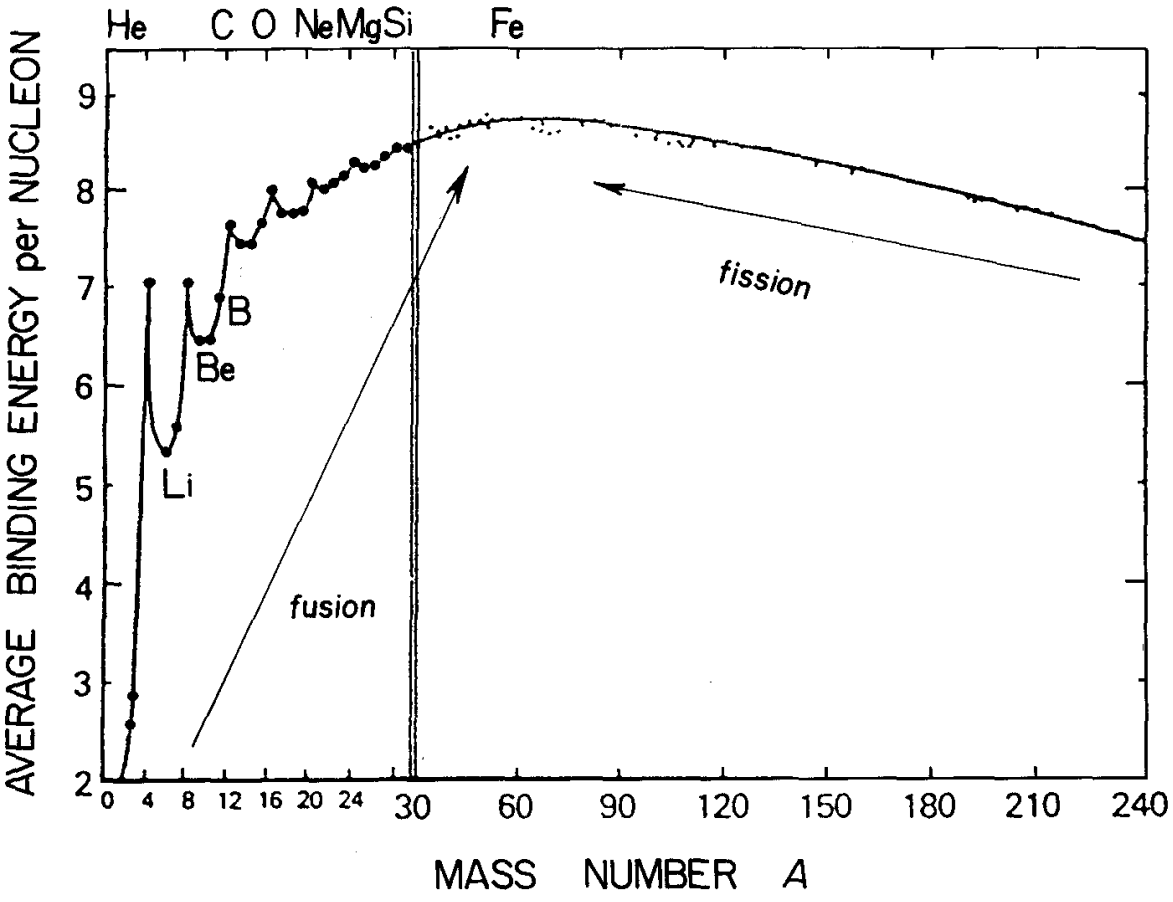

Figure 2.1: Binding energy per nucleon, as a function of mass number A. The iron-group nuclei are the most tightly bound, with the maximum at ^{56}Fe (8.8 MeV/nucleon). Adapted from Rolfs & Rodney (1988).

B. Cross sections

$\rightsquigarrow$ measure of probability that a certain reaction occurs
$\rightarrow$ much more difficult to obtain than Q-value

For R_p = projectile radius and R_t = target radius $\Rightarrow$

- classical geometrical cross section: $\sigma = \pi(R_p + R_t)^2$
- good approximation to nuclear radii: $R = R_0 \cdot A^{1/3}$ with $R_0 = 1.3 \cdot 10^{-13}$ cm

  $\Rightarrow$ $\mathrm{p} + \mathrm{p}$: $\sigma = 0.2 \cdot 10^{-24}$ cm^2
  $\mathrm{p} + {}^{238}\mathrm{U}$: $\sigma = 2.8 \cdot 10^{-24}$ cm^2
  ${}^{238}\mathrm{U} + {}^{238}\mathrm{U}$: $\sigma = 4.8 \cdot 10^{-24}$ cm^2

  new unit: 1 barn (b) := 10^{-24} cm^2

- quantum mechanics: de Broglie-wave of particles

$$\Rightarrow \sigma = \pi\lambda^2 \quad \text{with} \quad \lambda = \left(\frac{m_p + m_t}{m_t}\right)^{1/2} \frac{\hbar}{(2m_p E)^{1/2}}$$

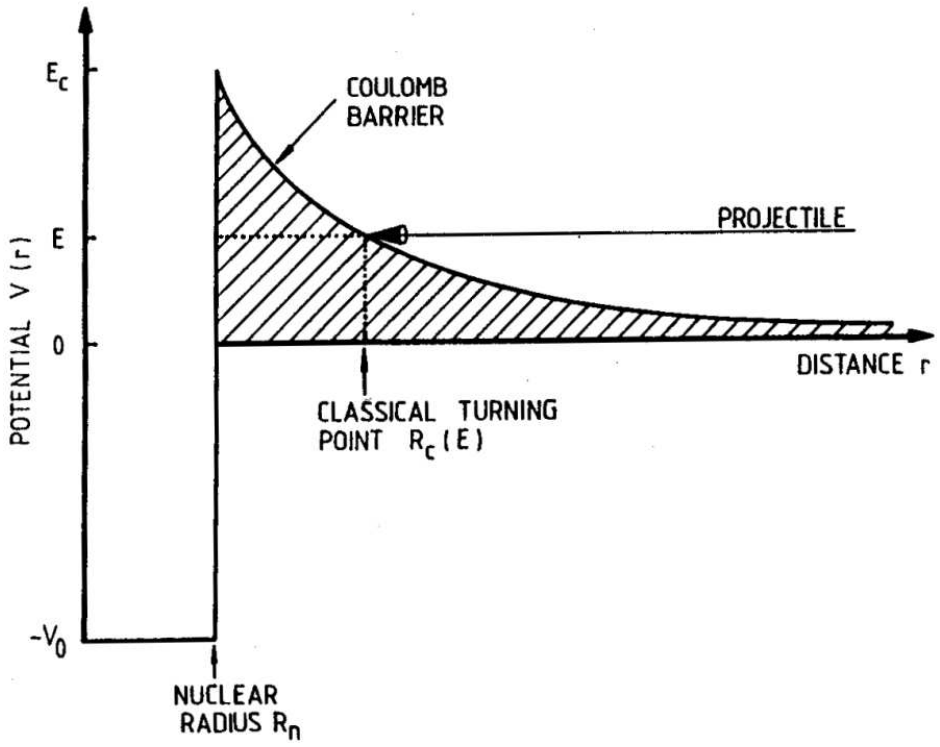

Figure 2.2: Nuclear potential for a charged particle reaction, consisting of the repulsive Coulomb potential ($V > 0$) for $r > R_n$ and the attractive potential of the strong nuclear force ($V < 0$) for $r < R_n$.

• complications:
- Coulomb-barrier may prevent reaction
- centrifugal barrier may prevent reaction
- nuclear structure effects may influence σ
- nature of the force determines strength of interaction:

strong force:	$^{15}\mathrm{N(p,\alpha)^{12}C}$	$\sigma \simeq 0.5$ b at $E_p = 2$ MeV
el. mag. force:	$^{3}\mathrm{He}(\alpha,\gamma)^{7}\mathrm{Be}$	$\sigma \simeq 10^{-6}$ b at $E_\alpha = 2$ MeV
weak force:	$\mathrm{p(p,e^+\nu)D}$	$\sigma \simeq 10^{-20}$ b at $E_p = 2$ MeV

C. Nuclear reaction rate

Definition: nuclear reaction rate $\boxed{r_{xy} := N_x \cdot N_y \cdot v \cdot \sigma(v)}$

with: N_x, N_y number density of particles x, y (i.e., particles per cm^3)
v relative velocity between x and y
$\sigma(v)$ cross section
$[r]$ = reactions per cm^3 per s = cm^{-3} s^{-1}

• in stellar gas: Maxwell-Boltzmann distribution of velocities $\Phi(v)$

$\Rightarrow\ r_{xy} = N_x N_y \langle \sigma v \rangle$

with $\langle \sigma v \rangle := \displaystyle\int_0^\infty \Phi(v) v \sigma(v) dv$

$$\Phi(v) = 4\pi v^2 \left(\frac{m}{2\pi kT}\right)^{3/2} \exp\left(-\frac{mv^2}{2kT}\right) = f(T)$$

with $m = \dfrac{m_x m_y}{m_x + m_y}$ = "reduced mass"

$E = \frac{1}{2} m v^2$

$$\Rightarrow \boxed{\langle \sigma v \rangle = \left(\frac{8}{\pi m}\right)^{\frac{1}{2}} \frac{1}{(kT)^{\frac{3}{2}}} \int_0^\infty \sigma(E) E \exp\left(-\frac{E}{kT}\right) dE}$$

D. Tunnel effect

• at high $T \Rightarrow$ nuclei ionized

$\Rightarrow$ repulsive Coulomb potential $\qquad V_{\mathrm{C}}(r) = \dfrac{Z_x Z_y e^2}{r}$

• classical physics: reaction only possible if
particle energy > Coulomb threshold energy $:= V_{\mathrm{C}}(R_x + R_y)$

$\rightsquigarrow$ H-burning would need $T \simeq 6 \cdot 10^9$ K ...

- quantum mechanics: **tunnel effect** (Gamow $\sim$ 1928)
  even if $E_x < V_C(R_x + R_y) \rightarrow$ finite probability that projectile penetrates Coulomb barrier
- tunneling probability: $P = \exp(-2\pi\eta)$

$$\text{with } \eta = \frac{Z_x Z_y e^2}{\hbar v}$$

$$\Rightarrow 2\pi\eta = 31.29 \cdot Z_x Z_y \left(\frac{A}{E}\right)^{\frac{1}{2}}$$

where A is the reduced mass in units of m_u and E is in keV

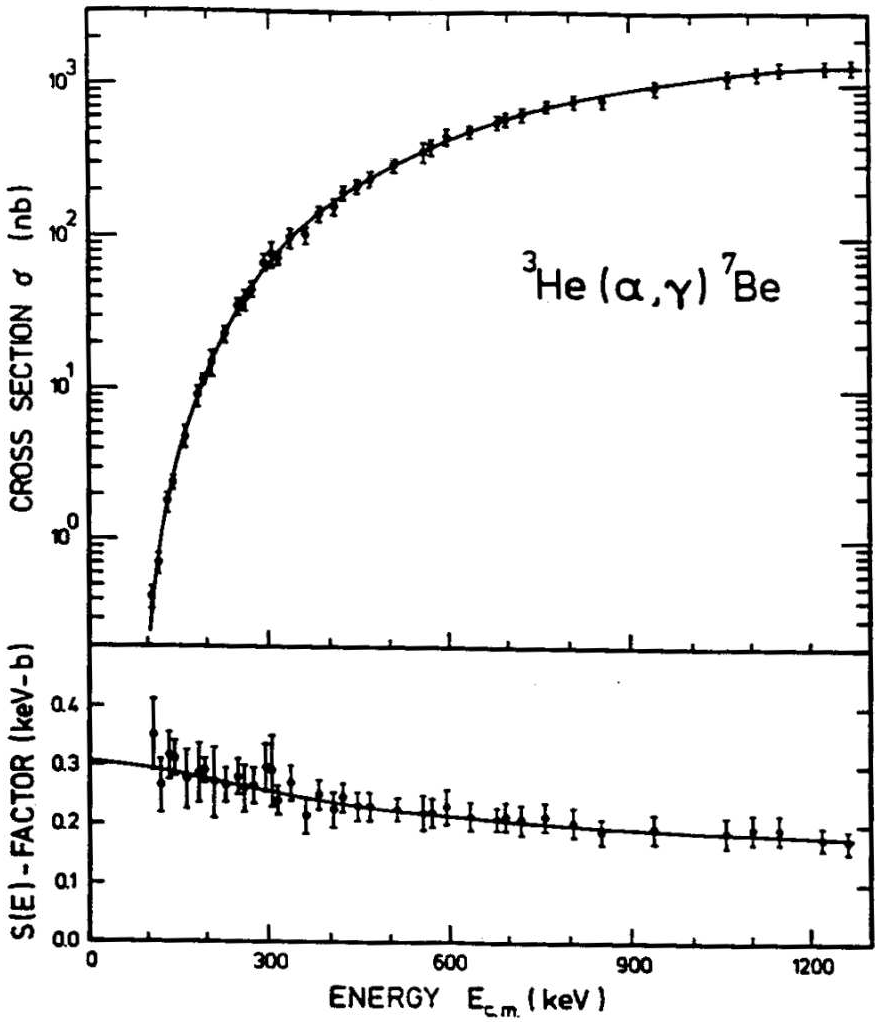

Figure 2.3: Energy dependence of the measured cross section (top) of the $^3\mathrm{He}(\alpha,\gamma)^7\mathrm{Be}$ reaction. An extrapolation to $E < 50\,\mathrm{keV}$, which is relevant in astrophysical environments, appears treacherous. However, the S-factor (bottom) is only weakly dependent on energy, and therefore much easier to extrapolate (solid line). Figure from Rolfs & Rodney (1988).

E. Astrophysical S-factor

Cross section (**B**) $\Rightarrow \sigma(E) \sim \pi\lambda^2 \sim 1/E$
Tunnel effect (**D**) $\Rightarrow \sigma(E) \sim \exp(-2\pi\eta),\ \eta \sim 1/\sqrt{E}$

$\Rightarrow$ define $S(E)$ such that

$$\sigma(E) = \frac{1}{E}\exp(-2\pi\eta)\cdot S(E)$$

$$\Rightarrow \langle\sigma v\rangle = \left(\frac{8}{\pi m}\right)^{1/2}\frac{1}{(kT)^{3/2}}\int_0^\infty S(E)\exp\left[-\frac{E}{kT}-\frac{b}{\sqrt{E}}\right]dE$$

with $b := (2m)^{1/2}\pi e^2 Z_x Z_y/\hbar$
$= 0.989 Z_x Z_y A^{1/2}$ $[(\mathrm{MeV})^{1/2}]$
(b^2 = "Gamow energy")

• often: S(E) varies slowly with E
→ **Gamow-peak** at energy $E_0 > kT$
→ for narrow T-range: $S(E) \simeq S(E_0) = \text{const.}$

$$\Rightarrow \langle\sigma v\rangle = \left(\frac{8}{\pi m}\right)^{1/2}\frac{1}{(kT)^{3/2}}S(E_0)\int_0^\infty \exp\left(-\frac{E}{kT}-\frac{b}{\sqrt{E}}\right)dE$$

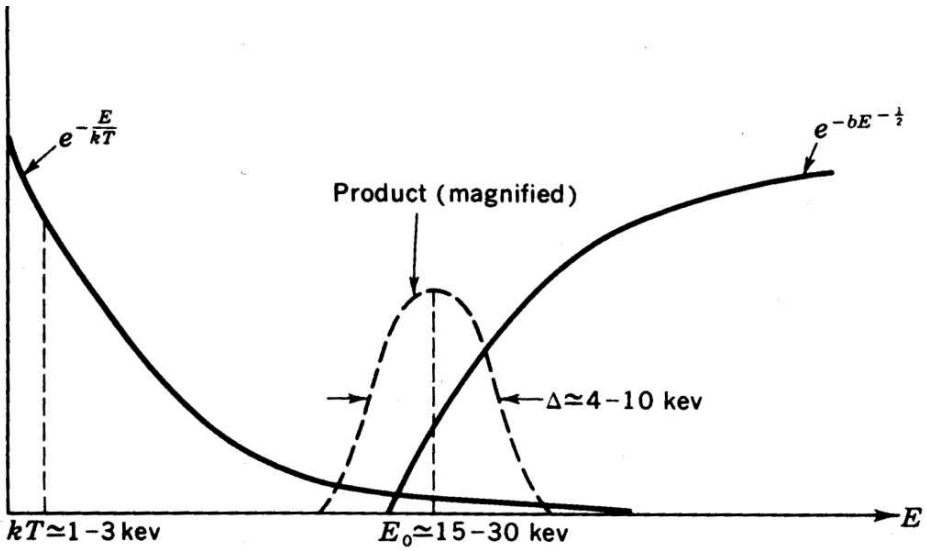

Figure 2.4: Dominant energy dependent factors in thermonuclear reactions. Most reactions occur in the overlap between the high-E tail of the Maxwell-Boltzmann distribution, giving a factor $\exp(-E/kT)$, and the probablity of tunneling through the Coulomb barrier, giving a factor $\exp(-b/\sqrt{E})$. Their product gives a fairly sharp peak called the **Gamow peak** at an energy E_0 which is generally much larger than kT. Figure from Clayton.

Look for $\frac{d}{dE}\langle\sigma v\rangle = 0 \rightarrow$ maximum

$$\Rightarrow E_0 = \left(\frac{bkT}{2}\right)^{2/3} = 1.22\left(Z_x^2 Z_y^2 A T_6^2\right)^{1/3} \text{ keV}$$

where $T_6 = T/10^6$ K

F. Temperature dependence

Gamow peak (**E**) $\Rightarrow E_0 \sim (Z_x Z_y)^{2/3} \Rightarrow$ shifted to higher E for heavier nuclei

$$\Rightarrow \text{approximate:} \quad \exp\left(-\frac{E}{kT} - \frac{b}{\sqrt{E}}\right) =: I_{\max} \exp\left[-\left(\frac{E-E_0}{\Delta/2}\right)^2\right]$$

↑ Gauss-function (see Fig 2.5)

$$\Rightarrow \Delta = 1/e - \text{folding width}$$
$$= \tfrac{4}{\sqrt{3}}\sqrt{E_0 kT} \simeq \text{geometric mean between } E_0 \text{ and } kT$$
$$I_{\max} = \exp\left(-\frac{3E_0}{kT}\right)$$

$$\Rightarrow \int_0^\infty \exp\left[-\frac{E}{kT} - \frac{b}{\sqrt{E}}\right] dE \simeq \Delta \cdot I_{\max}$$
$$= \tfrac{4}{\sqrt{3}}\sqrt{E_0 kT} \cdot \exp\left(-\tfrac{3E_0}{kT}\right)$$

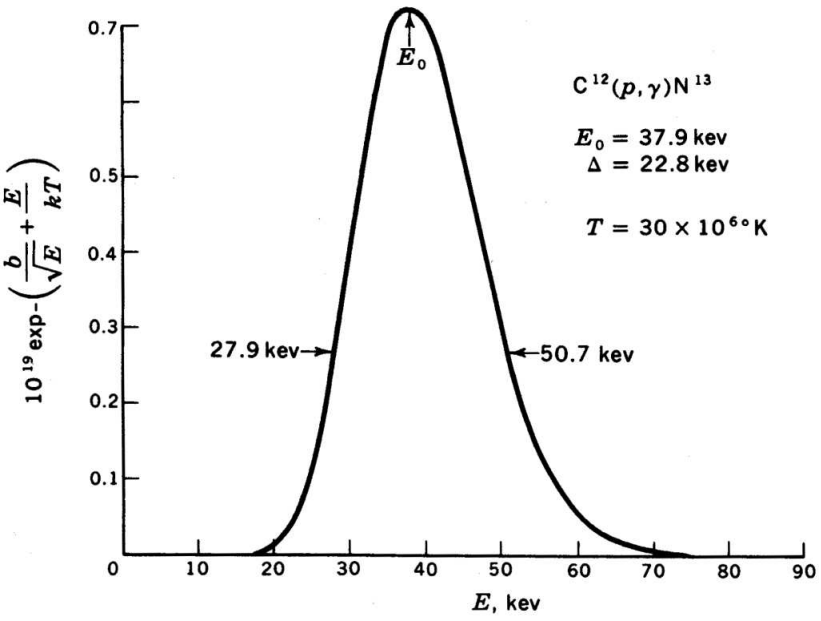

Figure 2.5: Gamow peak for the $^{12}\text{C}(\text{p},\gamma)^{13}\text{N}$ reaction at $T_6 = 30$. The peak is somewhat asymmetric about E_0, but is nevertheless adequately approximated by a Gaussian. Figure from CLAYTON.

Example:

$(T = 1.5 \cdot 10^7 K)$	$\Delta/2$	$\Delta \cdot I_{\max}$
$p + p$	3.2 keV	$7.0 \cdot 10^{-6}$ keV
$p + {}^{14}N$	6.8 keV	$2.5 \cdot 10^{-26}$ keV
$\alpha + {}^{12}C$	9.8 keV	$5.9 \cdot 10^{-56}$ keV
${}^{16}O + {}^{16}O$	20.2 keV	$2.5 \cdot 10^{-237}$ keV

$\Rightarrow$ $\boxed{\langle \sigma v \rangle \text{ drops enormously with increasing Coulomb-barrier}}$

$$\Rightarrow \langle \sigma v \rangle \simeq \left(\frac{2}{m}\right)^{1/2} \frac{\Delta}{(kT)^{3/2}} S(E_0) \exp\left(-\frac{3E_0}{kT}\right)$$

$$\text{with } \tau := \frac{3E_0}{kT}$$

$$\Rightarrow \langle \sigma v \rangle \simeq 7.20 \cdot 10^{-19} \frac{1}{AZ_xZ_y} \tau^2 e^{-\tau} \cdot S(E) \ \text{cm}^3 \ \text{s}^{-1}$$

$\Rightarrow$ $\boxed{\langle \sigma v \rangle \sim T^{\frac{\tau}{3} - \frac{2}{3}}}$

Example:

$(T = 1.5 \cdot 10^7 K)$	$\langle \sigma v \rangle \sim$	E_C
$p + p$	$T^{3.9}$	0.55 MeV
$p + {}^{14}N$	T^{20}	2.27 MeV
$\alpha + {}^{12}C$	T^{42}	3.43 MeV
${}^{16}O + {}^{16}O$	T^{182}	14.07 MeV

$\Rightarrow$ $\boxed{\text{thermonuclear cross sections are } \textbf{extremely } T\text{-dependent!}}$

$\Rightarrow$ $\boxed{\text{burning stages in stars occur at well-defined constant temperature}}$

G. Further effects affecting thermonuclear cross sections

Electron shielding

- in the laboratory: nuclei are surrounded by electrons
- stellar plasma contains nuclei and electrons
- electrons lower the effective repulsive Coulomb-potential between nuclei
  - $\Rightarrow$ weaker Coulomb-barrier (see Fig. 2.6)
  - $\Rightarrow$ increase of cross section for charged particle reactions

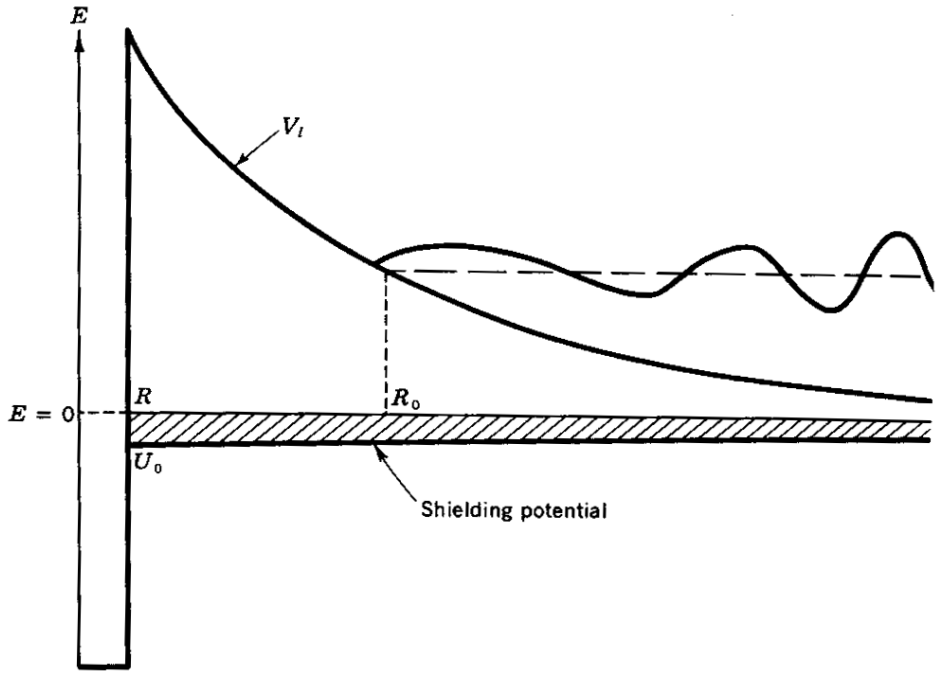

Figure 2.6: The effective potential modified by the screening potential. The polarization of the electron-ion plasma results in a small attractive potential (hatched area), which has the effect of reducing V and thereby increasing the penetrability of the Coulomb barrier. Figure from CLAYTON.

In the laboratory:

R_n = nuclear radius
R_a = atomic radius

$$\Rightarrow V_{c,\text{eff}} = \frac{Z_x Z_y e^2}{R_n} - \frac{Z_x Z_y e^2}{R_a}$$

as $R_a \gg R_n \rightarrow$ correction due to e^--shielding small in general

In stars:

nuclei ionized, but electrons "cluster" around nuclei in spherical shells with radius R_D: Debye-Hückel-radius

$$R_D = \left(\frac{kT}{4\pi e^2 \rho N_A \zeta}\right)^{1/2} \qquad \text{with} \qquad \zeta = \sum_i \left(Z_i^2 + Zi\right) \frac{X_i}{A_i}$$

high T, low ρ $\Rightarrow$ effect negligible
low T, high ρ $\Rightarrow$ effect important!

Resonances

direct capture reaction : $A(X,\gamma)B$

nucleus A captures projectile X directly to the low-energy state of nucleus B (see Fig. 2.7)

$\rightarrow$ σ varies smoothly with energy
$\rightarrow$ all projectile energies above Q-value are possible
$\rightarrow$ **non-resonant reaction**

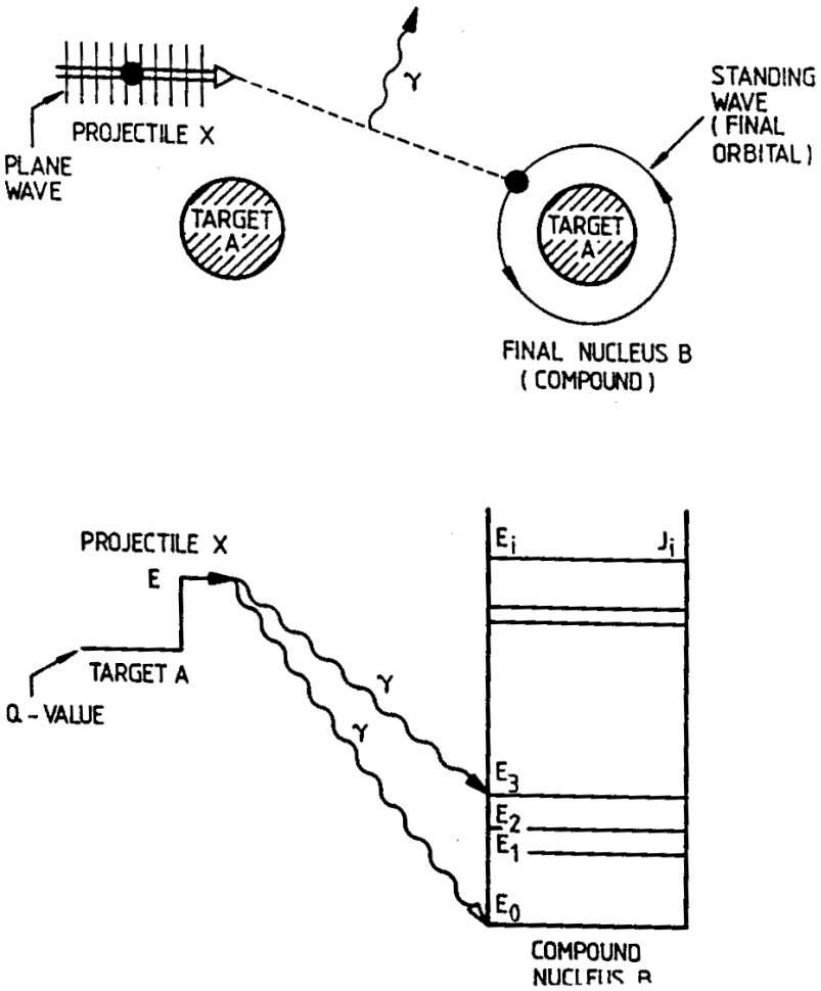

Figure 2.7: Illustration of a capture reaction $A(X,\gamma)B$ where the entrance channel $A+X$ goes directly to states in the final compound nucleus B under emission of a photon. This process is called a direct-capture reaction and can occur for all energies E of the projectile X.

resonant capture reaction : $A(X,\gamma)B$

$A + X$ form excited compound nucleus B^*, which later decays to low-energy state $B^* \to B + \gamma$ (see Fig. 2.8)

$\to$ 2 step process
$\to$ possible *only* if projectile energy matches the energy level of the excited state B^*!
$\to$ $\sigma(E)$ may have large local maxima
$\to$ **resonant reaction**

$\rightsquigarrow$ energy levels of nuclei often not accurately known ...

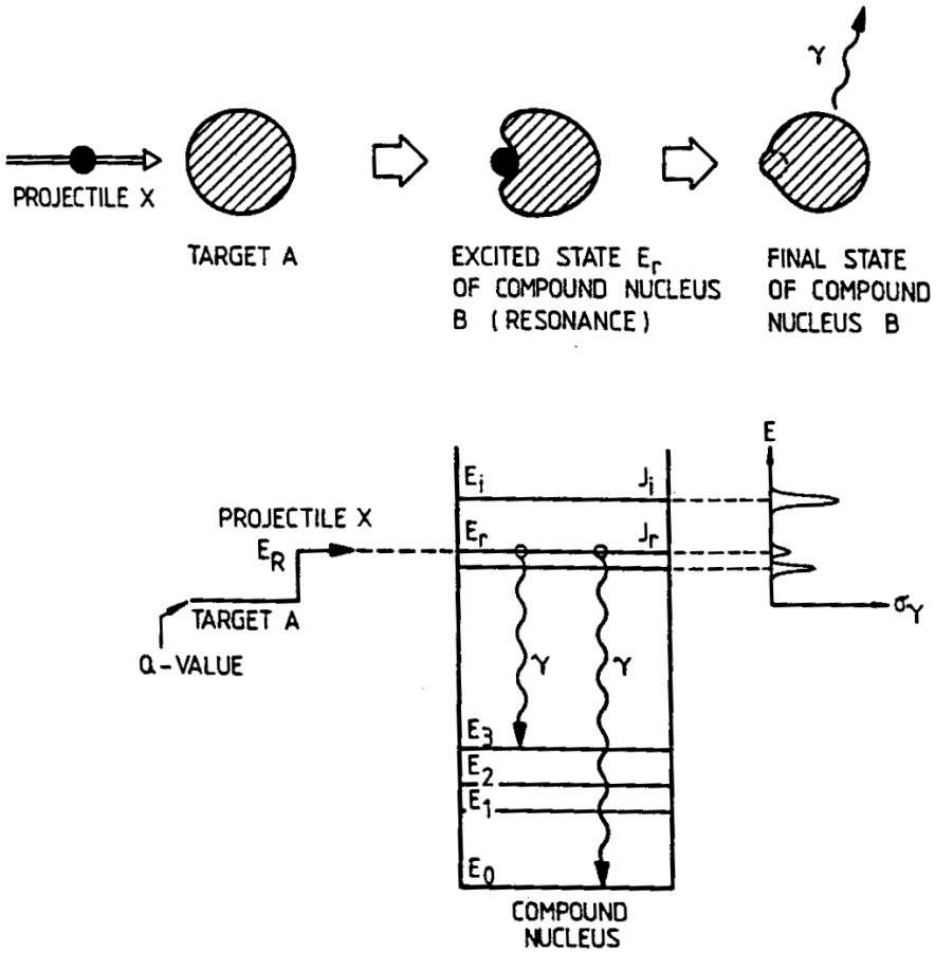

Figure 2.8: Illustration of a capture reaction $A(X,\gamma)B$ where the entrance channel $A + X$ forms an excited state E_r in the compound nucleus at an incident energy E_R. The excited state E_r decays into lower-lying states with the emission of a γ photon. This process is called a resonant capture reaction and can occur only at selected energies where $Q + E_R$ matches E_r. At these resonant energies E_R the capture cross section may exhibit large maxima.

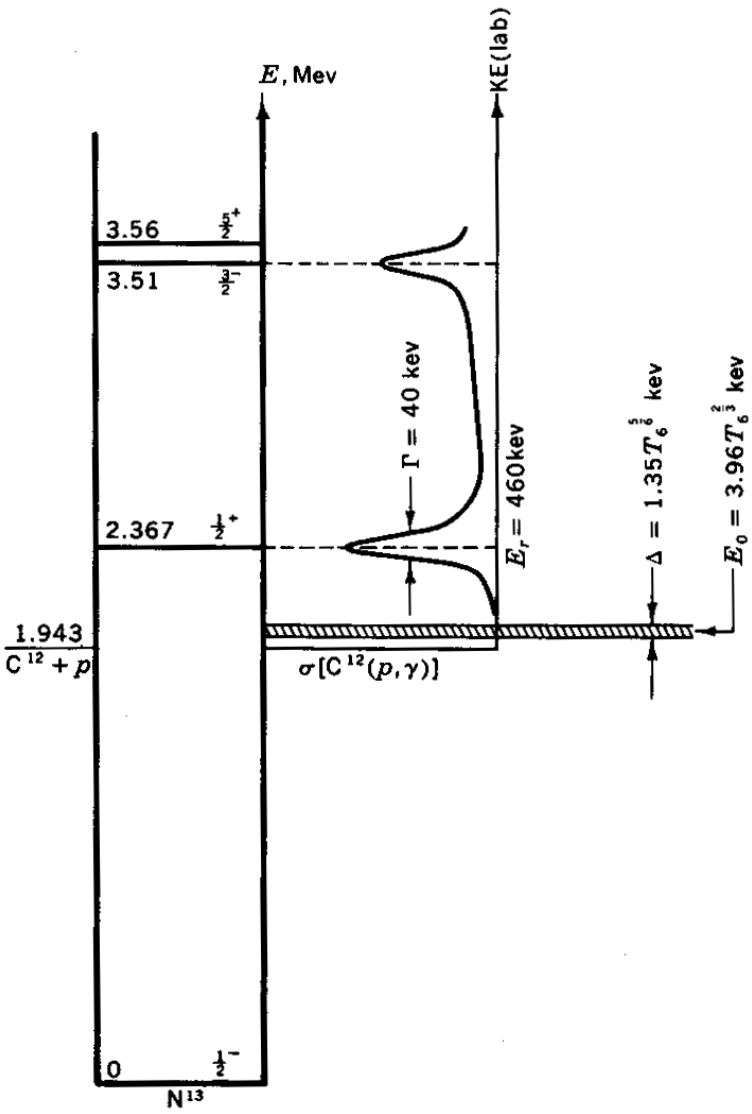

Figure 2.9: Energy-level diagram of ^{13}N, the compound nucleus for the reaction $^{12}\mathrm{C}(\mathrm{p},\gamma)^{13}\mathrm{N}$. The cross section for this reaction (displayed vertically on the right) is dominated by a resonance at $E_\mathrm{p} = 460\,\mathrm{keV}$. Shown as a hatched band is the range of effective stellar energies near E_0 (see Fig. 2.5). At that energy the protons are captured into the wing of the 460 keV resonance. Figure from Clayton.

Suggestions for further reading

– Chapter 2 of Pagel.
– For a very detailed but clearly written treatment of thermonuclear reaction rates, see Chapter 4 of Clayton.

Exercises

2.1 (a) Compute the Coulomb threshold energy for the $\mathrm{p(p, e^+\nu)D}$ reaction (in eV). Assume nuclear radii $R = R_0 A^{1/3}$ with $R_0 = 1.3 \cdot 10^{-13}$ cm.
Note: $e^2 = 1.44 \cdot 10^{-10}$ keV cm

(b) Compute the Coulomb threshold energy of the reaction $^{12}\mathrm{C}(\alpha, \gamma)^{16}\mathrm{O}$.

(c) Compare the results of (1) and (2). To which temperatures do these energies correspond?

2.2 Assume a temperature in the center of the sun of $T = 10^7$ K. How many $\mathrm{p(p, e^+\nu)D}$ reactions per unit time would take place if the tunnel-effect would not work? (Use the result of A).

2.3 (a) Compute the energy of the Gamow peak for the $\mathrm{p(p, e^+\nu)D}$ reaction at $T = 10^7$ K.

(b) Which fraction of the protons is found at this energy (order of magnitude)?

Chapter 3

Big Bang nucleosynthesis

A. Basics and background cosmology

'Hot' Big Bang theory: established theory for the beginning of the Universe

First proposed by Gamow, Alpher & Hermann in 1948:
$\Rightarrow$ going back in time, the Universe was smaller, *denser* and *hotter*
$\Rightarrow$ during the first few minutes (when $T \sim 10^9\,\mathrm{K}$), it acted like a nuclear reactor
$\rightsquigarrow$ but a 'defective' reactor because it was expanding and cooling rapidly...

Three independent fundamental tests:

1) Hubble expansion: distant galaxies recede with velocity $\propto$ distance $\rightarrow$
   $v = H_0 D$ with Hubble constant: $H_0 := 100\,h\,\mathrm{km\,s^{-1}\,Mpc^{-1}} \approx 70\,\mathrm{km\,s^{-1}\,Mpc^{-1}}$.

2) Cosmic microwave background (CMB) radiation: blackbody with $T = 2.73 \pm 0.01\,\mathrm{K}$.

3) *Nucleosynthesis* $\rightarrow$ abundances of light elements D(^{2}H), ^{3}He, ^{4}He, ^{7}Li
   in particular: deuterium (D) which is later only destroyed in stars

Big Bang cosmology:

Assumptions: – normal laws of physics hold at all times and places
– general relativity
– the *cosmological principle*: the Universe is *homogeneous* and *isotropic*

Define: R = scale factor $\propto$ physical size of a region comoving with the Hubble flow

Photon redshift z is related to the scale factor: $\quad 1 + z = \dfrac{\lambda}{\lambda_{\mathrm{lab}}} = \dfrac{R_0}{R_z} \quad (0 = \text{now})$

Adiabatic expansion of CMB photons:
• entropy, i.e. number N of photons in a comoving volume $V \propto R^3$ is conserved
• blackbody radiation: energy density $U = aT^4$; average energy per photon $\langle E_\gamma \rangle = 2.7kT$
$\Rightarrow$ number density of photons $n = N/V = U/\langle E_\gamma \rangle \propto T^3$

$\Rightarrow$ $\boxed{T \cdot R = \text{constant}}$ $\Rightarrow$ at early times, the background radiation was *hotter*!

GR ⇒ expansion rate follows from Einstein's field equations:

$$H^2 := \left(\frac{\dot{R}}{R}\right)^2 = \frac{8\pi G}{3}\rho + \frac{\Lambda}{3} - \frac{kc^2}{R^2} \tag{3.1}$$

with: ρ = mass-energy density (g/cm^3)
k = curvature constant → $k = 0$ flat geometry
$k > 0$ closed geometry
$k < 0$ open geometry
Λ = cosmological constant (postulated by Einstein)

⇒ **critical density** for a flat Universe with $k = \Lambda = 0$:

$$\boxed{\rho_{\rm crit} := \frac{3H^2}{8\pi G}} \qquad \text{define } \Omega := \frac{\rho}{\rho_{\rm crit}} \tag{3.2}$$

Today: $\rho_{\rm crit} = 1.88 \times 10^{-24} h^2\,{\rm g\,cm^{-3}} \approx 0.9 \times 10^{-24}\,{\rm g\,cm^{-3}}$ ($h \approx 0.7$)

Current evidence from:

- distant supernovae ⇒ expansion is *accelerating* (Riess et al. 1998)
- anisotropy of the CMB, as measured by the WMAP satellite (Spergel et al. 2003)
- galaxy clustering on large scales, e.g. derived from the Sloan Digital Sky Survey (SDSS) (Tegmark et al. 2004)

⇒ Universe is flat ($k = 0$) but $\Lambda > 0$

Define $\Omega_\Lambda := \Lambda/(3H^2)$, $\Omega_{\rm M} := \rho/\rho_{\rm crit}$ ⇒ $k = 0$ means $\Omega = \Omega_{\rm M} + \Omega_\Lambda = 1$

⇒ Today: $\Omega_\Lambda \approx 0.7$ ("dark energy")
$\Omega_{\rm M} \approx 0.3$ (mostly dark, non-baryonic matter)
Baryon (normal matter) density: $\Omega_{\rm b} = \rho_{\rm b}/\rho_{\rm crit} \approx 0.05$ $\quad (\Omega_{\rm b} h^2 = 0.023 \pm 0.001)$

B. History of the early Universe

Early Universe: T was very high
⇒ energy density ρ dominated by radiation (and other relativistic particles)
⇒ $\rho \propto R^{-4}$ (number density $\propto R^{-3}$, energy per photon $\propto T \propto R^{-1}$ due to redshift)
⇒ terms in eq. (3.1) involving k and Λ are negligible compared to ρ

⇒ $\boxed{\rho = \rho_{\rm crit}}$ independent of current properties

⇒ expansion rate H is fixed by total energy density ⇒ ρ is a known function of t:

$$\rho = \frac{3}{32\pi G} t^{-2} \tag{3.3}$$

Thermal equilibrium (TE) between particle-antiparticle pairs and photons: $\quad x + \bar{x} \leftrightarrow 2\gamma$
as long as $kT \gg m_x c^2$ ⇒ roughly equal numbers of particles and photons, $N_x \sim N_\gamma$

When $kT < m_x c^2$, most particle-antiparticle pairs annihilate: $\quad x + \bar{x} \to 2\gamma$

Assume a small matter/antimatter asymmetry, $N_x - N_{\bar{x}} \ll N_\gamma$
$\Rightarrow$ trace amounts of particles 'condense out' and remain...

E.g. baryons (protons, neutrons), $m_\mathrm{p} = 1.67 \times 10^{-24}\,\mathrm{g}$: $\quad m_\mathrm{p}c^2 = kT \quad \Rightarrow \quad T \simeq 10^{13}\,\mathrm{K}$

Nucleosynthesis is possible only after: $\quad E_\gamma \lesssim$ binding energy of nuclei $\simeq$ MeV
$\Rightarrow T \lesssim 10^{10}$ K $\Rightarrow t \gtrsim 1$ s

At that time:

- Baryons have condensed out and become non-relativistic; only trace amounts left
  $\Rightarrow$ negligible contribution to ρ.
- Universe is dominated by extremely relativistic particles in TE:
  photons, $\mathrm{e}^-\mathrm{e}^+$ pairs and $\nu\bar{\nu}$ pairs (N_ν families)
  Standard model of particle physics: $N_\nu = 3$ (ν_e, ν_μ and ν_τ).

$$\Rightarrow \rho = \rho_\gamma + \rho_{\mathrm{e}^\pm} + N_\nu \rho_\nu := (g_*/2)\rho_\gamma$$

with: $\rho_\gamma c^2 = aT^4$
$g_* = \frac{11}{2} + \frac{7}{4}N_\nu \quad \rightsquigarrow \quad 2 + 0.45\,N_\nu$ after $\mathrm{e}^\pm$ pairs annihilate

$$\Rightarrow T = \left(\frac{3c^2}{16\pi g_* a G}\right)^{1/4} t^{-1/2} \tag{3.4}$$

Hence in the Standard model[1], both ρ and T are known functions of $t \Rightarrow$ the outcome of Big Bang nucleosynthesis (BBN) depends only on a single parameter: the relative *baryon density*.

Baryon-to-photon ratio: $\boxed{\eta := \dfrac{N_\mathrm{b}}{N_\gamma} = \dfrac{n_\mathrm{b}}{n_\gamma}}$

$T \gg 10^{13}\,\mathrm{K}$: $\quad \mathrm{p} + \bar{\mathrm{p}} \leftrightarrow \gamma \quad \Rightarrow \quad \eta \simeq 1$

$T \sim 10^{13}\,\mathrm{K}$: $\quad \mathrm{p}\bar{\mathrm{p}}$ pairs annihilate $\quad \Rightarrow \quad \eta \downdownarrows$
Since then: $N_\mathrm{b} =$ constant

$T \sim 10^{10}\,\mathrm{K}$: $\quad \mathrm{e}^\pm$ pairs annihilate $\quad \Rightarrow \quad N_\gamma \uparrow$
Since then ($t \gtrsim 1\,\mathrm{s}$): $N_\gamma =$ constant $\Rightarrow$ $\boxed{\eta = \text{constant} \simeq 10^{-9} \ldots 10^{-10}}$

- Since η is conserved, particularly during BBN, it is a useful measure of the baryon density
- η is related to the baryon density *today* (expressed as $\rho_\mathrm{b} = \Omega_\mathrm{b}\rho_\mathrm{crit}$):

$$\eta = 2.73 \times 10^{-8}\Omega_\mathrm{b}h^2 \tag{3.5}$$

$\Rightarrow$ Value of η at epoch of BBN ($t \sim 100\,\mathrm{s}$) should correspond to the measurement of $\Omega_\mathrm{b}h^2$ from the CMB, when the Universe was 3.8×10^5 yrs old:

WMAP $\Rightarrow \Omega_\mathrm{b}h^2 = 0.023 \pm 0.001 \Rightarrow \eta = (6.1 \pm 0.3) \times 10^{-10}$

[1]With non-standard particle physics, e.g. $N_\nu > 3 \Rightarrow T$ is smaller at a particular t or $\rho \Rightarrow$ expansion rate is higher at a particular T.

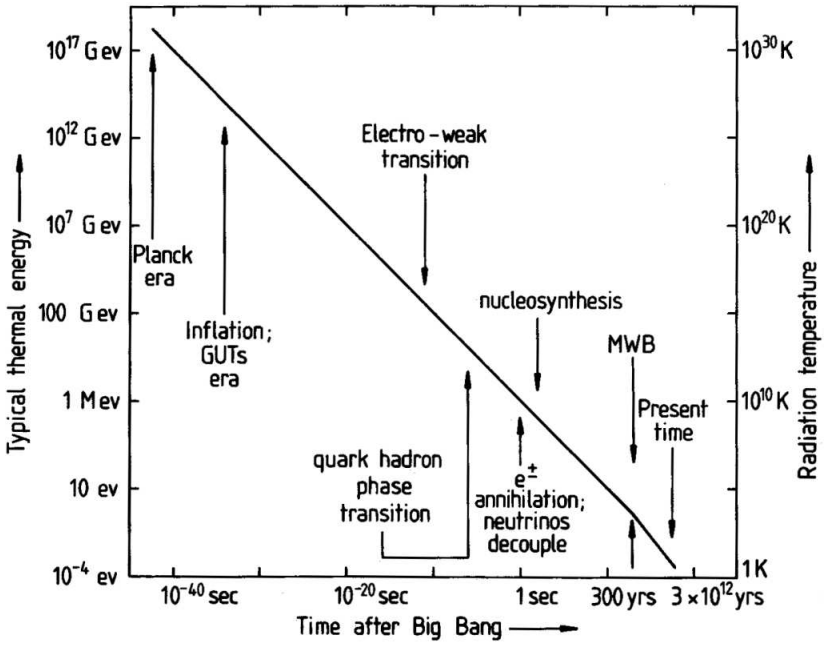

Figure 3.1: Schematic thermal history of the universe, showing the major episodes envisaged in the standard Hot Big Bang model. Note the logarithmic time axis, which runs from the Planck time (10^{-42} s) up to the present. Between the end of nucleosynthesis, $\approx 10^3$ s, and the decoupling of matter and radiation (i.e. last cattering of the microwave backgroud; MWB) at $\approx 3 \times 10^5$ yrs, nothing happens. This last event corresponds to (re)combination of atomic hydrogen at $T \approx 10^4\,\mathrm{K}$. The energy-density of the universe was dominated by radiation up to approximately this point, and by matter afterwards. Figure from PAGEL.

C. The n/p ratio

• As long as T is high enough: neutrons and protons in equilibrium through *weak interactions*:

$$\mathrm{n} + \mathrm{e}^+ \longleftrightarrow \mathrm{p} + \bar{\nu}_\mathrm{e}$$
$$\mathrm{n} + \nu_\mathrm{e} \longleftrightarrow \mathrm{p} + \mathrm{e}^-$$

$\Rightarrow$ equilibrium ratio:

$$\frac{\mathrm{n}}{\mathrm{p}} = \exp\left(-\frac{(m_\mathrm{n} - m_\mathrm{p})c^2}{kT}\right) = \exp\left(-\frac{1.29\,\mathrm{MeV}}{kT}\right)$$

• When $T \lesssim T_\mathrm{crit} (\simeq 10^{10}\mathrm{K})$: $\Rightarrow$ weak interactions become *slower* than the expansion rate

$\Rightarrow$ n/p "freezes out" to a constant value: $\dfrac{\mathrm{n}}{\mathrm{p}} = \exp\left(-\dfrac{(m_\mathrm{n} - m_\mathrm{p})c^2}{kT_\mathrm{crit}}\right)$

• Afterwards, n/p slowly decreases due to neutron decay:

$$\mathrm{n} \to \mathrm{p} + \mathrm{e}^- + \bar{\nu} \quad \text{with} \quad \tau_{1/2} = 10.3\ \mathrm{min}$$

Without further reactions, there would be no neutrons left in the Universe. However, most neutrons are bound by nucleosynthesis before much decay can occur (see Fig. 3.2).

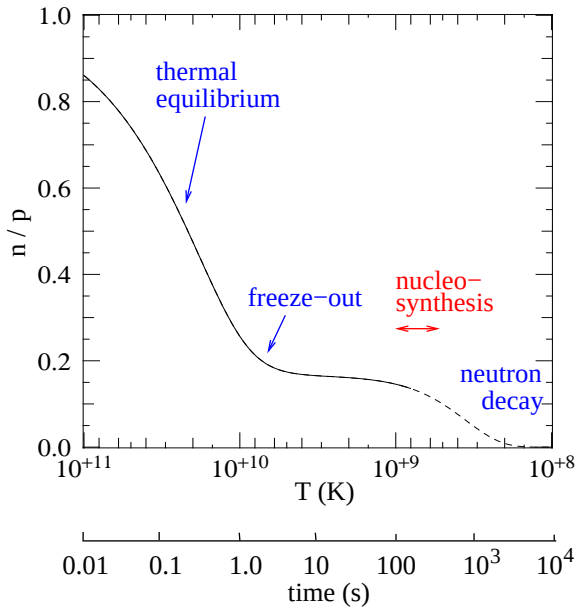

Figure 3.2: The neutron-to-proton ratio as a function of temperature and time in the early Universe. After $t \approx 100$ sec, nucleosynthesis starts and binds the remaining nuetrons into ^{4}He. Further neutron decay (the dashed portion of the line) does not play a role.

D. Deuterium: a bottleneck

• Nucleosynthesis has to go through

$$\mathrm{p} + \mathrm{n} \to \mathrm{D} + \gamma \to \ldots$$

(because the alternative $\mathrm{p} + \mathrm{p} \to \mathrm{D} + \mathrm{e}^+ + \gamma$ is too slow)

• $T \sim T_{\rm crit}$ is high enough for nuclear reactions to be in equilibrium: $\mathrm{n} + \mathrm{p} \longleftrightarrow \mathrm{D} + \gamma$

$kT_{\rm crit} < E_B(\mathrm{D}) = 2.2\,\mathrm{MeV} \Rightarrow$ synthesis of D is possible.

However: $\mathrm{D}(\gamma,\mathrm{n})\mathrm{p}$ (rate $\propto n_\gamma \exp[-E_B/kT]$) is still much faster than
$\mathrm{p}(\mathrm{n},\gamma)\mathrm{D}$ (rate $\propto n_{\rm b}$)

because $\eta = n_{\rm b}/n_\gamma \lll 1$

$\Rightarrow$ have to wait until $T \simeq 10^9\,\mathrm{K}$ ($t \simeq 100\,\mathrm{s}$) for photodisintegrations to become slow enough, so that (equilibrium) D abundance can build up (Fig. 3.4)

$\Rightarrow$ only after $\sim 100\,\mathrm{s}$, nucleosynthesis can really start

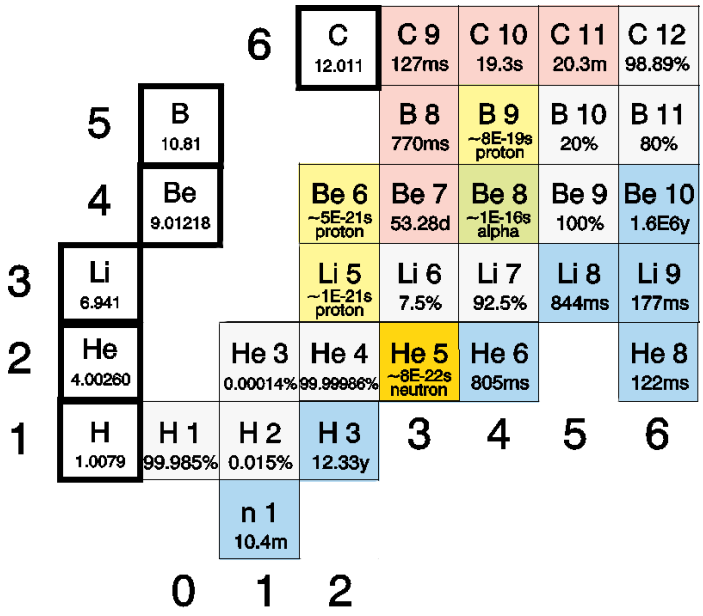

Figure 3.3: Lower-left section of the nuclide chart, showing the nuclei relevant for Big Bang nucleosynthesis. White squares are stable isotopes, coloured isotopes are unstable with the mode of decay and half-life as indicated (blue: β^- unstable; pink: β^+ unstable). Note that all nuclei with $A = 5$ and $A = 8$ are violently unstable, due to the vicinity of the very tightly bound ^{4}He nucleus.

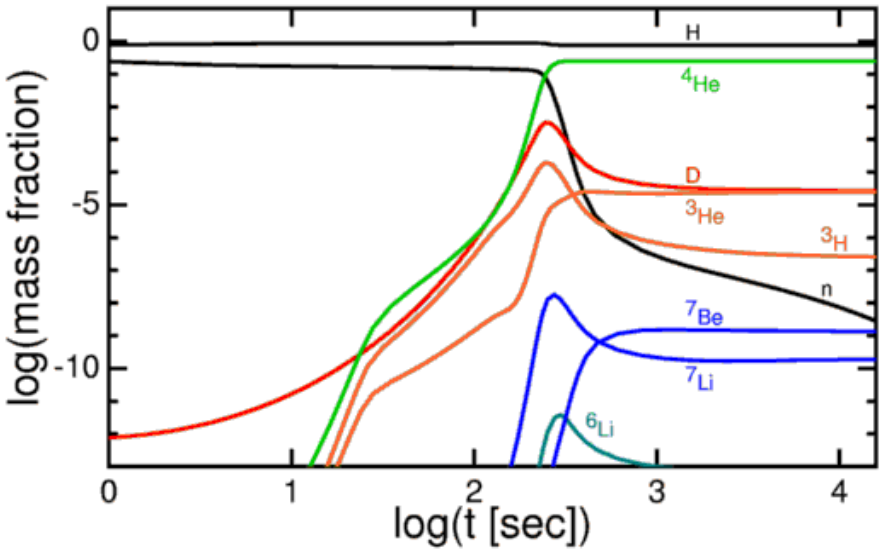

Figure 3.4: The evolution of light-element abundances with time in the standard BBN model, computed for $\eta = 7.9 \times 10^{-10}$ (Burles et al. 1999). Deuterium (red line) is in nuclear statistical equilibrium until $t \sim 200\,\mathrm{s}$ but its abundance is too low to allow other reactions to proceed. After $t \sim 200\,\mathrm{s}$ when the reactions get going, ^{4}He soaks up virtually all neutrons and only tiny amounts of other nuclei are left. Note that ^{3}H later decays into ^{3}He and ^{7}Be decays into ^{7}Li (by electron capture). Figure from `http://www.astro.ucla.edu/~wright/BBNS.html`.

E. Nucleosynthesis in the Big Bang

After D survives ($T \simeq 10^9\,\mathrm{K}$, $\rho \simeq 10^{-5}\,\mathrm{g/cm^3}$, $t \simeq 100\,\mathrm{s}$) quickly more reactions follow, the most important of which are:

$$\begin{aligned} \mathrm{D} + \mathrm{p} &\to {}^3\mathrm{He} + \gamma \\ \mathrm{D} + \mathrm{D} &\to {}^3\mathrm{He} + \mathrm{n} \\ \mathrm{D} + \mathrm{D} &\to {}^3\mathrm{H} + \mathrm{p} \\ {}^3\mathrm{He} + \mathrm{n} &\to {}^3\mathrm{H} + \mathrm{p} \\ {}^3\mathrm{He} + \mathrm{D} &\to {}^4\mathrm{He} + \mathrm{p} \\ {}^3\mathrm{H} + \mathrm{D} &\to {}^4\mathrm{He} + \mathrm{n} \end{aligned}$$

Note: 1) the weak interaction is too slow to be important:

$$\begin{aligned} \mathrm{n}(\mathrm{e}^-\bar{\nu}_e)\mathrm{p} \quad & \tau_{1/2} = 10 \text{ min} \\ {}^3\mathrm{H}(\mathrm{e}^-\bar{\nu}_e){}^3\mathrm{He} \quad & \tau_{1/2} = 12 \text{ yr} \end{aligned}$$

2) most reactions involving γ emission (i.e. electromagnetic interaction):

$$\mathrm{D}(\mathrm{n},\gamma){}^3\mathrm{H} \quad {}^3\mathrm{H}(\mathrm{p},\gamma){}^4\mathrm{He} \quad \ldots$$

are slower than those given above, which involve only the *strong* interaction

Next bottleneck: there is no stable isotope with **mass number 5** (Fig. 3.3)

i.e. $\left\{ \begin{array}{l} {}^4\mathrm{He}(\mathrm{n},\gamma){}^5\mathrm{He} \\ {}^4\mathrm{He}(\mathrm{p},\gamma){}^5\mathrm{Li} \end{array} \right.$ are impossible

Some *traces* of ^{7}Li, ^{7}Be produced due to

$$\begin{aligned} {}^3\mathrm{He} + {}^4\mathrm{He} &\to {}^7\mathrm{Be} + \gamma \qquad \text{(later followed by } {}^7\mathrm{Be}(\mathrm{e}^-,\nu_\mathrm{e}){}^7\mathrm{Li} \text{ with } \tau_{1/2} = 53\,\mathrm{d}) \\ {}^3\mathrm{H} + {}^4\mathrm{He} &\to {}^7\mathrm{Li} + \gamma \\ {}^7\mathrm{Be} + \mathrm{n} &\to {}^7\mathrm{Li} + \mathrm{p} \\ {}^7\mathrm{Li} + \mathrm{p} &\to 2\,{}^4\mathrm{He} \end{aligned}$$

After $\sim$ 1000 seconds, T gets so low that Coulomb barriers cause the reactions to stop (Fig. 3.4). Final mass fractions (order of magnitude):

$$\begin{aligned} \mathrm{D} &\sim 10^{-4} \\ {}^3\mathrm{He} &\sim 10^{-4} \ldots 10^{-5} \\ {}^7\mathrm{Li} &\sim 10^{-9} \end{aligned}$$

These are determined by competition between the *expansion rate* H and the *rates of the nuclear reactions* involved

$\Rightarrow$ effectively, all neutrons go into ^{4}He

$\Rightarrow$ Final mass fraction Y of ^{4}He is determined by the n/p ratio (i.e. by competition between *expansion* and *weak interactions*, cf. **C**), and *not* by nuclear reaction rates

$$Y = 2\,X_\mathrm{n} = 2\,\frac{\mathrm{n/p}}{1 + \mathrm{n/p}} \qquad \text{at } T \approx 10^9\,\mathrm{K} \quad (X_\mathrm{n} = \text{neutron mass fraction})$$

Example: $T_\mathrm{crit} = 8 \cdot 10^9$ K $\Rightarrow \dfrac{\mathrm{n}}{\mathrm{p}}(T_\mathrm{crit}) = 0.165 \simeq \frac{1}{6} \rightsquigarrow \frac{1}{7}$ after n-decay ($t \simeq 100\,\mathrm{s}$)

$\Rightarrow X_\mathrm{n} \simeq \frac{1}{8} \quad \Rightarrow \quad Y \simeq 0.25, \quad X = 1 - Y \simeq 0.75$

$\rightsquigarrow$ realistic time-dependent nuclear network calculations required to be more accurate

F. Two factors affect BB nucleosynthesis

1) the **baryon-to-photon ratio** $\eta = n_{\rm b}/n_\gamma$

$\eta \uparrow$ $\Rightarrow$ (1) $\Rightarrow$ particle density $n_{\rm b}$ larger
$\Rightarrow$ nuclear reactions are more frequent (§**E**) $\Rightarrow$ e.g. D $\downarrow$, ^{3}He $\downarrow$
(2) $\Rightarrow$ equil. D $\uparrow$ (§**D**) $\Rightarrow$ BBN can start earlier
$\Rightarrow$ fewer neutrons have had time to decay (§**C**) $\Rightarrow Y \uparrow$

Y (^{4}He) depends only weakly on η because it is mainly determined by the weak interaction rate ($\Rightarrow$ n/p) and not by nuclear reaction rates.

Other abundances are very sensitive to η (Fig. 3.5, 3.6), in particular deuterium $\Rightarrow$ D provides a sensitive measure of the baryon density (D is a "baryometer").

2) the **number of ν-families** N_ν

$N_\nu \uparrow$ $\Rightarrow$ energy density $\uparrow$ at a particular T (§**B**)
$\Rightarrow$ expansion more rapid at a particular T (§**B**)
$\Rightarrow T_{\rm crit} \uparrow$, n/p freezes out earlier (§**C**) $\Rightarrow Y \uparrow$

Hence: Y is sensitive to non-standard particle physics ($N_\nu \neq 3$).
The abundances of D, ^{3}He and ^{7}Li are much less sensitive to N_ν.

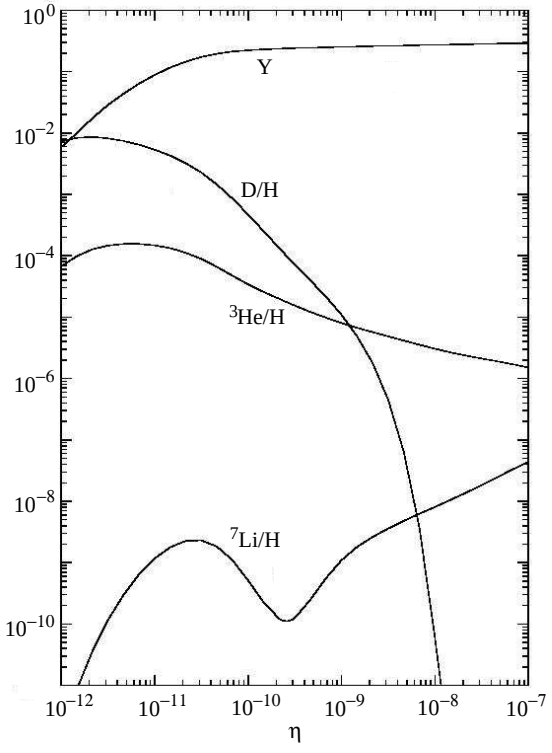

Figure 3.5: Predicted final abundances in standard BBN, as a function of the baryon-to-photon ratio η. Y is the ^{4}He mass fraction and D/H, ^{3}He/H and ^{7}Li/H are the number density ratios relative to hydrogen (protons). Adapted from G. Steigman (2000), `http://nedwww.ipac.caltech.edu/level5/Steigman/frames.html`.

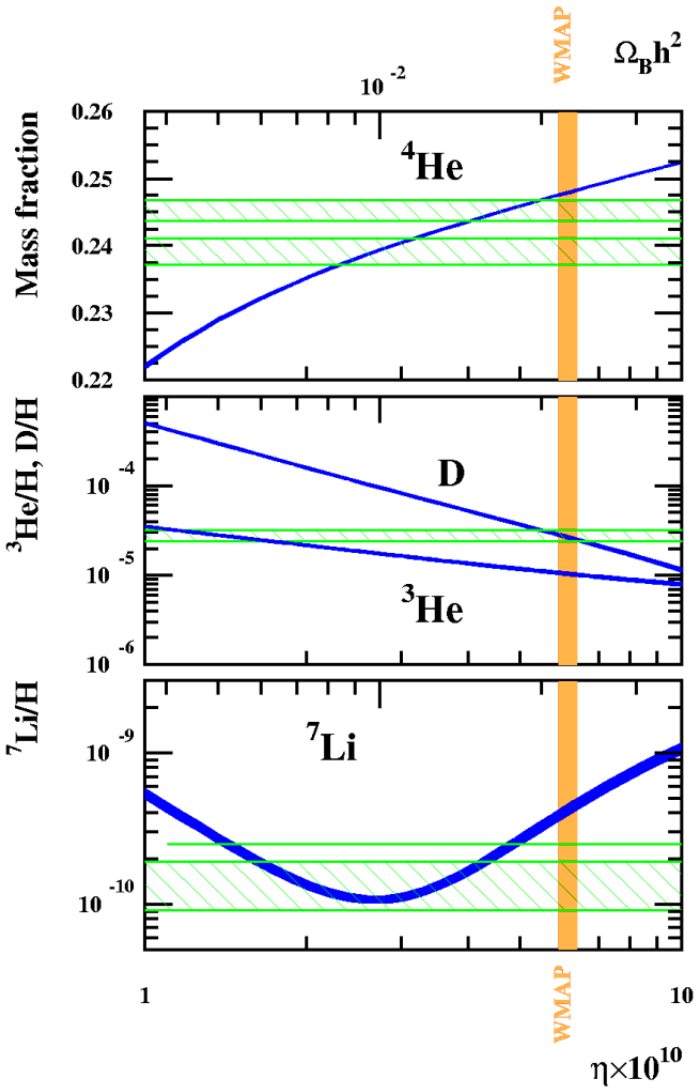

Figure 3.6: As Fig. 3.5, showing recent calculations by Coc et al. (2004) for the region $10^{-10} < \eta < 10^{-9}$. The width of the lines indicate the theoretical 1-σ errors resulting from reaction rate uncertainties. The green hatched areas represent primordial ^{4}He, D and ^{7}Li abundances derived by different groups. The vertical stripe represents the 1-σ limits on η provided by the WMAP measuremnt of the CMB anisotropy (Spergel et al. 2003). Along the top are the equivalent values of $\Omega_b h^2$. Figure from Coc et al. (2004).

G. Comparison of BBN with Solar-system abundances

Table 3.1 $\Rightarrow$ **chemical evolution** has played an important role between the Big Bang and the formation of the Solar System

In particular: isotopes with $A > 7$ are **not** produced by BBN

Stellar models:	D is always **destroyed**	$\downarrow$
	^{3}He is produced or destroyed	?
	^{4}He is always produced	$\uparrow$

Table 3.1: Result of standard BBN calculations versus Solar-system abundances

mass fraction	BBN[1]	Solar System
^{1}H	0.752	0.702
^{2}H	3.9×10^{-5}	2.3×10^{-5}
^{3}He	2.3×10^{-5}	3.4×10^{-5}
^{4}He	0.248	0.281
^{7}Li	2.2×10^{-9}	1.0×10^{-8}
$A > 7$	$\varnothing$	0.017

[1]using $\eta = 6.1 \times 10^{-10}$ corresponding to the WMAP measurement of $\Omega_{\rm b} h^2$

H. Observations of primordial abundances

To test the consistency of BBN: compare to primordial abundances of D, ^{3}He, ^{4}He and ^{7}Li
$\rightsquigarrow$ not *directly* observed, but *inferred* from observed abundances
- in very **old** objects
- in very **unevolved** objects

^{4}He: not measurable in stars
$\Rightarrow$ emission lines from gaseous nebulae in dwarf galaxies, with low metallicity
$\Rightarrow Y_P = 0.238 \pm 0.007$ (Fields & Olive 1998), see Fig. 3.7
however: different groups obtain somewhat different results...

D: from quasar absorption lines $\Rightarrow$ nearly unprocessed gas
(still small sample, systematic errors...)
$\Rightarrow$ D/H $= (2.8 \pm 0.4) \times 10^{-5}$ on average (Fig. 3.8)

^{3}He: difficult to measure in unevolved objects + uncertain chemical evolution (§**G**)
$\rightsquigarrow$ less useful as an observational test

^{7}Li: from metal-poor stars in the Galactic halo
$\Rightarrow$ constant Li/H as function of metal content $\Rightarrow$ interpreted as primordial
$\Rightarrow$ Li/H $= (1.0 \ldots 2.5) \times 10^{-10}$ (Fig. 3.8)

Conclusions:

• Primordial abundances of H, D, ^{3}He (if $\sim$ solar), ^{4}He, ^{7}Li do not contradict standard BB nucleosynthesis: all abundances fit (almost) a *single* value of the parameter η (Fig. 3.6).

• The implied value of η during BBN corresponds to the value derived from the CMB (§**B**):
$\eta \approx 6 \times 10^{-10}$
Hence, the Universe at $t \simeq 100\,$s ($T \sim 10^9\,$K) and at $t \simeq 3.8 \times 10^5\,$yr ($T \sim 10^4\,$K) agree!

• Normal, baryonic matter makes up only $\approx 5\%$ of the critical density of the Universe

• Apparent discrepancy for ^{7}Li (Fig. 3.8) $\rightsquigarrow$
- destruction of ^{7}Li in stars, due to extra (e.g. rotational) mixing?
- systematic errors in the derived abundance?
- unknown rate of some of the nuclear reactions involved?

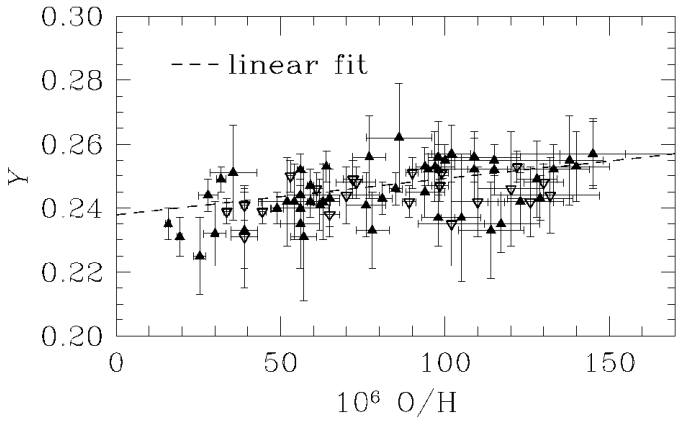

Figure 3.7: Observed mass fraction of ^{4}He in metal-poor extragalactic H II regions, as a function of the O/H ratio (for comparison, the solar O/H value is 8.3×10^{-4}). The intersection of the extrapolated relation with the vertical axis defines the primordial He abundance Y_P. Figure from Fields & Olive (1998).

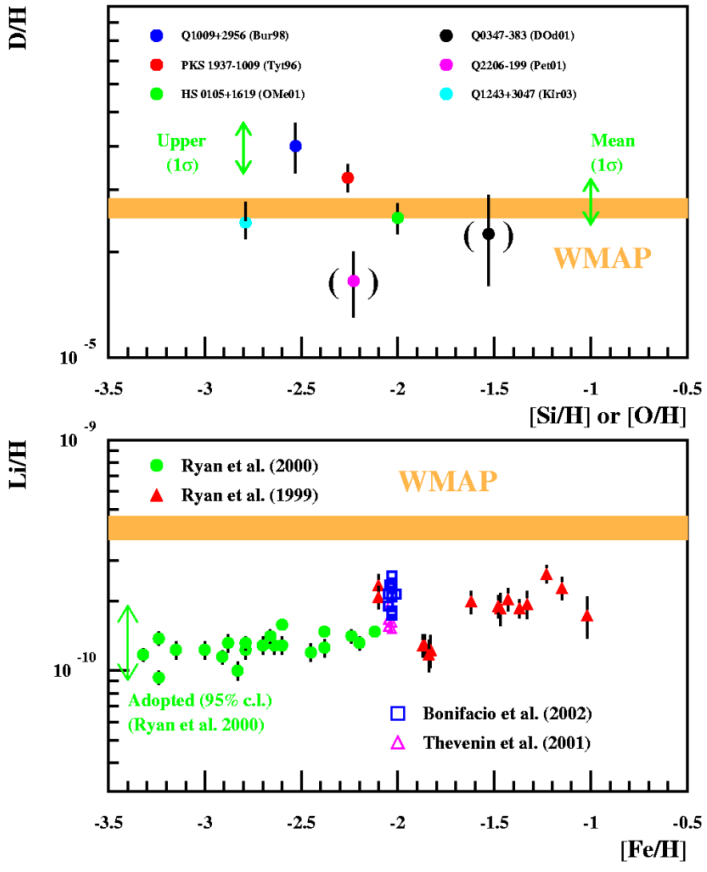

Figure 3.8: Observed abundances of D/H and Li/H as a function of metallicity (measured as $[\mathrm{O/H}] = \log(\mathrm{O/H}) - \log(\mathrm{O/H})_\odot$ in the upper panel, and [Fe/H] in the lower panel). The horizontal stripes represent the 1-σ limits derived from WMAP+BBN (Fig. 3.6). Figure from Coc et al. (2004).

Suggestions for further reading

– Chapter 4 of PAGEL.
– A good tutorial on Big Bang nucleosynthesis is: G. Steigman, "Light Element Nucleosynthesis", in *Encyclopedia of Astronomy and Astrophysics*, 2000. Available via internet at `http://nedwww.ipac.caltech.edu/level5/Steigman/frames.html`.

Exercises

3.1 Assume the big bang produced nuclei with the mass fractions as given in Table 3.1. What are the respective particle number fractions?

3.2 (a) Compute the critical density of the universe, assuming Newtonian gravity. The critical density is that density for which the sum of kinetic and potential energy in the universe is zero. Compare the answer you get to eq. (3.2).

(b) Is our universe today matter dominated? Is the assumption of Newtonian gravity reasonable?

3.3 Derive the relation between η and $\Omega_{\rm b}$, eq. (3.5). (Hint: calculate the current photon density n_γ, using the fact that the average energy per photon for blackbody radiation is $2.7kT$. Answer: $n_\gamma = 413\,{\rm cm}^{-3}$ for $T_\gamma = 2.73\,{\rm K}$.)

3.4 (a) How much energy is liberated from fusing 4 protons to ^{4}He? What does this have to do with the lifetime of the Sun?

(b) How much energy is liberated from decaying a neutron into a proton? What does this have to do with the Big Bang?

Chapter 4

Hydrostatic nucleosynthesis in stars (A < 56)

4.1 Stellar evolution and nuclear burning

A. The virial theorem determines the evolution of stars

The **virial theorem** connects two important energy reservoirs of a star: the gravitational potential energy $E_{\rm grav}$ and the total internal inergy $E_{\rm int}$. The virial theorem is valid for all gas spheres (stars) that are in **hydrostatic equilibrium**.

Consider a gaseous sphere of mass M, in which the physical quantities depend on the radial coordinate r, such as density $\rho(r)$, pressure $P(r)$, internal energy per unit mass $u(r)$.

Often it is more useful to take a *Lagrangian coordinate*, which follows the mass shells:
$\Rightarrow$ volume of a shell with thickness dr: $dV_r = 4\pi r^2 dr$
mass of this shell: $dM_r = \rho dV_r = 4\pi r^2 \rho\, dr$
Langragian coordinate: $M_r = \int_0^r 4\pi r'^2 \rho\, dr'$

Hydrostatic equilibrium (HE): the forces on all mass elements balance each other $\Rightarrow$

$$\frac{1}{\rho}\frac{dP}{dr} = -\frac{GM_r}{r^2} \qquad \Rightarrow \qquad \frac{dP}{dM_r} = -\frac{GM_r}{4\pi r^4}$$

multiply both sides by $4\pi r^3$ and integrate over dM_r $\Rightarrow$

right-hand side: $$-\int_0^M 4\pi r^3 \frac{GM_r}{4\pi r^4} dM_r \;=\; -\int_0^M \frac{GM_r}{r} dM_r \;=\; E_{\rm grav} \quad \text{(negative!)}$$

left-hand side: $$\int_0^M 4\pi r^3 \frac{dP}{dM_r} dM_r \;=\; 3\int_{\rm centre}^{\rm surf} V_r\, dP \;=\; 3\,[\,V_r P\,]_{\rm c}^{\rm s} - 3\int_{\rm c}^{\rm s} P\, dV_r$$
$$= \; -3\int_{\rm c}^{\rm s} P\, dV_r \;=\; -3\int_0^M \frac{P}{\rho}\, dM_r$$

This is the general form of the virial theorem: $$\boxed{-E_{\rm grav} = 3\int_{\rm c}^{\rm s} P\, dV}$$

Interpretation: a star that *contracts slowly* (while maintaining HE), and thereby becomes more strongly bound, must obtain a *higher internal pressure*.

The factor P/ρ is related to the internal energy per unit mass u:

$$\frac{P}{\rho} = \frac{\zeta}{3}\,u \quad \text{where e.g.} \quad \begin{cases} \zeta = 2 & \text{for an ideal gas} \\ \zeta = 1 & \text{for radiation pressure} \end{cases}$$

$$\Rightarrow \int_0^M 3\frac{P}{\rho}\,dM_r \;=\; \int_0^M \zeta u\,dM_r \;=\; \zeta\,E_{\rm int} \quad \text{(if } \zeta = \text{constant throughout the star)}$$

Virial theorem: $\boxed{-E_{\rm grav} = \zeta E_{\rm int}}$ $\qquad \zeta \simeq 1 \ldots 2$

Consequence for an *ideal gas*: hydrostatic contraction leads to a higher temperature

Qualitative behaviour of the pressure:

$E_{\rm grav} = -\int_0^M \frac{GM_r}{r} dM_r \sim \frac{G}{\langle r\rangle} M^2$

$E_{\rm int} = c\int_0^M P\,dV \sim \langle P\rangle\, V \sim \langle P\rangle\langle r\rangle^3$

$$\text{VT} \quad \Rightarrow \quad \frac{GM^2}{\langle r\rangle} \sim \langle P\rangle\,\langle r\rangle^3 \quad \Rightarrow \quad \langle P\rangle \sim GM^2\langle r\rangle^{-4} \sim GM^2\left(\sqrt[3]{M/\langle\rho\rangle}\right)^{-4} = GM^{2/3}\langle\rho\rangle^{4/3}$$

$\boxed{\langle P\rangle \sim GM^{2/3}\langle\rho\rangle^{4/3}}$

Theory of polytropes $\Rightarrow$ relation between central P and ρ: $\boxed{P_c = c\,GM^{2/3}{\rho_c}^{4/3}}$
where $c = 0.35 \ldots 0.5$.

Consequence: gas sphere of fixed mass $M \Rightarrow$
contraction in $\log P - \log\rho$ diagram (Fig. 4.1) according to $\log P \sim \frac{4}{3}\log\rho$
independent of the equation of state (EOS)

To find the **temperature evolution**: compare to *isothermals* in $\log P$ - $\log\rho$ diagram

- radiation dominated: $P = \frac{1}{3}aT^4 \;\neq f(\rho)$ $\quad \Rightarrow P_{T=\text{const}} \sim \rho^0$
- ideal gas: $P = \dfrac{\Re}{\mu}\rho T$ $\quad \Rightarrow P_{T=\text{const}} \sim \rho^1$
- non-relativistic degeneracy: $P = K_1\rho^{5/3} \;\neq f(T)$ $\quad \Rightarrow P_{T=\text{const}} \sim \rho^{5/3}$
- relativistic degeneracy: $P = K_2\rho^{4/3} \;\neq f(T)$ $\quad \Rightarrow P_{T=\text{const}} \sim \rho^{4/3}$

B. Evolution in the $\log P$ - $\log\rho$ diagram

From comparing the evolutionary tracks of stellar cores in the $\log P$ - $\log\rho$ diagram with isothermals (Fig. 4.1), we can draw the following conclusions:

- As long as the gas is ideal, contraction ($\rho\uparrow$) leads to a higher T, because the slope of the evolution track is steeper than that of ideal-gas isotherms: the evolution track crosses isotherms of increasing T.
  Note: this is consistent with what we have concluded from the virial theorem for an ideal gas (§**A**).

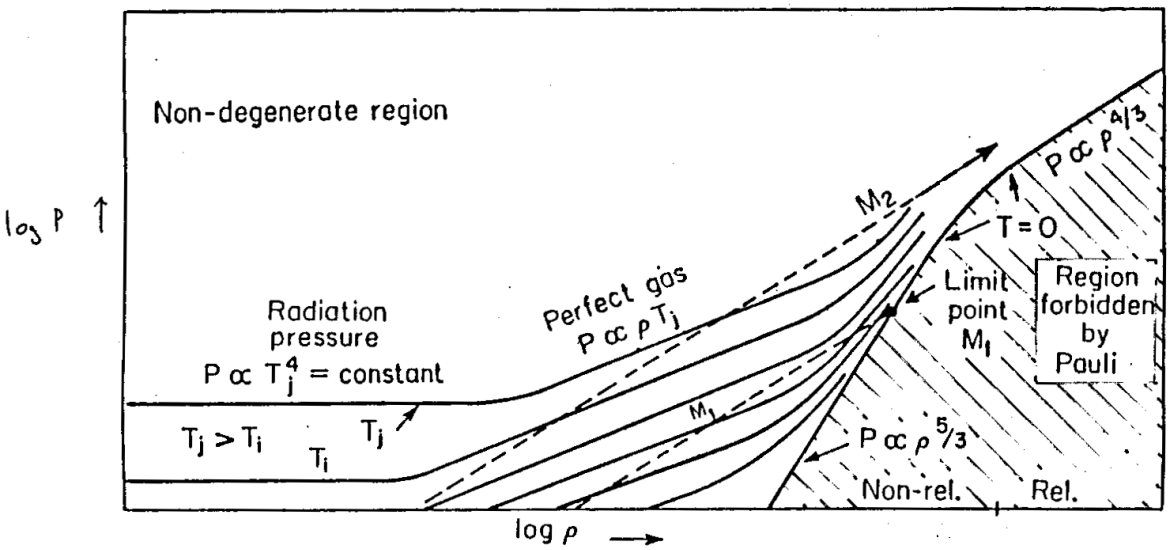

Figure 4.1: Schematic evolutionary tracks of stellar cores in the $\log\rho - \log P$ plane for two different masses, $M_1 < M_2$ (dashed straight lines with slope $\frac{4}{3}$). The solid lines are lines of constant temperature, which have slopes of 0, 1, $\frac{5}{3}$ and $\frac{4}{3}$ for the various equations of state (radiation pressure, ideal gas, non-relativistic and relativistic degeneracy, respectively). The hatched area is forbidden by Pauli's exclusion principle and bounded by the isotherm for $T = 0$.

- There exists a critical mass $M_{\rm Ch}$ such that stars (cores) with $M > M_{\rm Ch}$ can reach arbitrarily high temperatures (within the considered EOS), while stars (cores) with $M < M_{\rm Ch}$ can not.
- For $M < M_{\rm Ch}$:
  1) there is a maximum achievable temperature $T_{\rm max}(M)$
  2) every isothermal curve is reached twice $\Rightarrow T_{\rm final} = 0$
     This endpoint is a state of complete electron degeneracy.
  3) there is a maximum achievable pressure and density such that $P_{\rm max} = P_{\rm final}(M)$ and $\rho_{\rm max}(M) = \rho_{\rm final}(M)$
  4) $T_{\rm max}$, $P_{\rm max}$ and $\rho_{\rm max}$ are larger for larger M
- $M_{\rm Ch}$ is the so called **Chandrasekhar mass**

C. The evolution of stellar cores

- Star formation: gas cloud contracting under its own gravity.
- Ideal gas: contraction $\Rightarrow$ heating, $T \uparrow$ (§**A**)
- Hot gas must radiate $\Rightarrow$ star shines without nuclear fusion $\Rightarrow$ energy loss $L = \dot{E} \simeq -\dot{E}_{\rm grav}$
  $\Rightarrow$ further contraction and heating

  thermal timescale: $\tau \simeq \tau_{\rm KH} = \dfrac{-E_{\rm grav}}{L}$

- At $T = T_{\text{H burning}}$: contraction stops $\Rightarrow L = \dot{E} \simeq \dot{E}_{\text{nuc}}$
  T, ρ remain roughly constant

  nuclear timescale: $\tau \simeq \tau_{\text{nuc}} := \dfrac{E_{\text{nuc}}}{L}$
- When hydrogen is exhausted $\Rightarrow$ contraction of the H-exhausted core
  $L_{\text{core}} = \dot{E}_{\text{core}} \simeq \dot{E}_{\text{grav,core}}$
- Core contraction (on thermal timescale of the core) $\Rightarrow T_{\text{core}} \uparrow$
- At $T_{\text{core}} = T_{\text{He burning}}$: contraction stops $\Rightarrow L_{\text{core}} = \dot{E}_{\text{core}} \simeq \dot{E}_{\text{nuc,core}}$
  T, ρ remain roughly constant

  $\vdots$

$\Rightarrow$ Periods of contraction (on a thermal timescale) and nuclear burning (on a nuclear timescale) alternate each other, see Figure 4.2.

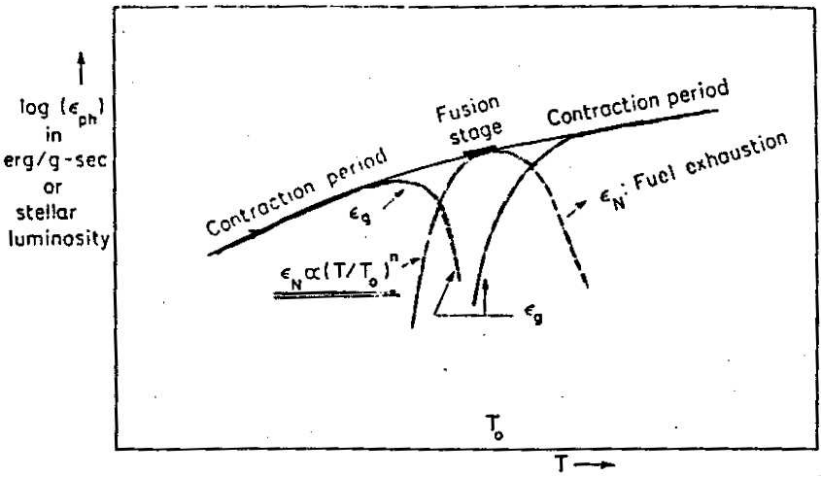

Figure 4.2: Interplay of contractional energy generation and nuclear energy generation in the course of stellar evolution. Because the nuclear energy generation rate is very sensitive to the temperature, $\epsilon_{\text{nuc}} \propto T^{\nu}$ with $\nu \gg 1$ (see Chapter 2), nuclear fusion stages take place at a roughly constant temperature, indicated as T_0.

Consequences of the existence of a **maximum temperature** for $M_{\text{core}} < M_{\text{Ch}}$ (§**B**):

- There is a **minimum (core) mass** M_{min} required for the ignition of each nuclear fuel (H, He, C, etc). Since heavier nuclei burn at higher T (Chapter 2), the minimum mass for each successive fusion stage is larger, see Table 4.1.
- The (cores of) stars with $M_{\text{core}} < M_{\text{Ch}}$ will eventually become **degenerate stars** (white dwarfs), with a composition determined by the last nuclear burning cycle for which $M_{\text{core}} > M_{\text{min}}$.
- Since $M_{\text{Ch}} > M_{\text{min}}$ for all nuclear fuels, the cores of stars with $M_{\text{core}} > M_{\text{Ch}}$ will undergo all nuclear burning cycles until an Fe core has formed, from which no further nuclear energy can be extracted. The Fe core must **collapse** in a cataclysmic event (a supernova or a gamma-ray burst) and become a neutron star or a black hole (§**D**). These explosions have important consequences for nucleosynthesis.

Figure 4.3 shows evolution tracks following from detailed stellar evolution calculations for various masses.

D. Degenerate stars and the Chandrasekhar mass

$$\text{HE} \quad \Rightarrow \quad \frac{dP}{dr} = -\frac{GM_r}{r^2}\rho \quad \rightsquigarrow \quad \frac{\langle P\rangle}{R} \propto \frac{M}{R^2}\frac{M}{R^3} \quad \Rightarrow \quad \langle P\rangle \propto \frac{M^2}{R^4}$$

- Non-relativistic degeneracy: $P \propto \rho^{5/3} \propto \left(\frac{M}{R^3}\right)^{5/3} = \frac{M^{5/3}}{R^5}$

  $$\text{HE} \Rightarrow \quad \frac{M^{5/3}}{R^5} \propto \frac{M^2}{R^4} \quad \Rightarrow \quad \boxed{R \propto M^{1/3}}$$

  This is the **mass-radius relation** for white dwarfs

- Extremely relativistic degeneracy: $P \propto \rho^{4/3} \propto \frac{M^{4/3}}{R^4}$

  $$\text{HE} \Rightarrow \quad \frac{M^{4/3}}{R^4} \propto \frac{M^2}{R^4} \quad \Rightarrow \quad \boxed{M = \text{constant}}$$

  This is the **Chandrasekhar mass** $M_{\rm Ch}$:
  the maximum mass for a star supported by electron degeneracy

Stars (cores) with $M > M_{\rm Ch}$ can **not** become completely degenerate **and** be in hydrostatic equilibrium at the same time $\Rightarrow$ must undergo core collapse $\rightsquigarrow$ supernova

Table 4.1: Characteristics of subsequent gravitational contraction and nuclear burning stages. Column (3) gives the total gravitational energy emitted since the beginning, and column (5) the total nuclear energy emitted since the beginning. Column (6) gives the minimum mass required to ignite a certain burning stage (column 4). The last two columns give the fraction of energy emitted as photons and neutrinos, respectively.

phase	T (10^6 K)	total $E_{\rm grav}$	net reactions	total $E_{\rm nuc}$	$M_{\rm min}$	γ (%)	ν (%)
Grav.	$0 \to 10$	~ 1 keV/n				100	
Nucl.	$10 \to 30$		$4\ ^1\text{H} \to\ ^4\text{He}$	6.7 MeV/n	0.08 $M_\odot$	∼95	∼5
Grav.	$30 \to 100$	~ 10 keV/n				100	
Nucl.	$100 \to 300$		$3\ ^4\text{He} \to\ ^{12}\text{C}$ $4\ ^4\text{He} \to\ ^{16}\text{O}$	≈ 7.4 MeV/n	0.3 $M_\odot$	∼100	∼0
Grav.	$300 \to 800$	~ 100 keV/n				∼50	∼50
Nucl.	$800 \to 1100$		$2\ ^{12}\text{C} \to$ Mg, Ne, Na, Al	≈ 7.7 MeV/n	1.0 $M_\odot$	∼0	∼100
Grav.	$1100 \to 1400$	~ 150 keV/n					∼100
Nucl.	$1400 \to 2000$		$2\ ^{16}\text{O} \to$ S, Si, P	≈ 8.0 MeV/n	1.3 $M_\odot$		∼100
Grav.	$2000 \to 5000$	~ 400 keV/n	$\ldots \to$ Fe	≈ 8.4 MeV/n			∼100

To compute the Chandrasekhar mass ⇒ theory of *polytropes* ⇒

$$\boxed{M_{\rm Ch} = \frac{0.1976}{m_{\rm p}^2}\left(\frac{hc}{G}\right)^{3/2}\mu_{\rm e}^{-2} = \frac{5.836}{\mu_{\rm e}^2}M_\odot}$$

with $\mu_{\rm e} := \left(\sum_i \frac{X_i Z_i}{A_i}\right)^{-1}$

Examples: 1) C/O-mixture: $Z_i/A_i = 2 \;\Rightarrow\; \mu_{\rm e} = 2$
$\Rightarrow\; M_{\rm Ch} = 1.459 M_\odot$

2) ^{56}Fe core: $Z = 26, A = 56 \;\Rightarrow\; \mu_{\rm e} = 2.154$
$\Rightarrow\; M_{\rm Ch} = 1.26 M_\odot$

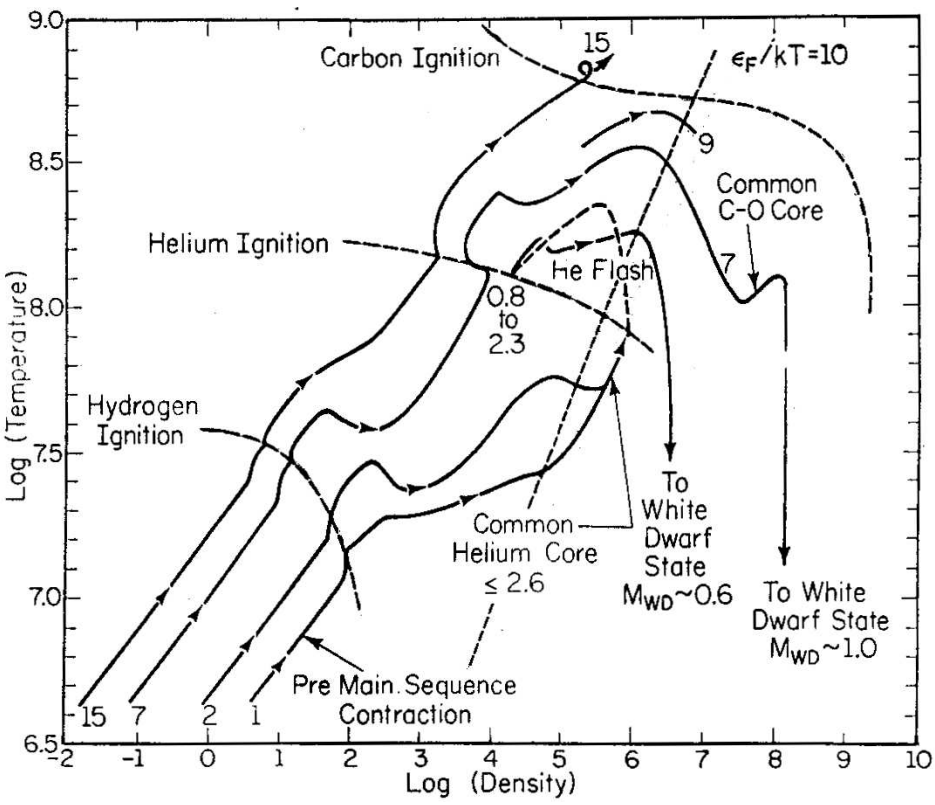

Figure 4.3: Evolution of the cores of stars of different mass in the $\log\rho - \log T$ plane, as it follows from detailed evolution calculations. Stars with core masses below a critical mass (the Chandrasekhar mass) reach a maximum temperature (which is lower for smaller masses) and then cool at a finite density, while stars above the critical mass keep getting hotter. Compare this figure to Fig. 4.1.

Suggestions for further reading

– Chapter 5.1–5.4 of PAGEL.
– To brush up on stellar evolution theory, consult the textbook by Kippenhahn & Weigert (1990), *Stellar Structure and Evolution.*

Exercises

4.1 Compute the thermal time scale of the Sun; assume $\rho = \langle\rho\rangle = M_\odot/V_\odot$, and the equation of state of an ideal gas.

4.2 The internal energy per unit mass is related to the pressure and density of a gas as:

$$\frac{P}{\rho} = \frac{c}{3}\,u \quad \text{where} \quad \begin{array}{l} c = 2 : \text{ideal gas} \\ c = 1 : \text{radiation pressure} \end{array}$$

(a) Use the first law of thermodynamics to show that the adiabatic exponent, $\gamma := (\partial \ln P/\partial \ln \rho)_{\rm ad}$, is equal to:

$$\gamma = 1 + \frac{c}{3}$$

(b) Write the virial theorem in terms of γ. For which values of γ can a star in hydrostatic equilibrium be gravitationally bound (i.e. total energy < 0) ?

4.3 (a) Determine the "borderline" between the areas of radiation pressure and ideal gas pressure being dominant, in the $\log T - \log \rho$ plane.

(b) Derive qualitatively how a slowly contracting star of certain fixed mass evolves in the $\log T - \log \rho$ plane, if the equation of state is that of an ideal gas.

4.2 Hydrogen burning

A. The pp reaction

Net effect of hydrogen burning:

$$4\,{}^1\mathrm{H} \rightarrow {}^4\mathrm{He} + 2\,\mathrm{e}^+ + 2\,\nu \quad (Q = 26.73\,\mathrm{MeV})$$

Puzzle of which reactions are involved first solved by von Weizsäcker in 1937, and Hans Bethe in 1938–'39

- simultaneous interaction of 4 protons is *extremely* unlikely
  $\Rightarrow$ series of 2-body interactions instead
- strong interaction:

  $\mathrm{p} + \mathrm{p} \rightarrow {}^2\mathrm{He}$ does not work, ${}^2\mathrm{He}$ is extremely unstable: ${}^2\mathrm{He} \rightarrow 2\mathrm{p}$ immediately

(for the same reason $\mathrm{p} + {}^4\mathrm{He} \rightarrow {}^5\mathrm{Li}$ is impossible, Fig. 3.3)
$\rightsquigarrow$ no exothermic strong interaction possible in $\mathrm{H} + \mathrm{He}$ gas[1]

- weak interaction (Bethe 1938):

  $\mathrm{p} + \mathrm{p} \rightarrow \mathrm{D} + \mathrm{e}^+ + \nu$ *does* work $(Q = 1.44\,\mathrm{MeV})$

Requires $\mathrm{p} \rightarrow \mathrm{n} + \mathrm{e}^+ + \nu$ (endothermic) to occur *during* a $\mathrm{p} + \mathrm{p}$ scattering.
Cross section of this **pp reaction** is 20 orders of magnitude smaller than for strong interaction $\Rightarrow$ unmeasurable! Only known from theory.

The binding energy of deuterium (2.225 MeV) exceeds the energy required for $\mathrm{p} \rightarrow \mathrm{n} + \mathrm{e}^+ + \nu$ (1.805 MeV), so that the reaction is exothermic, releasing 0.420 MeV. This energy goes into kinetic energy of the positron and the neutrino, in roughly equal parts. The subsequent annihilation of the positron ($\mathrm{e}^+ + \mathrm{e}^- \rightarrow \gamma$, 1.022 MeV) gives a total energy release of $Q =$ 1.442 MeV. The average kinetic energy of the neutrino is $\langle E_\nu \rangle = 0.265$ MeV.

pp-reaction rate:

$$\begin{aligned} r_{\mathrm{pp}} &= \tfrac{1}{2} n_{\mathrm{p}}^2 \langle \sigma v \rangle_{\mathrm{pp}} \\ &\approx 3.09 \times 10^{-37} n_{\mathrm{p}}^2\, T_6^{-2/3} \exp\left(-33.81 T_6^{-1/3}\right) \\ &\quad \times \left(1 + 0.0123 T_6^{1/3} + 0.0109 T_6^{2/3} + 0.00095 T_6\right) \quad \mathrm{cm}^{-3}\mathrm{s}^{-1} \end{aligned} \tag{4.1}$$

B. The ppI chain

Once ${}^2\mathrm{H}$ is produced by the pp reaction $\Rightarrow$
in principle: all possible reactions have to be considered
in practice: many reaction are negligibly slow

[1] Note that strong interactions between ${}^1\mathrm{H}$ and minor isotopes such as ${}^2\mathrm{H}$ are possible, e.g. $\mathrm{D}(\mathrm{p},\gamma)^3\mathrm{He}$ ($Q = 5.49$ Mev), but too little D is present (Chapter 3) $\Rightarrow$ not a major energy source. However this reaction occurs during pre-MS evolution, temporarily slowing contraction.

E.g. $\mathrm{D} + \mathrm{D} \to {}^4\mathrm{He} + \gamma$ is *unimportant*:

a) cross section is too small

b) D-abundance is too small (see below)

For similar reasons: ${}^3\mathrm{He}(\mathrm{D},\mathrm{p}){}^4\mathrm{He}$ and ${}^3\mathrm{He}(\mathrm{p},\mathrm{e}^+\nu){}^4\mathrm{He}$ are unimportant.

Table 4.2: Reactions in the ppI chain.

reaction:	rate:	Q (MeV)	$\langle E_\nu \rangle$ (MeV)
$\mathrm{H} + \mathrm{H} \to \mathrm{D} + \mathrm{e}^+ + \nu$	$r_{\mathrm{pp}} = \frac{1}{2}\mathrm{H}^2 \langle\sigma v\rangle_{\mathrm{pp}}$	1.442	0.265
$\mathrm{D} + \mathrm{H} \to {}^3\mathrm{He} + \gamma$	$r_{\mathrm{pD}} = \mathrm{H}\,\mathrm{D} \langle\sigma v\rangle_{\mathrm{pD}}$	5.493	
${}^3\mathrm{He} + {}^3\mathrm{He} \to {}^4\mathrm{He} + 2\,\mathrm{H}$	$r_{33} = \frac{1}{2}({}^3\mathrm{He})^2 \langle\sigma v\rangle_{33}$	12.860	

The reactions that follow in the so-called ppI chain are given in Table 4.2. With the reaction rates in Table 4.2, we can write down the following four differential equations that govern the abundances (number densities) of nuclei involved in the ppI chain. Notation e.g. $\mathrm{H} := n_{\mathrm{p}}$, $\mathrm{D} := n_{\mathrm{D}}$, etc:

$$\frac{d\mathrm{H}}{dt} = -\mathrm{H}^2 \langle\sigma v\rangle_{\mathrm{pp}} - \mathrm{H}\,\mathrm{D} \langle\sigma v\rangle_{\mathrm{pD}} + ({}^3\mathrm{He})^2 \langle\sigma v\rangle_{33} \tag{4.2}$$

$$\frac{d\mathrm{D}}{dt} = \frac{\mathrm{H}^2}{2} \langle\sigma v\rangle_{\mathrm{pp}} - \mathrm{H}\,\mathrm{D} \langle\sigma v\rangle_{\mathrm{pD}} \tag{4.3}$$

$$\frac{d\,{}^3\mathrm{He}}{dt} = \mathrm{H}\,\mathrm{D} \langle\sigma v\rangle_{\mathrm{pD}} - ({}^3\mathrm{He})^2 \langle\sigma v\rangle_{33} \tag{4.4}$$

$$\frac{d\,{}^4\mathrm{He}}{dt} = \frac{({}^3\mathrm{He})^2}{2} \langle\sigma v\rangle_{33} \tag{4.5}$$

The D-abundance

Consider the differential equation (4.3) for D $\Rightarrow$ it is **self-regulating**

- if D-abundance is small $\Rightarrow$ first term $<$ second term $\Rightarrow d\mathrm{D}/dt > 0$
  $\Rightarrow$ D-abundance grows
- if D-abundance is large $\Rightarrow$ first term $>$ second term $\Rightarrow d\mathrm{D}/dt < 0$
  $\Rightarrow$ D-abundance decreases

Hence the D-abundance tends to an *equilibrium abundance* such that $\dfrac{d\mathrm{D}}{dt} = 0 \Rightarrow$

$$\left(\frac{\mathrm{D}}{\mathrm{H}}\right)_{\mathrm{e}} = \frac{\langle\sigma v\rangle_{\mathrm{pp}}}{2\langle\sigma v\rangle_{\mathrm{pD}}} \approx 3 \times 10^{-18} \quad (T \sim 10^7\mathrm{K}) \tag{4.6}$$

$\rightsquigarrow$ extremely small, $\ll$ initial $\mathrm{D/H} \sim (2 \ldots 3) \times 10^{-5}$ of interstellar gas from which stars form

Definition: **lifetime** of species X against reacting with particle a:

$$\tau_a(X) := \left| \frac{n(X)}{[dn(X)/dt]_a} \right| \tag{4.7}$$

E.g. the lifetimes of H and D against proton capture are, at $T_6 \approx 15$:

$$\tau_{\rm p}({\rm H}) \;=\; \frac{n_{\rm p}}{(dn_{\rm p}/dt)_{\rm p}} \;=\; \frac{n_{\rm p}}{n_{\rm p}^2\,\langle\sigma v\rangle_{\rm pp}} \;=\; \frac{1}{n_{\rm p}\,\langle\sigma v\rangle_{\rm pp}} \;\approx\; 10^{10}\ {\rm yr}$$

$$\tau_{\rm p}({\rm D}) \;=\; \frac{n_{\rm D}}{(dn_{\rm D}/dt)_{\rm p}} \;=\; \frac{n_{\rm D}}{n_{\rm p}\,n_{\rm D}\,\langle\sigma v\rangle_{\rm pD}} \;=\; \frac{1}{n_{\rm p}\,\langle\sigma v\rangle_{\rm pD}} \;\approx\; 1.6\ {\rm sec}$$

Note: the factor $\frac{1}{2}$ from the pp-reaction rate disappears because each reaction destroys two protons. It follows that

$$\frac{\tau_{\rm p}({\rm D})}{\tau_{\rm p}({\rm H})} \;=\; \frac{\langle\sigma v\rangle_{\rm pp}}{\langle\sigma v\rangle_{\rm pD}} \quad\Rightarrow\quad \left(\frac{\rm D}{\rm H}\right)_{\rm e} \;=\; \frac{\tau_{\rm p}({\rm D})}{2\,\tau_{\rm p}({\rm H})}$$

Because $\tau_{\rm p}({\rm H}) \gg \tau_{\rm p}({\rm D})$, the H abundance remains essentially constant while the D abundance changes. Then one can show that D exponentially approaches its equilibrium abundance on a timescale $\tau_{\rm p}({\rm D})$, whatever its starting abundance.

In other words: deuterium reaches equilibrium *within seconds*.

The ^{3}He abundance

We can assume that ${\rm D/H} = ({\rm D/H})_{\rm e} \Rightarrow$ can eliminate differential equation (4.3) for D in ppI-chain $\Rightarrow$ equations for H and ^{3}He become

$$\frac{d{\rm H}}{dt} \;=\; -\frac{3}{2}{\rm H}^2\,\langle\sigma v\rangle_{\rm pp} + ({}^3{\rm He})^2\,\langle\sigma v\rangle_{33} \tag{4.8}$$

$$\frac{d\,{}^3{\rm He}}{dt} \;=\; \frac{\rm H^2}{2}\,\langle\sigma v\rangle_{\rm pp} - ({}^3{\rm He})^2\,\langle\sigma v\rangle_{33} \tag{4.9}$$

New equation for ^{3}He: *also* self-regulating $\Rightarrow$ equilibrium abundance

$$\left(\frac{{}^3{\rm He}}{\rm H}\right)_{\rm e} \;=\; \left(\frac{\langle\sigma v\rangle_{\rm pp}}{2\langle\sigma v\rangle_{33}}\right)^{\frac{1}{2}} \;\approx\; 10^{-5} \quad (T \approx 1.5\times10^7{\rm K})$$

but depending rather strongly on temperature, see Fig. 4.4.

Note: lifetime of ^{3}He against itself $\tau_3({}^3{\rm He}) \approx 10^5$ yr in the centre of the Sun ($T_6 = 15$), and increasing rapidly for lower T: for $T_6 \lesssim 8$, $\tau_3({}^3{\rm He}) \gtrsim 10^9$ yr
$\Rightarrow$ equilibrium is reached in the center of the Sun
$\Rightarrow$ equilibrium is *not* reached outside central parts of the Sun

If ^{3}He reaches equilibrium $\Rightarrow$ eq. (4.9) can also be eliminated ($2r_{33} = r_{\rm pp}$) $\Rightarrow$ equations for H and ^{4}He become very simple:

$$\frac{d{\rm H}}{dt} \;=\; -\,{\rm H}^2\,\langle\sigma v\rangle_{\rm pp} \;=\; -2r_{\rm pp} \tag{4.10}$$

$$\frac{d{}^4{\rm He}}{dt} \;=\; \frac{\rm H^2}{4}\,\langle\sigma v\rangle_{\rm pp} \;=\; \tfrac{1}{2}r_{\rm pp} \tag{4.11}$$

The rate of H-burning is then set completely by the pp reaction, the slowest in the chain. Equation (4.11) reflects that for each ^{4}He nucleus made by the ppI chain, *two* pp reactions are required.

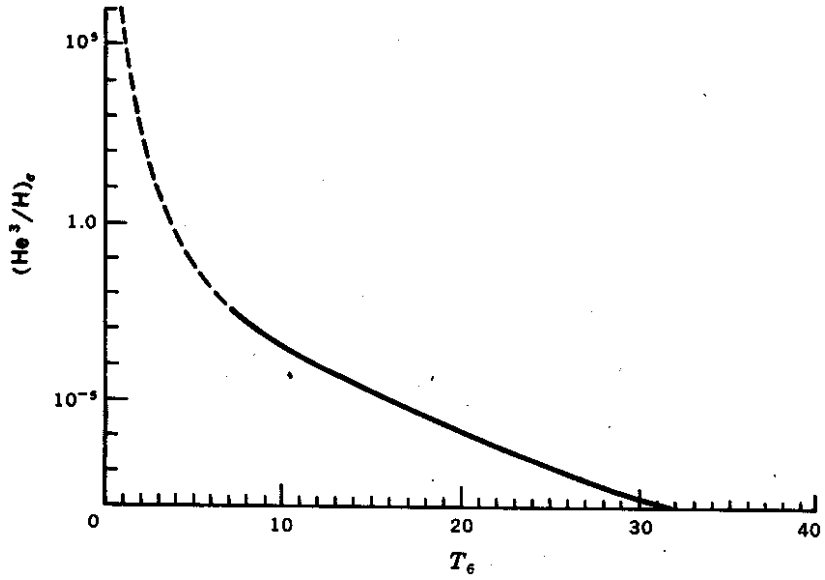

Figure 4.4: The equilibrium ratio of ^{3}He to H during hydrogen burning. The curce is dashed for $T_6 < 8$ becuase the time required for ^{3}He to reach equilibrium is longer than the H-burning lifetime at such low temperature. Figure from CLAYTON.

Effective energy release of the ppI chain: $Q_{\rm eff} = Q - 2\langle E_\nu \rangle = 26.21$ MeV per ^{4}He
$\Rightarrow$ effective energy generation rate in erg g^{-1} s^{-1}:

$$\epsilon_{\rm ppI} = \frac{Q_{\rm eff}}{\rho} \frac{d^4{\rm He}}{dt} = Q_{\rm eff} \frac{r_{\rm pp}}{2\,\rho} \tag{4.12}$$

Note: the above is only valid for ^{3}He equilibrium.

ppI summary:

- D is *destroyed* (in fact already on the pre-main sequence)
- ^{3}He is destroyed in the center, enriched above the core of the Sun
- the pp-reaction is the slowest, and (when ^{3}He is in equilibrium) sets the pace of the overall rate of the ppI chain

C. The ppII and ppIII chains

The ppI chain can operate in a *pure hydrogen gas.*
If ^{4}He is abundant, and the temperature is not too low, the reaction

$$^3{\rm He} + {}^4{\rm He} \rightarrow {}^7{\rm Be} + \gamma \tag{4.13}$$

competes with the ^{3}He + ^{3}He reaction. Because of a stronger T sensitivity (larger reduced mass of the reacting nuclei), the ^{3}He + ^{4}He reaction starts to dominate at high temperature.

This initiates 2 new branches to complete $4\,{\rm p} \rightarrow {}^4$He reaction chain, Fig. 4.5

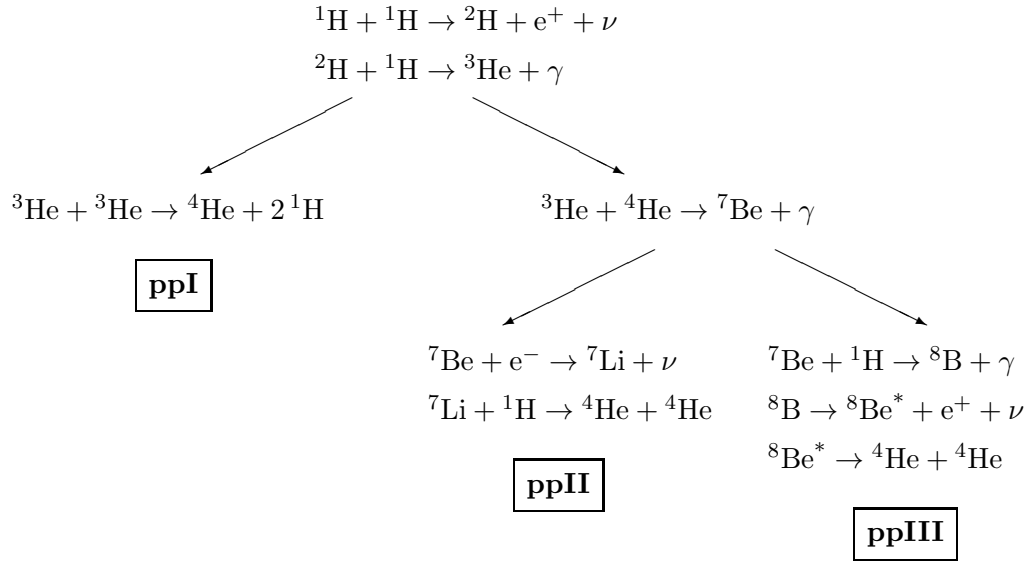

Figure 4.5: Reaction flows in the proton capture chains

Lifetimes of the radioactive species: $\tau(^7\mathrm{Be}) \simeq 0.3$ yr
$\tau(^8\mathrm{B}) \simeq 1$ s
$\tau(^8\mathrm{Be}) \simeq 10^{-22}$ s

Note on the $^7\mathrm{Be}(\mathrm{e}^-, \nu)^7\mathrm{Li}$ reaction:

- This is an *electron capture* reaction, governed by the weak interaction
- on earth: ^{7}Be nucleus captures one of its bound electrons (most likely from the K-shell) with $\tau_{1/2} = 53.3$ d $\Rightarrow \tau_\mathrm{e}(^7\mathrm{Be}) = 76.9$ d (lifetime defined as in eq. 4.7)
- in stars: ^{7}Be is completely ionized $\Rightarrow$ lifetime can be longer
  $\tau_\mathrm{e}(^7\mathrm{Be})$ depends on stellar conditions, i.e. on electron density n_e and temperature
  e-capture rate $r_{\mathrm{e}7} := n(^7\mathrm{Be}) n_\mathrm{e} \lambda_{\mathrm{e}7}$ with $\lambda_{\mathrm{e}7} \propto T^{-1/2}$ ($\Rightarrow$ decreasing with T !)
  $\Rightarrow \tau_\mathrm{e}(^7\mathrm{Be}) \simeq 7.06 \times 10^8 \dfrac{T_6^{1/2}}{\rho(1+X)}$ (X = H mass fraction)
  $\rightsquigarrow$ solar center: $\tau_\mathrm{e}(^7\mathrm{Be}) = 140$ d (^{7}Be lifetime against capture of continuum electrons)
  $\rightsquigarrow$ a small K-shell contribution is still present in the Sun
  $\rightsquigarrow \tau(^7\mathrm{Be}) \simeq 120$ d
- $^7\mathrm{Be}(\mathrm{e}^-, \nu)^7\mathrm{Li}$ has a Q-value of 0.862 MeV, emitted as one 0.862 MeV neutrino (89.6% of the time), or one 0.384 MeV neutrino and one 0.478 MeV photon (10.4%)
- enhanced lifetime of ^{7}Be makes $^7\mathrm{Be}(\mathrm{p}, \gamma)$ more likely at higher T

Comparing ppI, ppII and ppIII

- ppII, III start with $^3\mathrm{He}(\alpha, \gamma)^7\mathrm{Be}$, but the α-particle is used only as a catalyst: it is liberated in the end, by $^7\mathrm{Li}(\mathrm{p}, \alpha)^4\mathrm{He}$ or by $^8\mathrm{B}(\alpha)^4\mathrm{He}$
- ppII, III need the (slow) pp-reaction only *once* to produce one ^{4}He nucleus, whereas ppI needs *two* pp-reactions per ^{4}He nucleus $\Rightarrow$ at high temperature: ppII, III may dominate

Table 4.3: Reactions of the pp chains. Cross section factors are taken from Bahcall (1989), except for the pp and ^{3}He-^{3}He reactions which are from Angulo et al. (1999). The last column gives the order of magnitude of the lifetime of the reacting nuclei in the center of the Sun.

reaction	Q (MeV)	$\langle E_\nu \rangle$ (MeV)	$S(0)$ (keV barn)	dS/dE (barn)	τ (yr)
$^1\mathrm{H}(\mathrm{p},\mathrm{e}^+\nu)^2\mathrm{H}$	1.442	0.265	3.94×10^{-22}	4.61×10^{-24}	10^{10}
$^2\mathrm{H}(\mathrm{p},\gamma)^3\mathrm{He}$	5.493		2.5×10^{-4}	7.9×10^{-6}	10^{-8}
$^3\mathrm{He}(^3\mathrm{He},2\mathrm{p})^4\mathrm{He}$	12.860		5.18×10^{3}	-1.1×10^{1}	10^{5}
$^3\mathrm{He}(\alpha,\gamma)^7\mathrm{Be}$	1.587		5.4×10^{-1}	-3.1×10^{-4}	10^{6}
$^7\mathrm{Be}(\mathrm{e}^-,\nu)^7\mathrm{Li}$	0.862	0.814			10^{-1}
$^7\mathrm{Li}(\mathrm{p},\alpha)^4\mathrm{He}$	17.347		5.2×10^{1}	0	10^{-5}
$^7\mathrm{Be}(\mathrm{p},\gamma)^8\mathrm{B}$	0.137		2.4×10^{-2}	-3×10^{-5}	10^{2}
$^8\mathrm{B}(\mathrm{e}^+\nu)^8\mathrm{Be}^*(\alpha)^4\mathrm{He}$	18.071	6.710			10^{-8}

- branching ratios (see Fig. 4.7):

$$\frac{f_{\mathrm{ppI}}}{f_{\mathrm{ppII}} + f_{\mathrm{ppIII}}} = \frac{r_{33}}{r_{34}} = \frac{\langle \sigma v \rangle_{33}}{2\langle \sigma v \rangle_{34}} \frac{^3\mathrm{He}}{^4\mathrm{He}}. \tag{4.14}$$

  $\Rightarrow$ ppI dominates over ppII, III for small ^{4}He and/or large ^{3}He abundance
  $\Rightarrow$ ppI also dominates at low T, because $\langle \sigma v \rangle_{34}$ increases more steeply with T than $\langle \sigma v \rangle_{33}$

$$\frac{f_{\mathrm{ppII}}}{f_{\mathrm{ppIII}}} = \frac{r_{\mathrm{e}7}}{r_{\mathrm{p}7}} = \frac{\lambda_{\mathrm{e}7}}{\langle \sigma v \rangle_{\mathrm{p}7}} \frac{n_{\mathrm{e}}}{n_{\mathrm{p}}} = \frac{\lambda_{\mathrm{e}7}}{\langle \sigma v \rangle_{\mathrm{p}7}} \frac{1+X}{2X} \tag{4.15}$$

  (note: $n_{\mathrm{p}} = n(\mathrm{H}) = X\rho/m_{\mathrm{H}}$, $n_{\mathrm{e}} = \rho/\mu_{\mathrm{e}} m_{\mathrm{H}}$ and $1/\mu_{\mathrm{e}} = \frac{1}{2}(1+X)$)

  $\Rightarrow$ ppII dominates over ppIII when hydrogen gets depleted
  $\Rightarrow$ ppIII dominates over ppII at high T, because $\lambda_{\mathrm{e}7}$ decreases with T while $\langle \sigma v \rangle_{\mathrm{p}7}$ increases with T

Differential equations

In practice: D, ^{8}B, ^{7}Li and ^{7}Be have very short lifetimes (see Table 4.3) $\Rightarrow$ they can be assumed to be always in equilibrium $\Rightarrow$ only H, ^{3}He and ^{4}He are important:

$$\frac{d\mathrm{H}}{dt} = -\frac{3}{2}\mathrm{H}^2 \langle \sigma v \rangle_{\mathrm{pp}} + (^3\mathrm{He})^2 \langle \sigma v \rangle_{33} - {}^3\mathrm{He}\,{}^4\mathrm{He} \langle \sigma v \rangle_{34} \tag{4.16}$$

$$\frac{d\,^3\mathrm{He}}{dt} = \frac{\mathrm{H}^2}{2} \langle \sigma v \rangle_{\mathrm{pp}} - (^3\mathrm{He})^2 \langle \sigma v \rangle_{33} - {}^3\mathrm{He}\,{}^4\mathrm{He} \langle \sigma v \rangle_{34} \tag{4.17}$$

$$\frac{d\,^4\mathrm{He}}{dt} = \frac{(^3\mathrm{He})^2}{2} \langle \sigma v \rangle_{33} + {}^3\mathrm{He}\,{}^4\mathrm{He} \langle \sigma v \rangle_{34} \tag{4.18}$$

^{3}He $\Rightarrow$ self-regulating as for ppI, but equilibrium ^{3}He abundance now depends on ^{4}He/H as well as T (cf. Clayton, p. 380ff)

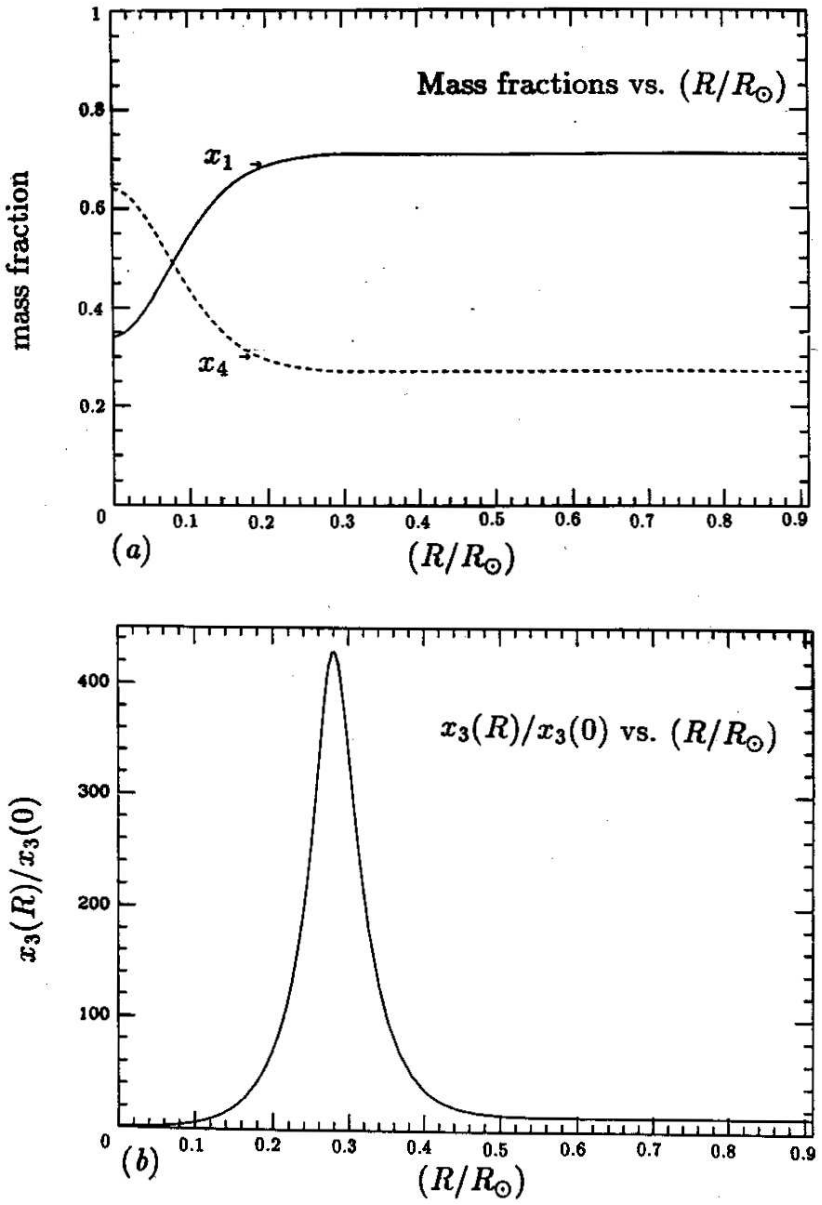

Figure 4.6: Composition profiles in a typical solar model. (a) Mass fractions of ^{1}H (X_1) and of ^{4}He (X_4) as a function of radius. (b) Mass fraction of ^{3}He (X_3) relative to its central value $X_3(0)$, as a function of radius. Figure from Bahcall (1989).

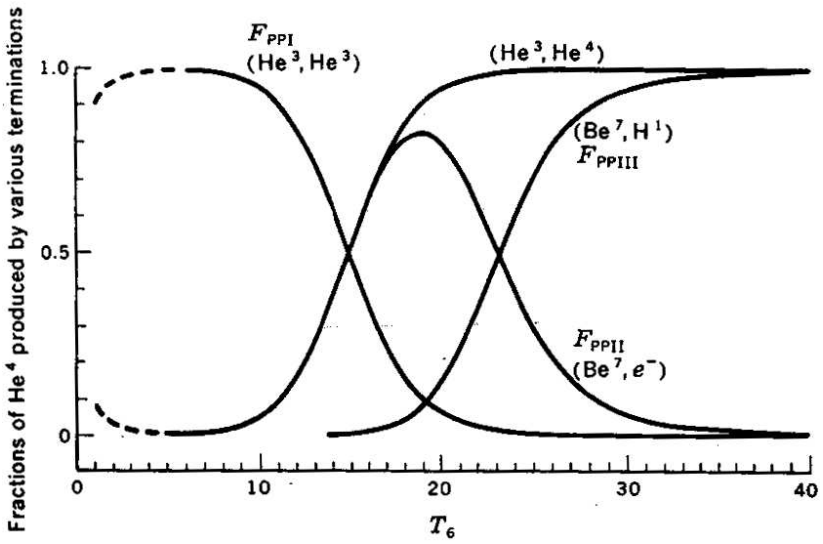

Figure 4.7: Fraction of ^{4}He produced by the ppI, ppII and ppIII chains, as a function of temperatute. The chains are assumed to be in equilibrium, and it was assumed that $Y = X$. Figure from CLAYTON.

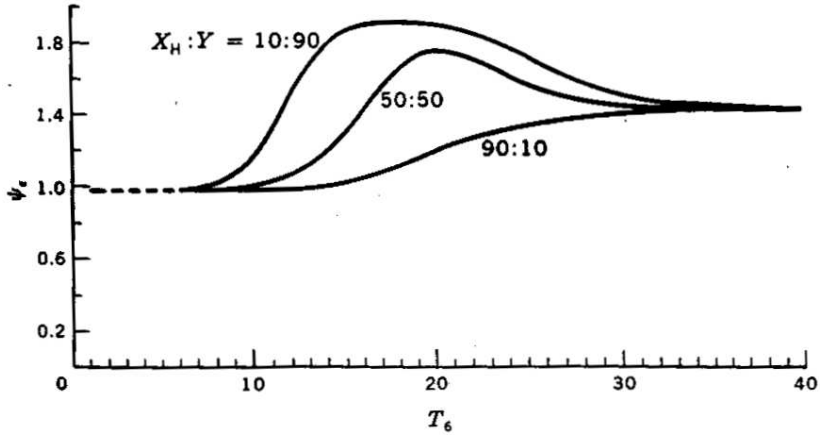

Figure 4.8: The function ψ, which measures the rate of thermal energy release relative to the rate of the pp reaction, as a function of temperature for three different choices of composition. Figure from CLAYTON .

If ^{3}He is in equilibrium, the equation for ^{4}He reduces to

$$\frac{d\,^4\mathrm{He}}{dt} \;=\; \frac{\mathrm{H}^2}{4}\,\langle\sigma v\rangle_{\mathrm{pp}} + \frac{^3\mathrm{He}\,^4\mathrm{He}}{2}\,\langle\sigma v\rangle_{34} \;\equiv\; \tfrac{1}{2} r_{\mathrm{pp}}\,\Phi(\alpha) \tag{4.19}$$

The function $\Phi(\alpha)$ depends on temperature and on the ^{4}He/H ratio
- for small α (low T and/or small ^{4}He/H) $\Rightarrow$ ppI dominates, $\Phi \approx 1$ (cf. eq. 4.11).
- for large α (high T and/or large ^{4}He/H) $\Rightarrow$ ppII or ppIII dominate, $\Phi \approx 2$
  $\Rightarrow$ eq. (4.19) gives $d\,^4\mathrm{He}/dt = r_{\mathrm{pp}}$ ($\Rightarrow$ *one* pp reaction required per ^{4}He)

The **energy** generated by ppI, ppII and ppIII is always the same ($Q = 26.73\,\mathrm{MeV}$ per net $4\,\mathrm{p} \rightarrow {}^4\mathrm{He}$ reaction). However, the ν-losses are different (see Table 4.3, Fig. 4.9):

For ppI, two pp neutrinos are released (§**B**). For ppII the second neutrino comes from ^{7}Be ($\Rightarrow Q_{\mathrm{eff}} = 25.67\,\mathrm{MeV}$), and for ppIII the energetic second neutrino comes from ^{8}B decay ($\Rightarrow Q_{\mathrm{eff}} = 19.70\,\mathrm{MeV}$). When ^{3}He is in equilibrium the energy generation rate is (Fig. 4.8):

$$\begin{aligned}\epsilon_{\mathrm{pp}} \;&=\; \frac{r_{\mathrm{pp}}}{2\rho}\cdot(4m_{\mathrm{p}} - m_\alpha)c^2\cdot\Phi(\alpha)\,(0.981 f_{\mathrm{ppI}} + 0.961 f_{\mathrm{ppII}} + 0.739 f_{\mathrm{ppIII}}) \\ &\equiv\; \frac{r_{\mathrm{pp}}}{2\rho}\cdot(4m_{\mathrm{p}} - m_\alpha)c^2\cdot\psi\end{aligned} \tag{4.20}$$

Nucleosynthesis: except for ^{4}He, the only nucleus which can be *produced* in significant amounts by the pp-chains is ^{3}He.

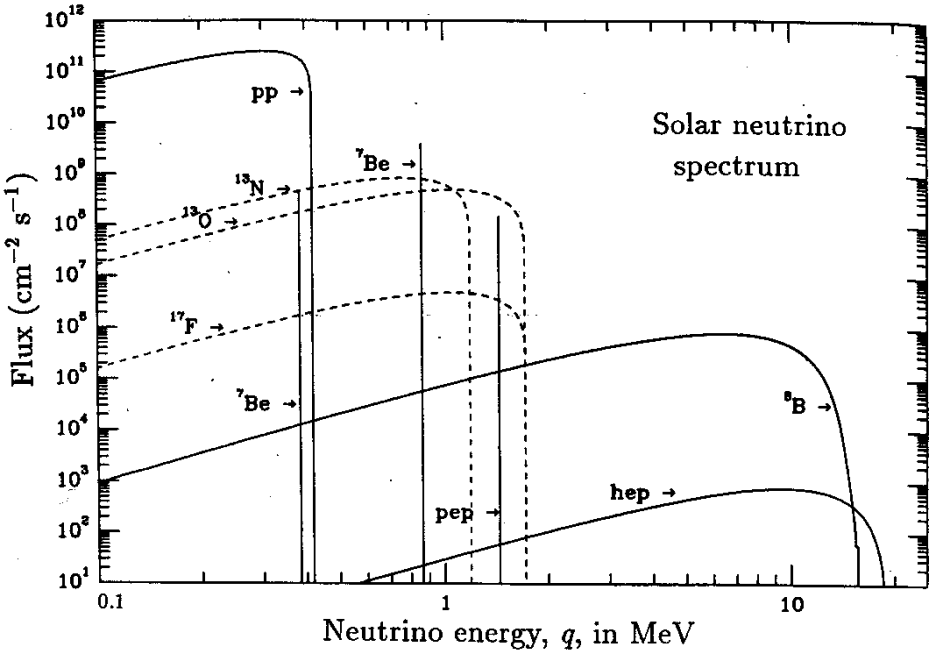

Figure 4.9: Energy spectrum of neutrinos, according to a solar model. Solid lines are for neutrinos from the pp chain, and dashed lines for the CNO cycle. Figure from Bahcall (1989).

D. The CNO-cycle

The pp chains can operate in a gas consisting only of H and He.
If *heavier elements* are present, e.g. in solar abundances, and for relatively high T and low ρ (i.e. in relatively massive stars):

$^{12}\mathrm{C}(\mathrm{p},\gamma)^{13}\mathrm{N}$ may compete, and win over $\mathrm{p}+\mathrm{p}$

suggested by Bethe and von Weizsäcker in 1938 $\Rightarrow$

The CN cycle

$$^{12}\mathrm{C}\,(\mathrm{p},\gamma)\,^{13}\mathrm{N}\,(\mathrm{e}^{+}\nu)\,^{13}\mathrm{C}\,(\mathrm{p},\gamma)\,^{14}\mathrm{N}\,(\mathrm{p},\gamma)^{15}\mathrm{O}\,(\mathrm{e}^{+}\nu)^{15}\mathrm{N}\,(p,\alpha)\,^{12}\mathrm{C}$$

This is a cyclic process, with the CNO-nuclei acting only as catalysts
Net effect, like the pp chains: $4\,\mathrm{H}\rightarrow{}^{4}\mathrm{He}+2\mathrm{e}^{+}+2\nu+\gamma$ ($Q=26.73\,\mathrm{MeV}$)

- two β-decays + ν-production:
  $^{13}\mathrm{N}(\mathrm{e}^{+}\nu):\ \tau\simeq 10$ min, $E_\nu\simeq 0.71$ MeV
  $^{15}\mathrm{O}(\mathrm{e}^{+}\nu):\ \tau\simeq 2$ min, $E_\nu\simeq 1.00$ MeV

- assume: $\tau_\beta(^{13}\mathrm{N})=\tau_\beta(^{15}\mathrm{O})=0\Rightarrow$ effectively $\quad ^{12}\mathrm{C}(\mathrm{p},\gamma\mathrm{e}^{+}\nu)^{13}\mathrm{C}$
  $^{14}\mathrm{N}(\mathrm{p},\gamma\mathrm{e}^{+}\nu)^{15}\mathrm{N}$

Differential equations for the CN cycle:

$$\frac{d\,^{12}\mathrm{C}}{dt} = \mathrm{H}\left(^{15}\mathrm{N}\,\langle\sigma v\rangle_{15}-{}^{12}\mathrm{C}\,\langle\sigma v\rangle_{12}\right) \tag{4.21}$$

$$\frac{d\,^{13}\mathrm{C}}{dt} = \mathrm{H}\left(^{12}\mathrm{C}\,\langle\sigma v\rangle_{12}-{}^{13}\mathrm{C}\,\langle\sigma v\rangle_{13}\right) \tag{4.22}$$

$$\frac{d\,^{14}\mathrm{N}}{dt} = \mathrm{H}\left(^{13}\mathrm{C}\,\langle\sigma v\rangle_{13}-{}^{14}\mathrm{N}\,\langle\sigma v\rangle_{14}\right) \tag{4.23}$$

$$\frac{d\,^{15}\mathrm{N}}{dt} = \mathrm{H}\left(^{14}\mathrm{N}\,\langle\sigma v\rangle_{14}-{}^{15}\mathrm{N}\,\langle\sigma v\rangle_{15}\right) \tag{4.24}$$

$$\frac{d\mathrm{H}}{dt} = -\mathrm{H}\left(^{12}\mathrm{C}\,\langle\sigma v\rangle_{12}+{}^{13}\mathrm{C}\,\langle\sigma v\rangle_{13}+{}^{14}\mathrm{N}\,\langle\sigma v\rangle_{14}+{}^{15}\mathrm{N}\,\langle\sigma v\rangle_{15}\right) \tag{4.25}$$

$$\frac{d\,^{4}\mathrm{He}}{dt} = \mathrm{H}\,^{15}\mathrm{N}\,\langle\sigma v\rangle_{15} \tag{4.26}$$

Consequences:

- total mass (nucleon number) is conserved
- also: total number of CNO-nuclei is conserved
- $d\mathrm{H}/dt<0$ and $d\,^{4}\mathrm{He}/dt>0$ always
- equations for CN nuclei are self-regulating $\Rightarrow$ $^{12}\mathrm{C}$, $^{13}\mathrm{C}$, $^{14}\mathrm{N}$ and $^{15}\mathrm{N}$ will seek equilibrium abundance

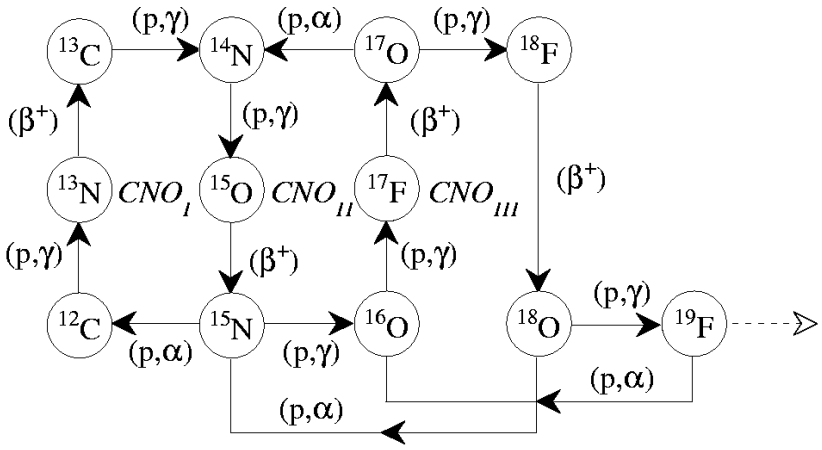

Figure 4.10: Reaction flows in the CNO cycles. $\mathrm{CNO_I}$ corresponds to the CN cycle, the main energy-producing cycle. $\mathrm{CNO_I}$ + $\mathrm{CNO_{II}}$ together form the CNO bi-cycle. $\mathrm{CNO_{III}}$ and $\mathrm{CNO_{IV}}$ are much slower than the bi-cycle, but when activated do affect the abundances of the nuclei involved, i.e. they tend to destroy ^{18}O and ^{19}F.

Lifetimes of CN-nuclei against p-capture

$$\tau_{\mathrm{p}}(^{12}\mathrm{C}) = \frac{n(^{12}\mathrm{C})}{(dn(^{12}\mathrm{C})/dt)_{\mathrm{p}}} = \frac{n(^{12}\mathrm{C})}{n_{\mathrm{p}} n(^{12}\mathrm{C}) \langle \sigma v \rangle_{12}} = \frac{1}{n_{\mathrm{p}} \langle \sigma v \rangle_{12}}$$

with $\langle \sigma v \rangle_{12}$ = Maxwellian-averaged cross section of $^{12}\mathrm{C}(\mathrm{p},\gamma)^{13}\mathrm{N}$
Similarly:

$$\tau_{\mathrm{p}}(^{13}\mathrm{C}) = \frac{1}{n_{\mathrm{p}} \langle \sigma v \rangle_{13}}, \qquad \tau_{\mathrm{p}}(^{14}\mathrm{N}) = \frac{1}{n_{\mathrm{p}} \langle \sigma v \rangle_{14}}, \qquad \tau_{\mathrm{p}}(^{15}\mathrm{N}) = \frac{1}{n_{\mathrm{p}} \langle \sigma v \rangle_{15}}$$

At $T \simeq 2 \cdot 10^7$ K (see Table 4.4):

$$\tau_{\mathrm{p}}(^{15}\mathrm{N}) \ll \tau_{\mathrm{p}}(^{13}\mathrm{C}) < \tau_{\mathrm{p}}(^{12}\mathrm{C}) \ll \tau_{\mathrm{p}}(^{14}\mathrm{N}) \ll \tau_{\mathrm{star}}!$$

i.e. $\quad 35 \text{ yr} \ll 1600 \text{ yr} < 6600 \text{ yr} \ll 9 \times 10^5 \text{ yr}$

$\Rightarrow$ 1) **Equilibrium** will be achieved in the stellar centre, as all lifetimes are smaller than the stellar lifetime

i.e. $\dfrac{d}{dt}{}^{12}\mathrm{C} = \dfrac{d}{dt}{}^{13}\mathrm{C} = \dfrac{d}{dt}{}^{14}\mathrm{N} = \dfrac{d}{dt}{}^{15}\mathrm{N} = 0$

2) The equilibrium abundance ratios are given by the cross section ratios of neighbouring reactions.
E.g. $\quad d(^{13}\mathrm{C})/dt = 0 \;\Leftrightarrow\; \mathrm{H}\,{}^{13}\mathrm{C}\,\langle \sigma v \rangle_{13} = \mathrm{H}\,{}^{12}\mathrm{C}\,\langle \sigma v \rangle_{12} \;\Leftrightarrow$

$$\boxed{\left(\frac{^{12}\mathrm{C}}{^{13}\mathrm{C}}\right)_{\mathrm{e}} = \frac{\langle \sigma v \rangle_{13}}{\langle \sigma v \rangle_{12}} = \frac{\tau_{\mathrm{p}}(^{12}\mathrm{C})}{\tau_{\mathrm{p}}(^{13}\mathrm{C})}} \quad \text{etc.}$$

Table 4.4: Reactions of the CNO bi-cycle. Cross section factors are taken from Bahcall (1989). The last column gives the lifetime of the CNO nuclei for $T_6 = 20$.

reaction	Q (MeV)	$\langle E_\nu \rangle$ (MeV)	$S(0)$ (MeV barn)	dS/dE (barn)	τ (yr)
$^{12}\mathrm{C}(\mathrm{p},\gamma)^{13}\mathrm{N}$	1.944		1.45×10^{-3}	2.45×10^{-3}	6.6×10^3
$^{13}\mathrm{N}(\mathrm{e}^+\nu)^{13}\mathrm{C}$	2.220	0.707			863 s
$^{13}\mathrm{C}(\mathrm{p},\gamma)^{14}\mathrm{N}$	7.551		5.50×10^{-3}	1.34×10^{-2}	1.6×10^3
$^{14}\mathrm{N}(\mathrm{p},\gamma)^{15}\mathrm{O}$	7.297		3.32×10^{-3}	-5.91×10^{-3}	9.3×10^5
$^{15}\mathrm{O}(\mathrm{e}^+\nu)^{15}\mathrm{N}$	2.754	0.997			176 s
$^{15}\mathrm{N}(\mathrm{p},\alpha)^{12}\mathrm{C}$	4.965		7.80×10^1	3.51×10^2	3.5×10^1
$^{15}\mathrm{N}(\mathrm{p},\gamma)^{16}\mathrm{O}$	12.127		6.4×10^{-2}	3×10^{-2}	3.9×10^4
$^{16}\mathrm{O}(\mathrm{p},\gamma)^{17}\mathrm{F}$	0.600		9.4×10^{-3}	-2.3×10^{-2}	7.1×10^7
$^{17}\mathrm{F}(\mathrm{e}^+\nu)^{17}\mathrm{O}$	2.761	0.999			93 s
$^{17}\mathrm{O}(\mathrm{p},\alpha)^{14}\mathrm{N}$	1.192		resonant reaction		1.9×10^7

CN nucleosynthesis

Lifetimes: $^{15}\mathrm{N} : {}^{13}\mathrm{C} : {}^{12}\mathrm{C} : {}^{14}\mathrm{N} \simeq 1 : 45 : 190 : 26\,000$
$\Rightarrow$ CN-equilibrium abundance distribution:

$$^{15}\mathrm{N} : {}^{13}\mathrm{C} : {}^{12}\mathrm{C} : {}^{14}\mathrm{N} \simeq \tfrac{1}{26\,000} : \tfrac{1}{600} : \tfrac{1}{140} : 1$$

independent of the initial composition

Comparison with solar system composition:

$$^{15}\mathrm{N} : {}^{13}\mathrm{C} : {}^{12}\mathrm{C} : {}^{14}\mathrm{N} = \tfrac{1}{1136} : \tfrac{1}{114} : \tfrac{4}{5} : \tfrac{1}{5}$$

$\Rightarrow$ $^{15}\mathrm{N}$, $^{13}\mathrm{C}$ and $^{12}\mathrm{C} \downarrow$ $\quad$ $^{14}\mathrm{N} \uparrow$
$\Rightarrow$ $^{14}\mathrm{N}$ is the major nucleosynthesis product of the CN-cycle (except for $^4\mathrm{He}$).

The CNO bi-cycle

Not all proton captures on $^{15}\mathrm{N}$ lead to $^{12}\mathrm{C} + \alpha$:

$$^{15}\mathrm{N} + \mathrm{p} \rightarrow {}^{16}\mathrm{O}^* \nearrow {}^{12}\mathrm{C} + \alpha \quad \text{for} \sim 99.9\%$$
$$\searrow {}^{16}\mathrm{O} + \gamma \quad \text{for} \sim 0.1\%$$

This initiates a second cycle (Fig. 4.10):

$$^{15}\mathrm{N}\,(\mathrm{p},\gamma)\,{}^{16}\mathrm{O}\,(\mathrm{p},\gamma)\,{}^{17}\mathrm{F}\,(\mathrm{e}^+\nu)\,{}^{17}\mathrm{O}\,(\mathrm{p},\alpha)\,{}^{14}\mathrm{N}\,(\mathrm{p},\gamma)\,{}^{15}\mathrm{O}\,(\mathrm{e}^+\nu)\,{}^{15}\mathrm{N} \quad \text{(CNO-II)}$$

ratio of 1:1000 $\Rightarrow$

- second cycle *not* relevant for energy generation
- but: very relevant for **nucleosynthesis**:
  it makes the $^{16}\mathrm{O}$-reservoir available to flow into the CN-cycle.

Two remarkable features:

1) CN-equilibrium is achieved much faster (typically in $\sim 10^4$ yr) than CNO-equilibrium.
   Reason: $\tau_{\mathrm{CN-eq.}} \simeq \tau_{\mathrm{p}}(^{12}\mathrm{C}) \ll \tau_{\mathrm{p}}(^{16}\mathrm{O}) \simeq \tau_{\mathrm{CNO-eq.}}$

2) Most of the original ^{16}O gets incorporated into the CN-cycle.
   Reason: whatever enters the CN-cycle remains there with 99.9% probability

The complete CNO-cycles

two more cycles can operate (Fig. 4.10):

$$^{17}\mathrm{O}\,(\mathrm{p},\gamma)\,^{18}\mathrm{F}\,(\mathrm{e}^{+}\nu)\,^{18}\mathrm{O}\,(\mathrm{p},\alpha)\,^{15}\mathrm{N}\,(\mathrm{p},\gamma)\,^{16}\mathrm{O}\,(\mathrm{p},\gamma)\,^{17}\mathrm{F}\,(\mathrm{e}^{+}\nu)\,^{17}\mathrm{O} \quad \text{(CNO-III)}$$

$$^{18}\mathrm{O}\,(\mathrm{p},\gamma)\,^{19}\mathrm{F}\,(\mathrm{p},\alpha)\,^{16}\mathrm{O}\,(\mathrm{p},\gamma)\,^{17}\mathrm{F}\,(\mathrm{e}^{+}\nu)\,^{17}\mathrm{O}(\mathrm{p},\gamma)\,^{18}\mathrm{F}\,(\mathrm{e}^{+}\nu)\,^{18}\mathrm{O} \quad \text{(CNO-IV)}$$

• General rule: the (p,α)-reactions – if leading to a stable nucleus – are *faster* than the (p,γ)-reactions (strong vs. electromagnetic force!)
Only exception: $^{13}\mathrm{C}(\mathrm{p},\gamma)^{14}\mathrm{N}$ is faster than $^{13}\mathrm{C}(\mathrm{p},\alpha)^{10}\mathrm{B}$.

$\Rightarrow$ speed of CNO-cycles: CN $\gg$ CNO-II $\gg$ CNO-III $\gg$ CNO IV

• If *all* cycles are fast enough $\rightsquigarrow$ complete CNO-equilibrium abundances (see Table 4.5)

$\Rightarrow$ 1) ^{14}N is strongly produced
2) ^{12}C, ^{15}N, ^{16}O, ^{18}O, ^{19}F are *destroyed*
3) ^{13}C and ^{17}O can be produced by the CNO-cycle

Table 4.5: CNO-equilibrium abundances

	^{12}C	^{13}C	^{14}N	^{15}N	^{16}O	^{17}O	^{18}O	^{19}F
equil. mass fraction ($Z = 2\,\%$, $T = 3 \cdot 10^7$ K)	10^{-4}	$6{\cdot}10^{-5}$	10^{-2}	$3 \cdot 10^{-7}$	$3 \cdot 10^{-4}$	$4 \cdot 10^{-6}$	10^{-9}	10^{-9}
solar mass fraction	$3.5 \cdot 10^{-3}$	$4 \cdot 10^{-5}$	10^{-3}	4.10^{-6}	10^{-2}	4.10^{-6}	2.10^{-5}	4.10^{-7}
ratio	$\frac{1}{30}$	1.5	10	$\frac{1}{10}$	$\frac{1}{30}$	1	$\frac{1}{20\,000}$	$\frac{1}{400}$

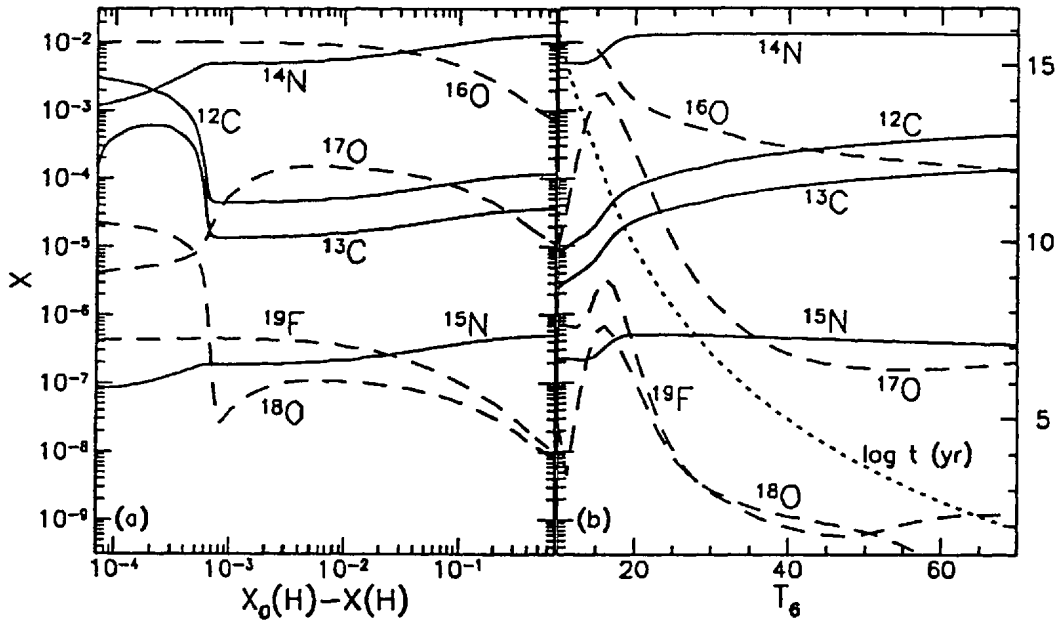

Figure 4.11: *(left)* Time evolution of the mass fractions of stable nuclides involved in the CNO cycles, versus the amount of H burnt at a constant temperature $T = 25 \times 10^6$ K and density $\rho = 100\,\mathrm{g\,cm^{-3}}$. $X_0(\mathrm{H}) = 0.7$ is the initial H mass fraction. *(right)* Final values of these mass fractions (at $X(\mathrm{H}) = 10^{-9}$) versus T_6, the temperature in 10^6 K. The dotted line indicates the logarithm of the H-burning time (in years) to be read on the right-hand side ordinate. Figure from Arnould & Mowlavi (1993).

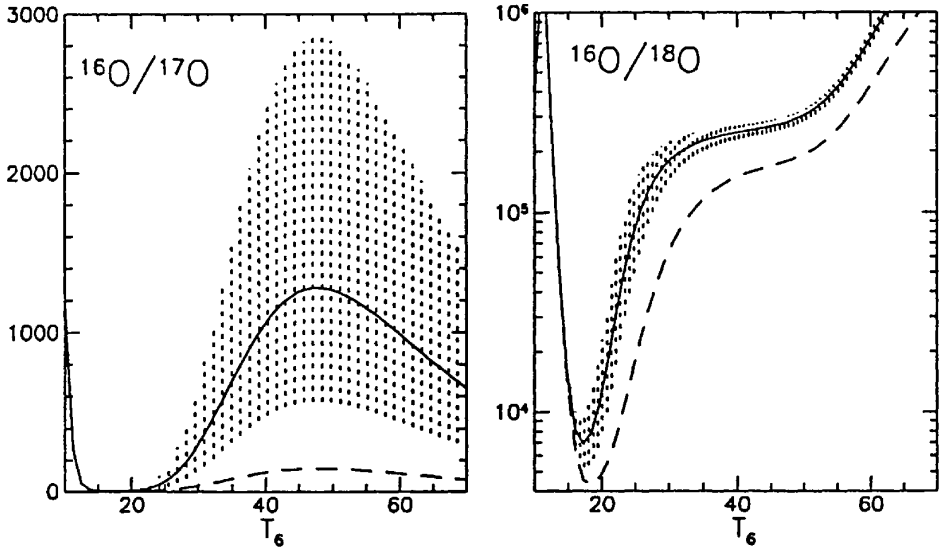

Figure 4.12: The effect of uncertainties in the reaction rates of $^{17}\mathrm{O}(\mathrm{p},\gamma)^{18}\mathrm{F}$ and $^{17}\mathrm{O}(\mathrm{p},\alpha)^{14}\mathrm{N}$ on the the final abundance ratios $^{16}\mathrm{O}/^{17}\mathrm{O}$ (left) and $^{16}\mathrm{O}/^{18}\mathrm{O}$ (right). The solid line is for the rates of Landré et al. (1990) with the effect of its uncertainty indicated as shading. The dashed line is for the rates of Berheide et al. (1992). Figure from Arnould & Mowlavi (1993).

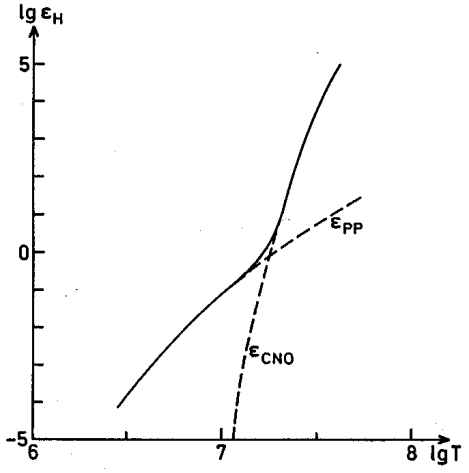

Figure 4.13: Temperature dependence of nuclear energy generation by the pp reactions and the CN cycle. Figure from Kippenhahn & Weigert (1990).

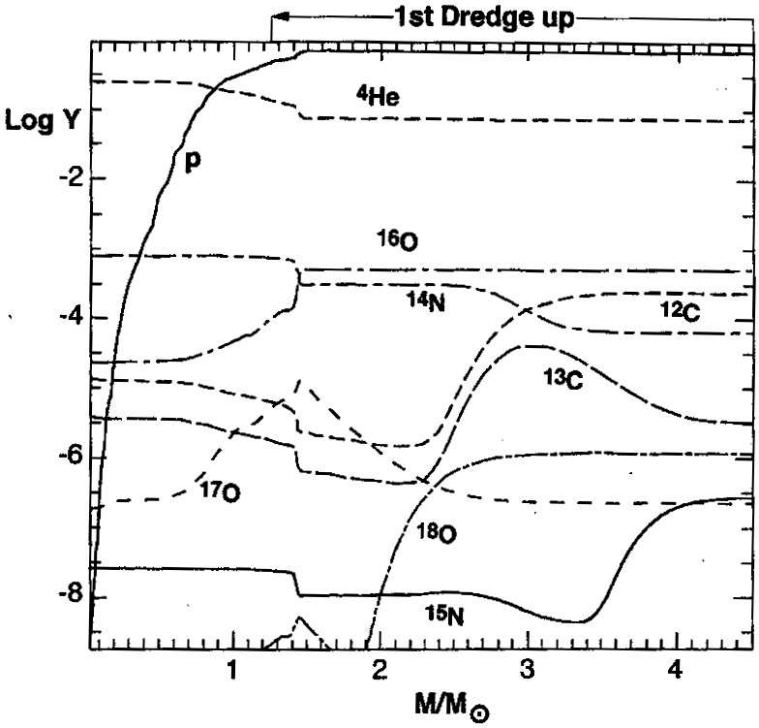

Figure 4.14: Abundance profiles of several light nuclei (plotted as the logarithm of $Y = X/A$, where X is the usual mass fraction) in the inner regions of a $5\,M_\odot$ star after core H-burning. The region that is subsequently mixed by the first dredge-up is indicated by the arrow along the top. Before the first dredge-up, the original composition is unchanged down to $\sim 4\,M_\odot$. Below $\sim 4\,M_\odot$, ^{13}C increases and ^{15}N decreases due to CN cycling, and somewhat deeper down, where the CN cycle has been more effective, ^{14}N increases while ^{12}C and ^{13}C decrease. After the first dredge-up, the envelope composition is homogeneously mixed to the average value down to the indicated depth. This means an increase in the surface ^{14}N/^{12}C and ^{13}C/^{12}C abundance ratios. Figure from Busso et al. (1999).

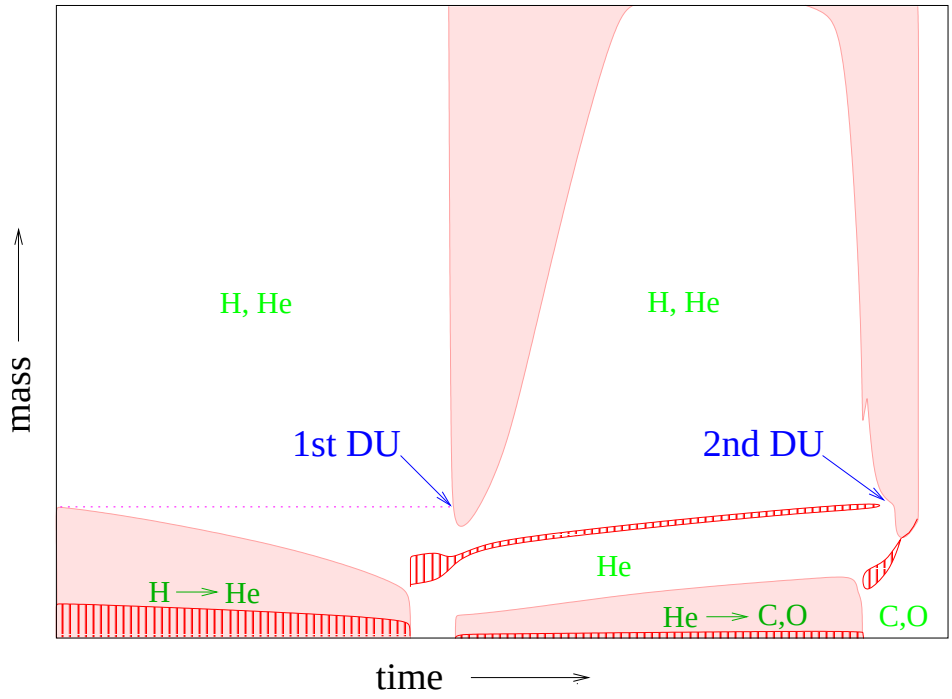

Figure 4.15: Schematic Kippenhahn diagram of a star of approximately $5\,M_\odot$. The shaded areas indicate mass ranges that are convective, and the vertically hatched regions undergo nuclear burning. The occurrence of the first and second dredge-up episodes are also indicated.

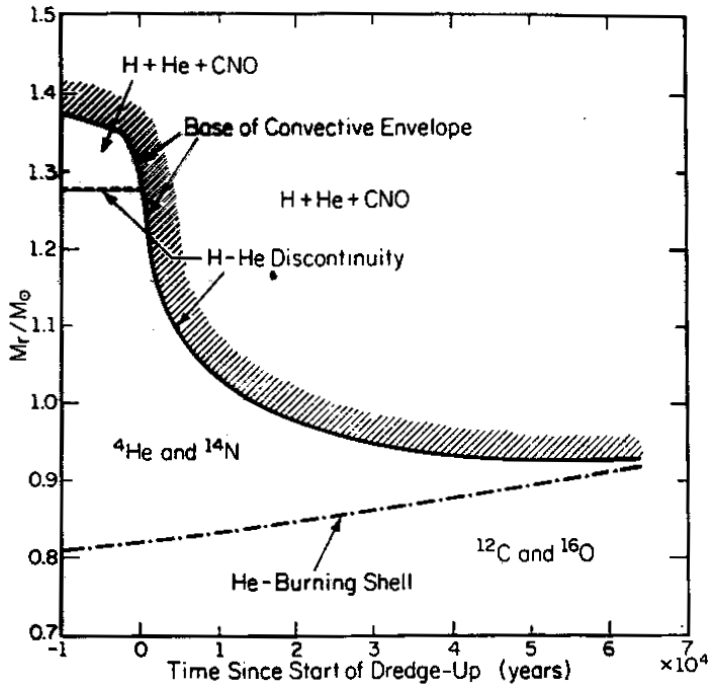

Figure 4.16: Close-up of a Kippenhahn diagram of a $7\,M_\odot$ star during the second dredge-up, which only occurs for stars more massive than $\sim 4\,M_\odot$. Contrary to the first dredge-up, the base of the convective envelope penetrates past the (inactive) H-burning shell into the helium core, mixing large amounts of ^{4}He and ^{14}N into the envelope. Figure from Iben (1991).

E. Beyond the CNO-cycle

Further hydrogen burning reactions can occur for sufficiently high temperature:

The NeNa-cycle

$$^{20}\mathrm{Ne}\,(\mathrm{p},\gamma)\,^{21}\mathrm{Na}\,(\mathrm{e}^{+}\nu)\,^{21}\mathrm{Ne}\,(\mathrm{p},\gamma)\,^{22}\mathrm{Na}\,(\mathrm{e}^{+}\nu)\,^{22}\mathrm{Ne}\,(\mathrm{p},\gamma)\,^{23}\mathrm{Na}\,(\mathrm{p},\alpha)\,^{20}\mathrm{Ne}$$

- *not* a true cycle at H-burning temperature
- most relevant reaction: $^{22}\mathrm{Ne}(\mathrm{p},\gamma)^{23}\mathrm{Na}$
  $\Rightarrow$ increase of *elemental* Na by factor 10! (^{23}Na is the only stable Na isotope)
  $\Rightarrow$ 1) Na-production
  2) Observational consequences in stellar surface abundances

The MgAl-cycle

$$^{24}\mathrm{Mg}\,(\mathrm{p},\gamma)\,^{25}\mathrm{Al}\,(\mathrm{e}^{+}\nu)\,^{25}\mathrm{Mg}\,(\mathrm{p},\gamma)\,^{26}\mathrm{Al}\;\nearrow(\mathrm{p},\gamma)\,^{27}\mathrm{Si}\,(\mathrm{e}^{+}\nu)\;\searrow$$
$$\searrow(\mathrm{e}^{+}\nu)\,^{26}\mathrm{Mg}\,(\mathrm{p},\gamma)\;\nearrow\;^{27}\mathrm{Al}\,(\mathrm{p},\alpha)\,^{24}\mathrm{Mg}$$

- also *not* a true cycle at H-burning temperature
- most relevant reaction: $^{25}\mathrm{Mg}(\mathrm{p},\gamma)^{26}\mathrm{Al}$
  $\Rightarrow$ production of radioactive nucleus ^{26}Al

Aluminium-26

- produced by the MgAl-cycle if $T \gtrsim 3 \cdot 10^7$ K
  $\Rightarrow$ ^{26}Al is always produced by stars which do H-burning via the CNO-cycle.
- production occurs in an unusual way:
  The $^{25}\mathrm{Mg}(\mathrm{p},\gamma)^{26}\mathrm{Al}$ reaction produces *two* "types" of ^{26}Al:

  a) ^{26}Al in its ground state = $^{26}\mathrm{Al}^{\mathrm{g}}$ with $\tau_{1/2}(^{26}\mathrm{Al}^{\mathrm{g}}) \simeq 10^6$ yr

  b) ^{26}Al in its first excited state = $^{26}\mathrm{Al}^{*}$ with $\tau_{1/2}(^{26}\mathrm{Al}^{*}) = 6$ s

The *branching ratio* is roughly: 85% of the produced ^{26}Al is $^{26}\mathrm{Al}^{\mathrm{g}}$, 15% is $^{26}\mathrm{Al}^{*}$.
This depends somewhat on temperature.

- When $^{26}\mathrm{Al}^{\mathrm{g}}$ decays to ^{26}Mg, it emits a γ-photon of 1.806 MeV
  $\rightsquigarrow$ COMPTEL has observed $\sim 3M_\odot$ of radioactive ^{26}Al "glowing" in the Milky Way
  Note: distribution is a) patchy
  b) confined to the Galactic plane
- One explanation of the origin of the Galactic ^{26}Al:

  1) Massive stars produce ^{26}Al during their CNO-burning within MgAl-cycle

  2) As lifetime of massive stars $\simeq$ lifetime of ^{26}Al
  $\Rightarrow$ ^{26}Al still present when stars explode as supernovae

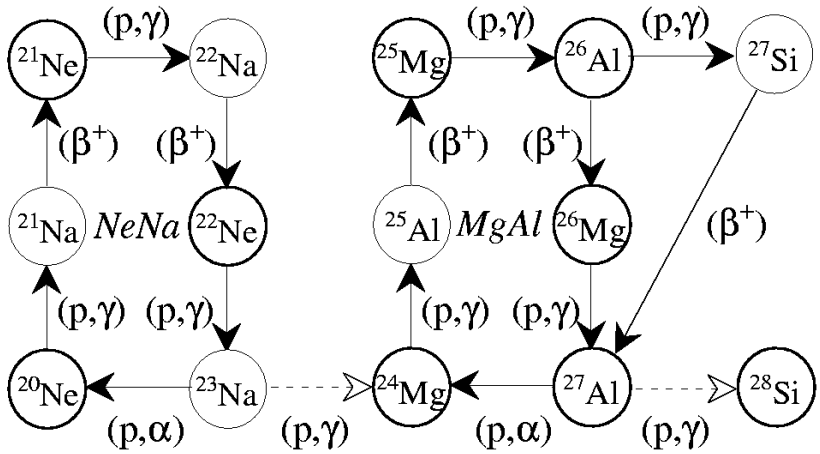

Figure 4.17: Reaction flows in the NeNa and MgAl cycles.

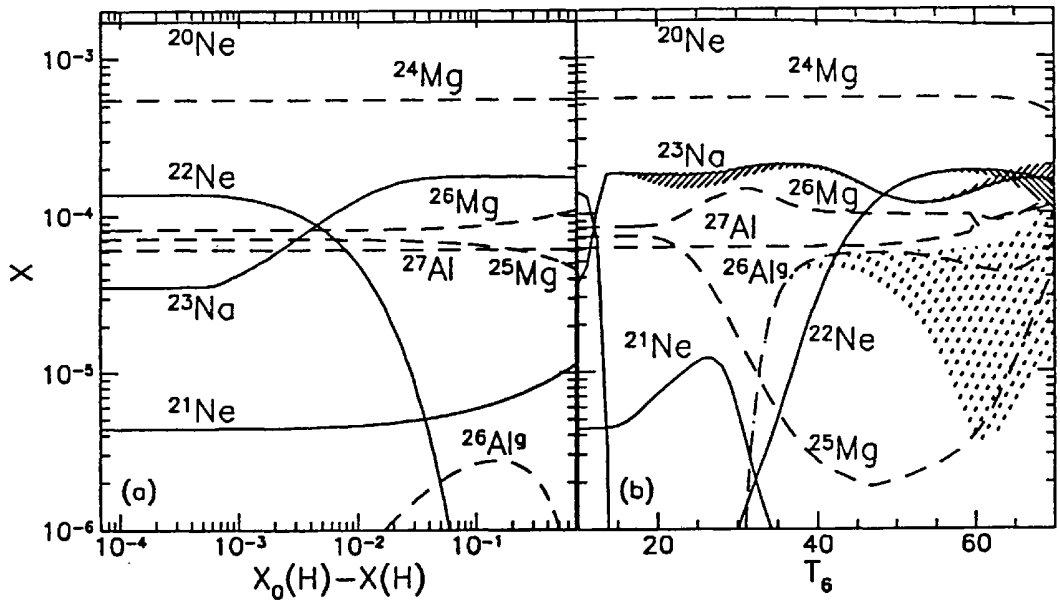

Figure 4.18: Same as Fig. 4.11, but for the nuclides involved in the NeNa (solid lines) and MgAl cycles (dashed lines). The hatched areas indicate the of ^{22}Ne, ^{23}Na and ^{26}Al^{g} due to uncertainties in the reaction rates. Figure from Arnould & Mowlavi (1993).

Suggestions for further reading

– Chapter 5.6–5.7 of Pagel.
– Chaper 5 of Clayton provides much more detail about the nuclear reactions involved in hydrogen burning. Some of this is used these lecture notes.

Exercises

4.4 Assume that the energy for the Sun's luminosity is provided by the conversion of $4\mathrm{H} \rightarrow {}^4\mathrm{He}$, and that neutrinos carry off 3% of the liberated energy.

(a) How many neutrinos are liberated in the Sun each second?

(b) What is the solar neutrino flux at earth?

4.5 Show that the differential equations describing the abundance changes in the ppI chain obey mass (or nucleon number) conservation.

4.6 Show that for constant H and ^{4}He abundances, the D abundance varies as

$$\left(\frac{\mathrm{D}}{\mathrm{H}}\right)(t) = \left(\frac{\mathrm{D}}{\mathrm{H}}\right)_{\mathrm{e}} - \left[\left(\frac{\mathrm{D}}{\mathrm{H}}\right)_{\mathrm{e}} - \left(\frac{\mathrm{D}}{\mathrm{H}}\right)_{t=0}\right] \cdot \exp\left(-\frac{t}{\tau_{\mathrm{p}}(\mathrm{D})}\right).$$

where the subscript 'e' stands for equilibrium value. Interpret this equation.

4.7 Show that the number of CNO nuclei is a conserved quantity in the CNO tri-cycle.

4.8 Compute the abundances of ^{12}C, ^{13}C, ^{14}N and ^{15}N in the center of a star where 1 out of 1000 nuclei is a carbon or nitrogen nucleus, assuming CN equilibrium. Assume the stellar center has a temperature of 2×10^7 K. Hint: use the lifetimes of the CN nuclei given in the lecture.

4.9 (a) Compute how much ^{26}Al is produced by stars of $20\,\mathrm{M}_\odot$ (lifetime $\simeq 7 \cdot 10^6$ yr) and $85\,\mathrm{M}_\odot$ stars (lifetime $\simeq 3 \cdot 10^6$ yr), by assuming that all initially present ^{25}Mg is burnt instantly to $^{26}\mathrm{Al}^{\mathrm{g}}$ during hydrogen burning. (Assume an initial ^{25}Mg mass fraction of 10^{-4}), and that $^{26}\mathrm{Al}(\mathrm{p},\gamma)$ is too slow to play a role.)

(b) How much ^{26}Al is ejected into the ISM by these stars? Can this explain the $3\,\mathrm{M}_\odot$ of ^{26}Al observed in the Milky Way? Are there ways to increase the ^{26}Al mass ejected by these stars?
(Lifetime of $^{26}\mathrm{Al} \simeq 10^6$ yr; Type II supernova rate $\simeq 0.01$/yr/Galaxy)

4.3 Advanced nuclear burning phases

A. Helium burning

Starting composition: ashes of hydrogen burning

For example ($Z = Z_\odot$): $X = 0.70$, $Y = 0.28$, $Z = 0.02$ (with $X(\mathrm{O}) \approx 0.01$)

$\Downarrow$

after H-burning: $X = 0$, $Y = 0.98$, $Z = 0.02$ (with $X(\mathrm{N}) \approx 0.014$)

Main reaction of helium burning: so called 3α-reaction

Starting point is the reaction $\alpha + \alpha \rightarrow {}^8\mathrm{Be}$ ($Q = -92\,\mathrm{keV}$).
Endothermic $\Rightarrow$ ^{8}Be is unstable against breakup in 2α, but $\tau_{1/2}({}^8\mathrm{Be}) \simeq 3 \times 10^{-16}\,\mathrm{s}$ is much larger than the timescale of an $\alpha + \alpha$ scattering!
$\Rightarrow$ a small concentration of ^{8}Be can build up until equilibrium is reached:

$$\alpha + \alpha \leftrightarrow {}^8\mathrm{Be}$$

Equilibrium ^{8}Be concentration increases with T: at $T \simeq 10^8\,\mathrm{K}$ it is ${}^8\mathrm{Be}/{}^4\mathrm{He} \simeq 10^{-9}$ $\Rightarrow$

$$^8\mathrm{Be} + \alpha \rightarrow {}^{12}\mathrm{C} + \gamma$$

becomes possible due to a resonance in the reaction ${}^8\mathrm{Be}(\alpha){}^{12}\mathrm{C}^*(\gamma){}^{12}\mathrm{C}$.
The existence of the resonance was predicted by Fred Hoyle in 1954, on the basis that otherwise there would be no carbon in the Universe!
Effectively:

$$\boxed{3\alpha \rightarrow {}^{12}\mathrm{C} + \gamma}$$

but note: it is **not** a three particle reaction!

Further reactions:

$\boxed{{}^{12}\mathrm{C}(\alpha,\gamma){}^{16}\mathrm{O}}$	very important
${}^{16}\mathrm{O}(\alpha,\gamma){}^{20}\mathrm{Ne}$	less important (only at very high T)

Remark: the $^{12}\mathrm{C}(\alpha,\gamma)$-rate is not very well known today.
$\Rightarrow$ unclear wether main product of He-burning is carbon or oxygen!

Secondary nucleosynthesis during helium burning:

$$^{14}\mathrm{N}(\alpha,\gamma){}^{18}\mathrm{F}(\beta^+){}^{18}\mathrm{O}(\alpha,\gamma){}^{22}\mathrm{Ne} \quad (\text{already at } T \simeq 10^8\,\mathrm{K})$$

$\Rightarrow$ production of ^{18}O and ^{22}Ne

$$^{22}\mathrm{Ne}(\alpha,\mathrm{n}){}^{25}\mathrm{Mg} \quad (\text{for } T \geq 3 \cdot 10^8\,\mathrm{K}$$

$\Rightarrow$ **n**-production !! $\Rightarrow$ s-process (Chapter 5).

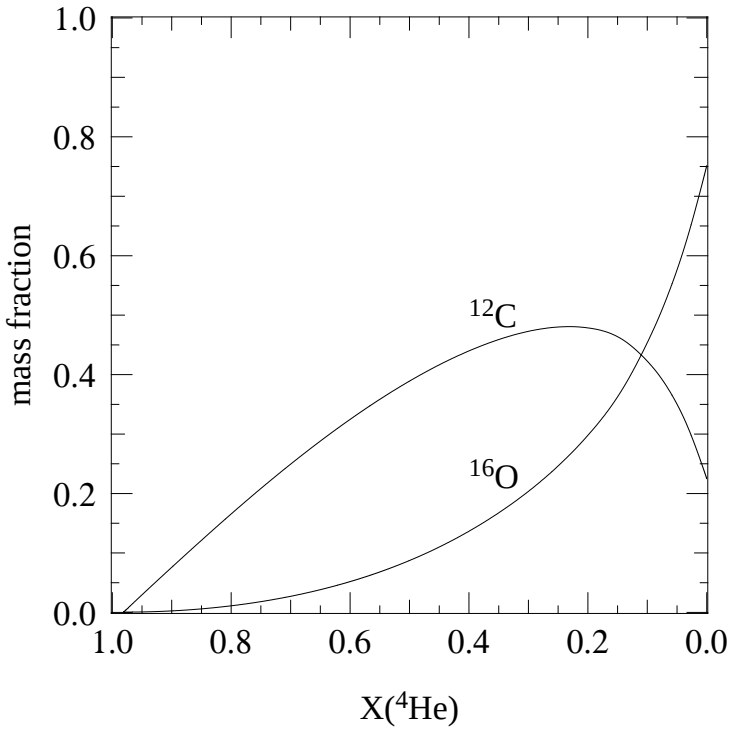

Figure 4.19: Mass fractions of ^{12}C and ^{16}O as a function of the decreasing He mass fraction, calculated for a $5\,M_\odot$ star with $Z = 0.02$.

B. Carbon burning

Starting composition: ashes of helium burning, mainly ^{12}C, ^{16}O
no light particles (p, n, α) available initially!

Main reaction of carbon burning: $^{12}C + {}^{12}C$

There are two main exit channels:

$$^{12}\mathrm{C} + {}^{12}\mathrm{C} \rightarrow {}^{24}\mathrm{Mg}^* \rightarrow {}^{20}\mathrm{Ne} + \alpha + 4.6\,\mathrm{MeV} \quad (\sim 50\%)$$
$$^{12}\mathrm{C} + {}^{12}\mathrm{C} \rightarrow {}^{24}\mathrm{Mg}^* \rightarrow {}^{23}\mathrm{Na} + \mathrm{p} + 2.2\,\mathrm{MeV} \quad (\sim 50\%)$$

$\Rightarrow$ production of p and α particles; those are immediately captured $\Rightarrow$

many side reactions, e.g.: $^{23}\mathrm{Na}(\mathrm{p},\alpha)^{20}\mathrm{Ne}$, $^{20}\mathrm{Ne}(\alpha,\gamma)^{24}\mathrm{Mg}$ ...
also $^{12}\mathrm{C}(\alpha,\gamma)^{16}\mathrm{O}$, $^{16}\mathrm{O}(\alpha,\gamma)^{20}\mathrm{Ne}$ ...

Composition after carbon burning: ^{16}O, ^{20}Ne, ^{24}Mg (together: 95%)

C. Neon burning

First expectation: oxygen burning should follow carbon burning, as ^{16}O is the lightest remaining nucleus, **but:**

^{16}O is doubly-magic nucleus (magic n and magic p number!)
$\Rightarrow$ extremely stable: α-separation energy: 7.2 MeV
^{20}Ne is much less stable: α-separation energy: 4.7 MeV

Consequence: $^{20}\mathrm{Ne}(\gamma,\alpha)^{16}\mathrm{O}$ occurs at lower temperatures than $^{16}\mathrm{O} + {}^{16}\mathrm{O}$

Main reactions of neon burning:

$$^{20}\mathrm{Ne} + \gamma \longleftrightarrow {}^{16}\mathrm{O} + \alpha$$
$$^{20}\mathrm{Ne} + \alpha \rightarrow {}^{24}\mathrm{Mg} + \gamma$$

Effectively: $2\,{}^{20}\mathrm{Ne} \rightarrow {}^{16}\mathrm{O} + {}^{24}\mathrm{Mg}$ $\Rightarrow$ effective energy generation > 0!

Composition after neon burning: ^{16}O, ^{24}Mg (together: 95%)

D. Oxygen burning

Starting composition: ashes of neon burning, mainly ^{16}O, ^{24}Mg
no light particles (p, n, α) available initially!

Main reaction of oxygen burning: $^{16}\mathbf{O} + {}^{16}\mathbf{O}$

There are two main exit channels:

$$^{16}\mathrm{O} + {}^{16}\mathrm{O} \rightarrow {}^{32}\mathrm{S}^* \rightarrow {}^{28}\mathrm{Si} + \alpha + 9.6\,\mathrm{MeV} \quad (\sim 60\%)$$
$$^{16}\mathrm{O} + {}^{16}\mathrm{O} \rightarrow {}^{32}\mathrm{S}^* \rightarrow {}^{31}\mathrm{P} + \mathrm{p} + 7.7\,\mathrm{MeV} \quad (\sim 40\%)$$

$\Rightarrow$ production of p and α particles (like in carbon burning) which are immediately captured $\Rightarrow$

many side reactions, e.g.: $^{31}\mathrm{P}(\mathrm{p},\alpha)^{28}\mathrm{Si}$, $^{28}\mathrm{Si}(\alpha,\gamma)^{32}\mathrm{S}$ ...
also $^{24}\mathrm{Mg}(\alpha,\gamma)^{28}\mathrm{Si}$, ... but $^{16}\mathrm{O}(\alpha,\gamma)^{20}\mathrm{Ne}$ is blocked!

Composition after oxygen burning: ^{28}Si, ^{32}S (together: 90%)

E. Silicon burning

Main ash of oxygen burning, and lightest remaining isotope: ^{28}Si
but: $^{28}\mathrm{Si} + {}^{28}\mathrm{Si}$ is prohibited by the high Coulomb-barrier

instead: $^{28}\mathrm{Si}(\gamma,\alpha)^{24}\mathrm{Mg}$ occurs for $T > 3 \cdot 10^9\,\mathrm{K}$
$\Rightarrow$ Si-burning occurs similar to Ne-burning: through (γ,α) and (α,γ)-reactions:

$$^{28}\mathrm{Si}\,(\gamma,\alpha)\,^{24}\mathrm{Mg}\,(\gamma,\alpha)\,^{20}\mathrm{Ne}\,(\gamma,\alpha)\,^{16}\mathrm{O}\,(\gamma,\alpha)\,^{12}\mathrm{C}\,(\gamma,\alpha)\,2\alpha$$

and

$$^{28}\mathrm{Si}\,(\alpha,\gamma)\,^{32}\mathrm{S}\,(\alpha,\gamma)\,^{36}\mathrm{Ar}\,(\alpha,\gamma)\,^{40}\mathrm{Ca}\,(\alpha,\gamma)\,^{44}\mathrm{Ti}\,(\alpha,\gamma)\,^{48}\mathrm{Cr}\,(\alpha,\gamma)\,^{52}\mathrm{Fe}\,(\alpha,\gamma)\,^{56}\mathrm{Ni}$$

For $T > 4{\cdot}10^9\,\mathrm{K}$: almost nuclear statistical equilibrium (NSE) may be reached (cf. Chapter 6)
As in the matter p/n < 1 due to β-decays and possibly e^--captures: final composition may be mostly ^{56}Fe.

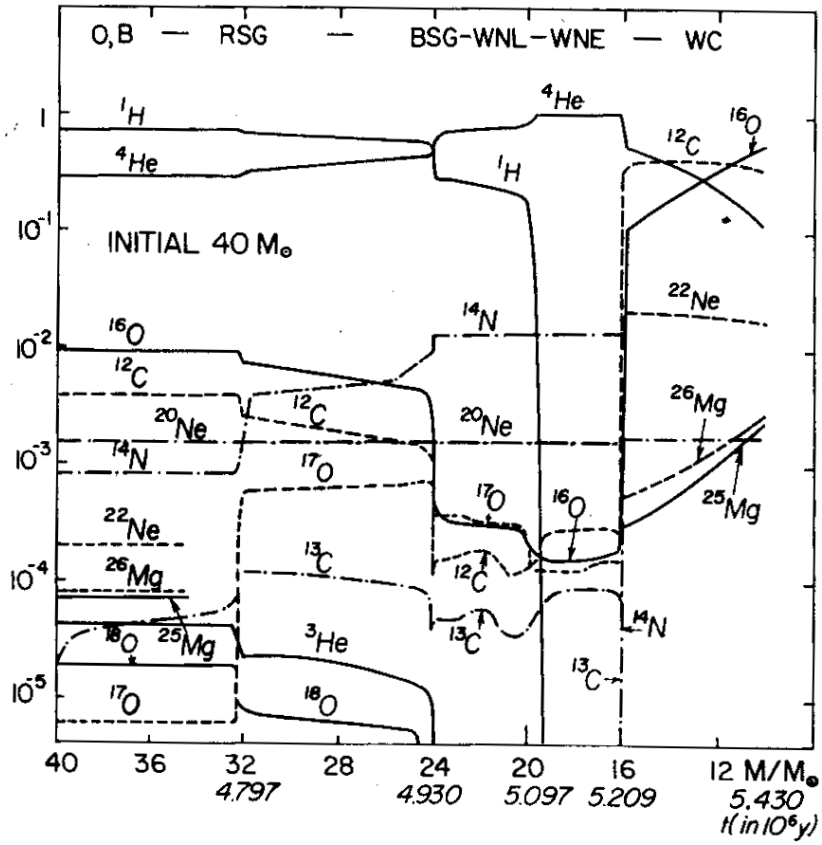

Figure 4.20: Evolution of surface abundances of a $40\,\mathrm{M}_\odot$ star that becomes a Wolf-Rayet star as a result of stellar-wind mass loss. As the star evolves from an O-star to a red supergiant (RSG) and back to a blue supergiant (BSG), the surface composition is changed as a result of the outer layers being peeled off in stellar winds. ^{4}He and ^{14}N become enriched at the surface. As the surface He mass fraction increases, the star becomes a nitrogen-rich Wolf-Rayet star evolving from late (WNL) to early, i.e. hotter (WNE) type. When the layers that have experienced He burning are exposed, the star becomes carbon-rich (WC). Mass loss from WC stars probably accounts for a substantial fraction of the ^{12}C in the Universe. Figure from Pagel.

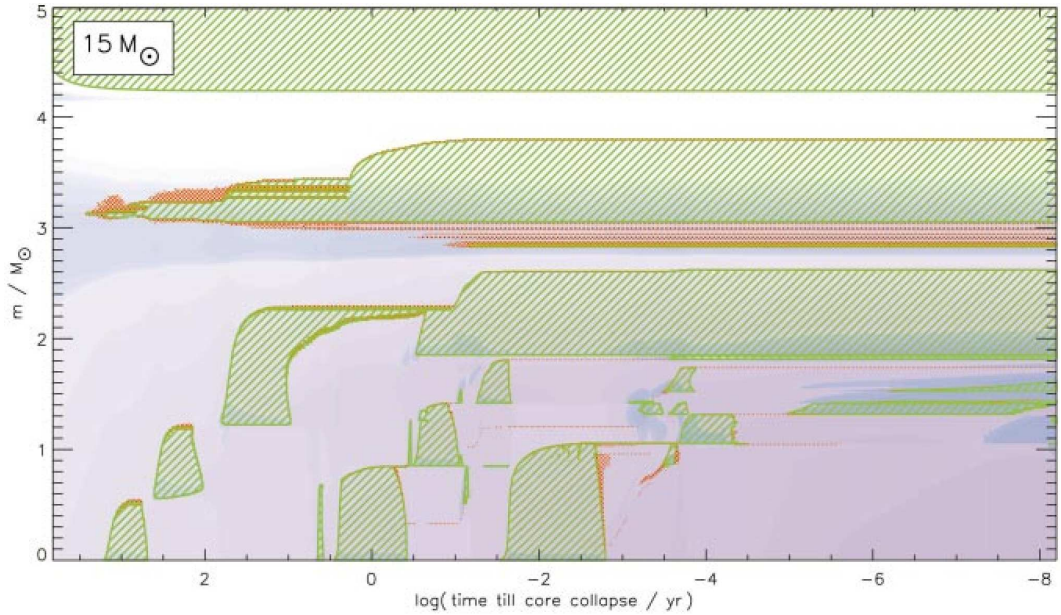

Figure 4.21: Kippenhahn diagram of the final evolution of the interior regions of a $15\,M_\odot$ star, showing the last 10^4 years until core collapse with time on a logarithmic scale. Cross-hatched regions are convective, while the grey scale indicates the energy generation rate. Note that the inner core of $\sim 1.4\,M_\odot$ has gone through all burning stages: central C-burning (at $\log t \approx 3$ before core collapse), Ne burning ($\log t \approx 0.6$) quickly followed by O burning ($\log t \approx 0$), and Si burning ($\log t \approx -2$). Figure from Woosley et al. (2002).

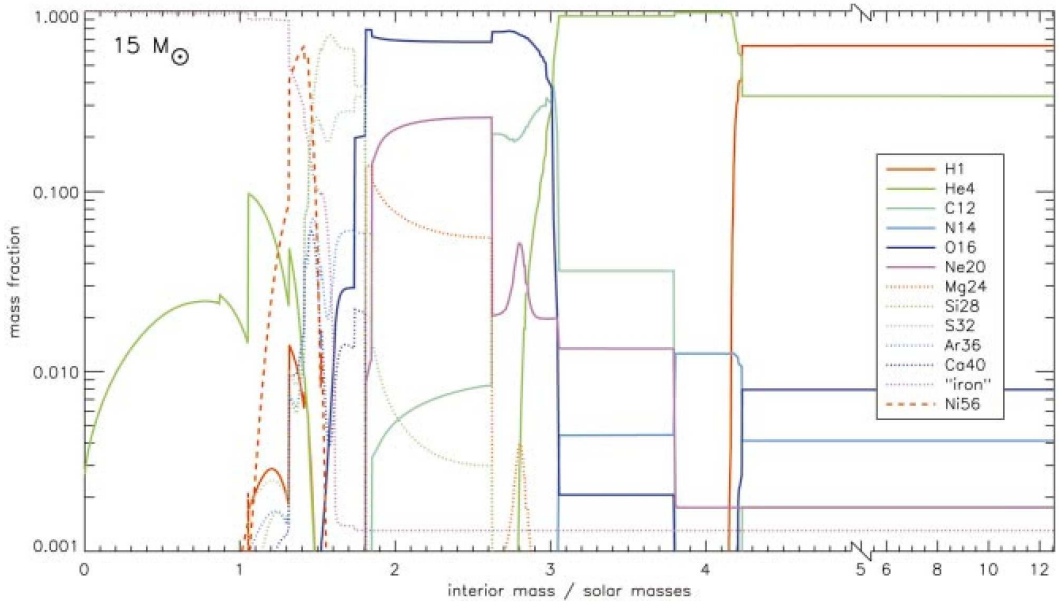

Figure 4.22: Final composition profiles of the $15\,M_\odot$ model shown in Fig. 4.21, just before core collapse. "Iron" refers to the sum of neutron-rich isotopes in the iron group, mainly ^{54}Fe, ^{56}Fe and ^{58}Fe. Figure from Woosley et al. (2002).

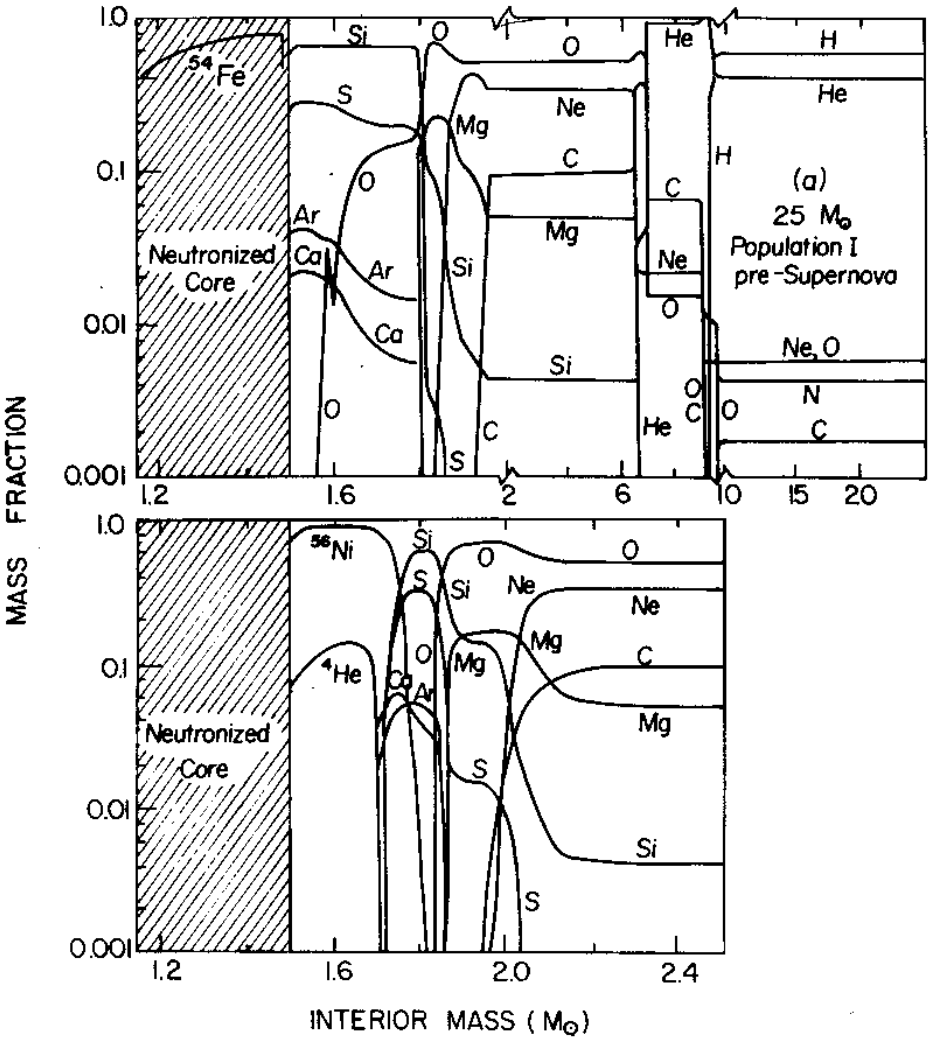

Figure 4.23: Chemical profile of a $25\,M_\odot$ star, immediately before core collapse (upper panel) and after modification by explosive nucleosynthesis in a supernova explosion (lower panel). Note the change in horizontal scale at $2\,M_\odot$ in the upper panel. The amount of ^{56}Ni (which later decays to ^{56}Fe) ejected depends on the mass cut between the core and envelope, and is uncertain by a factor ≈ 3. The mass cut is located somehere in the ^{28}Si–^{56}Ni transition zone. Figure from Pagel.

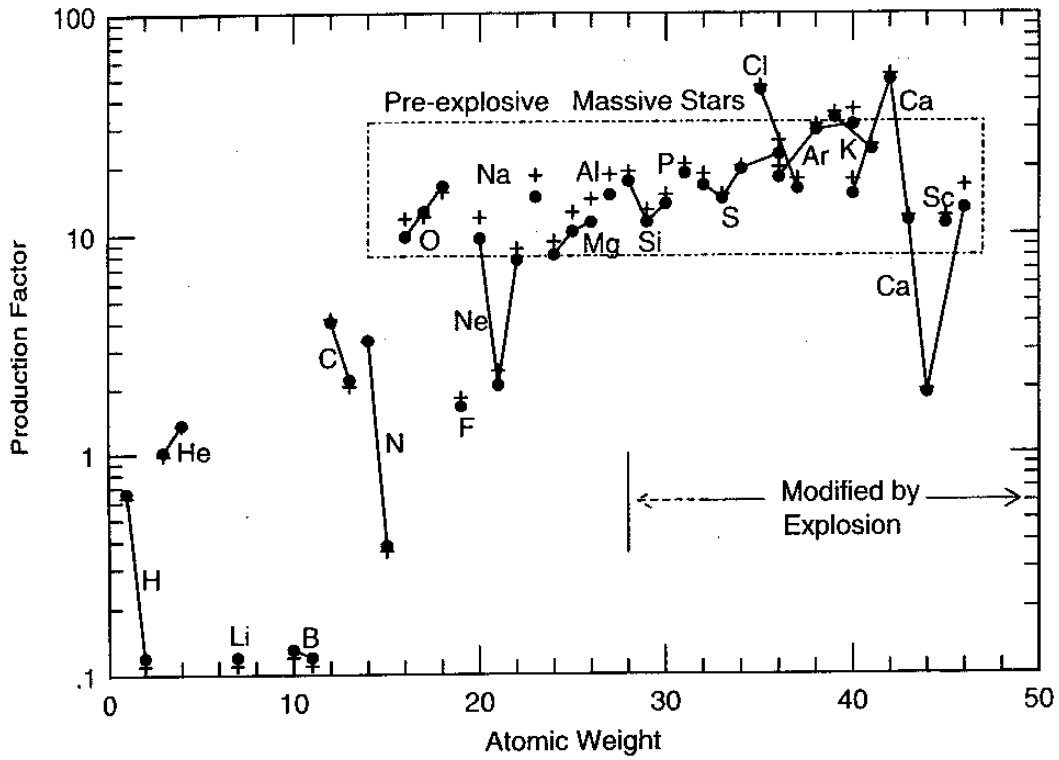

Figure 4.24: Production factors of nuclear species up to $A = 46$, resulting from hydrostatic evolution in one generation of massive stars at solar metallicity. The isotopes within the dashed box are produced in relative amounts corresponding within a factor 2 to solar system abundances, but note that iron would have a production factor of only ~ 2 on this diagram. Figure from Woosley & Weaver (1993).

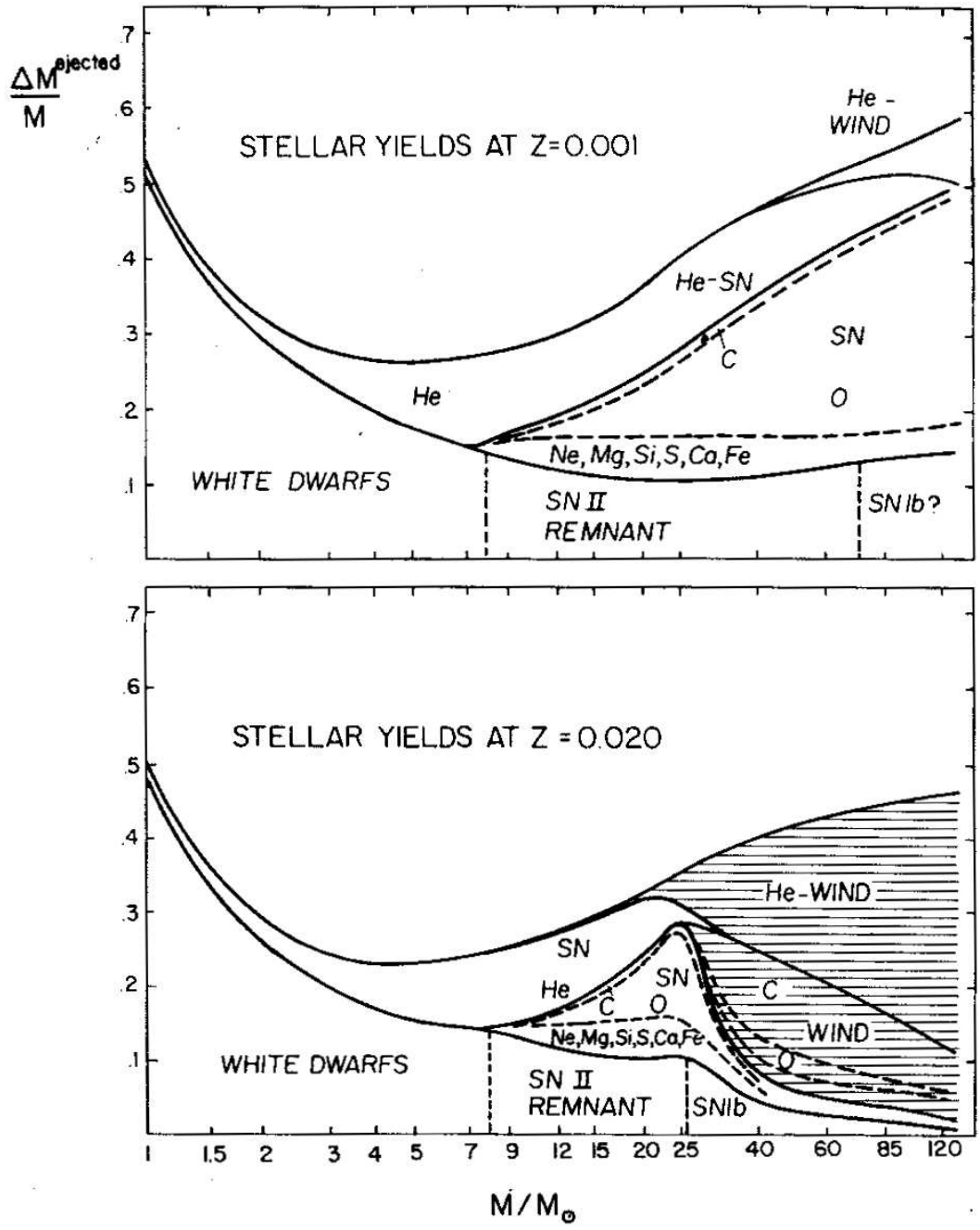

Figure 4.25: The fractions of stellar mass in the form of various elements (yields) ejected by stars in stellar winds and in supernovae, as a function of initial mass. The upper panel is for stars with about 1/20 solar metallicity, the lower panel for solar metallicity. The effects of mass loss, especially during the WR phase (hatched regions) are more drastic at higher metallicity. Figure from Pagel.

Suggestions for further reading

– Chapter 5.8–5.10 of PAGEL.
– Chapter 5.5–5.6 of CLAYTON.
– A good review article about advanced nuclear burning in massive stars is by Woosley, Heger & Weaver (2002), *The evolution and explosion of massive stas*, Rev. Mod. Phys., 74, 1015.

Exercises

4.10 Compute the Chandrasekhar mass for (a) pure hydrogen gas, (b) pure helium gas, (c) C/O-gas, and (d) pure ^{56}Fe-gas. Which of these are relevant for stellar evolution?

4.11 As the reaction $^{16}\mathrm{O}(\alpha,\gamma)^{20}\mathrm{Ne}$ releases 4.7 MeV of energy, the reverse reaction $^{20}\mathrm{Ne}(\gamma,\alpha)^{16}\mathrm{O}$ *consumes* energy. Why does neon burning produce energy nevertheless, and how much energy is produced by "burning" 1 g of neon?

4.12 Consider a massive star with $Z = 0.02$ and the following initial abundances (mass fractions) :

$$\begin{aligned} X(^{12}\mathrm{C}) &= 0.176Z \\ X(^{14}\mathrm{N}) &= 0.052Z \\ X(^{16}\mathrm{O}) &= 0.502Z \\ X(^{20}\mathrm{Ne}) &= 0.092Z \\ X(^{22}\mathrm{Ne}) &\approx 0 \end{aligned}$$

(a) What is the mass fraction of ^{14}N in the core after the star has gone through H-burning?

(b) What is the mass fraction of ^{22}Ne in the core after the star has gone through He-burning?

(c) What is the **number ratio** $^{22}\mathrm{Ne}/^{20}\mathrm{Ne}$ in the core after He-burning? (Neglect the $^{16}\mathrm{O}(\alpha,\gamma)^{20}\mathrm{Ne}$ reaction)

4.13 One generation of massive stars produces oxygen and iron with a ratio of [O/Fe] = 0.5 (reminder: $[\mathrm{O/Fe}] = \log \frac{(\mathrm{O/Fe})}{(\mathrm{O/Fe})_\odot}$), and [O/C] = 0.5. This is observationally confirmed in extremely metal poor galactic stars (cf. Chapter 8, Fig. 8.6). What are the conclusions?

Chapter 5

Neutron-capture nucleosynthesis

5.1 The s-process

A. Effects of slow neutron capture process

• Elements beyond the iron group:
- not produced by charged particle reactions (high Coulomb-barriers!)
- possibility: neutron captures
- are free neutrons available in stars? ($\rightarrow$ **C**)

• n-capture: $(Z, A) + \mathrm{n} \rightarrow (Z, A+1) + \gamma$
then if $(Z, A+1)$ is a stable nucleus, we may have
$(Z, A+1) + \mathrm{n} \rightarrow (Z, A+2) + \gamma$
or $(Z, A+1)$ is β^--unstable, i.e.
$(Z, A+1) \rightarrow (Z+1, A+1) + \mathrm{e}^- + \nu \quad (\beta^-\text{-decay})$

• β-decay times of nuclei close to the "valley of stability" in the nuclear chart are mostly of order of hours ($\pm$ a factor of $\sim 10^3$).
$\Rightarrow$ short compared to stellar evolution time scale

$\rightsquigarrow$ • Definition of "classical" s-process:

$$\boxed{\tau(\text{n-capture}) \gg \tau(\beta^-\text{-decay})}$$

$\rightsquigarrow$ "s" stands for slow

Neutron capture cross section:

- no Coulomb-barrier
- for thermal neutrons: often $\sigma(v) \sim \dfrac{1}{v}$
$\Rightarrow$ cross section **increases** for **low** energy!

$$\Rightarrow \langle \sigma v \rangle = \int_0^\infty \sigma v \Phi(v) dv \sim C \cdot \int_0^\infty \Phi(v) dv = \text{constant}$$

$\Rightarrow$ weak energy dependence of $\langle \sigma v \rangle$

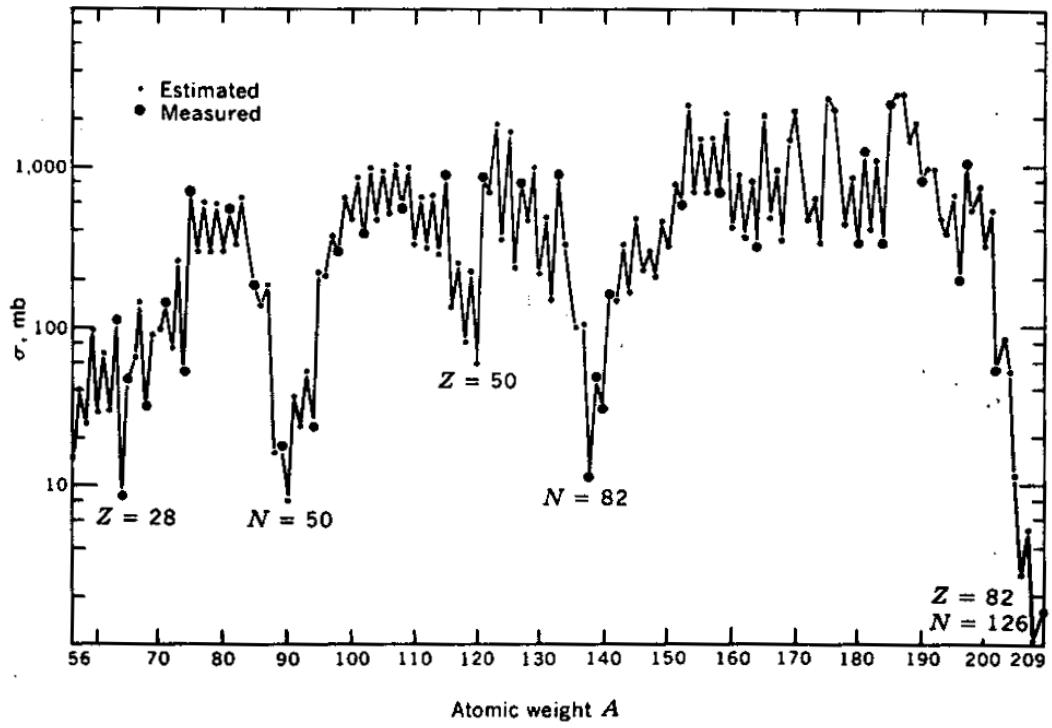

Figure 5.1: Measured and estimated neutron-capture cross sections of nuclei on the s-process path, for neutron energies near 25 keV. Odd mass numbers tend to have higher cross sections than even-A nuclei. However, the most obvious effect is the substantial lowering, by a factor of $10^2 - 10^3$, of the cross sections near magic numbers of neutrons ($N = 50$, 82 and 126) and to a lesser extent of protons (Z). Compare this figure to Fig. 1.1, and notice how the abundances of s-process elements anti-correlate with the n-capture cross sections. Figure from CLAYTON.

• define: $\langle\sigma\rangle := \dfrac{\langle\sigma v\rangle}{v_T}$, with $v_T = \left(\dfrac{2kT}{\mu_n}\right)^{\frac{1}{2}}$
and $\mu_{\rm n} = \dfrac{m_{\rm n} m_A}{m_{\rm n} + m_A}$

often: $\langle\sigma\rangle \simeq \sigma(v_T)$

exceptions: • close to magic neutron numbers: $\sigma \downarrow$
• light elements: more complicated

Time scales:

- nuclear time scale of the star: $\tau_{\rm nuc} \sim 10^{12}\,{\rm s}$
- mean life time of a heavy nucleus against n-capture : $\tau_A = \dfrac{1}{N_{\rm n}\langle\sigma v\rangle}$
  $\sigma \simeq 100\,{\rm mb}$, $v_T \simeq 3 \cdot 10^8\,{\rm cm/s} \rightarrow \tau_A \simeq 3 \cdot 10^{16}\,{\rm s}/N_{\rm n}$
  i.e., for $\tau_A \simeq \tau_{\rm nuc} \Rightarrow N_{\rm n} \simeq 3 \cdot 10^4\ {\rm cm}^{-3}$
- mixing time scale in stars: $\tau_{\rm mix} \simeq 10^6\,{\rm s}$ (convection)
- neutron decay $\tau_{\rm n-decay} \simeq 10^3\,{\rm s}$

- mean life time of neutron against capture by heavy nucleus $\tau_{\rm n} = \dfrac{1}{N_A \langle \sigma v \rangle} \simeq 10^{-3}\,{\rm s}$

- thermalisation time scale for neutrons : $\tau_{\rm therm} \simeq 10^{-5}\,{\rm s}$ (~ 40 scatterings)
  note: $\sigma(v)$ increases for smaller velocities!

$\Rightarrow \tau_{\rm therm} < \tau_{\rm n}$ $\quad\Rightarrow$ we can assume thermal velocities
$\tau_{\rm n} < \tau_{\rm n-decay}$ $\quad\Rightarrow$ we can neglect n-decay
$\tau_{\rm n} < \tau_{\rm mix}$ $\quad\Rightarrow$ neutrons are not transported by mixing

Differential equations:

$(Z, A) + {\rm n} \rightarrow (Z, A+1)$
$(Z, A-1) + {\rm n} \rightarrow (Z, A)$
$\Rightarrow \dfrac{dN_A}{dt} = -\langle \sigma v \rangle_A N_{\rm n} N_A + \langle \sigma v \rangle_{A-1} N_{\rm n} N_{A-1}$

- we can "short-cut" β-decays:
  $(Z, A) + {\rm n} \rightarrow (Z, A+1) \overset{\beta-{\rm decay}}{\longrightarrow} (Z+1, A+1)$
  $\rightsquigarrow \dfrac{dN_{A+1}}{dt} = -\langle \sigma v \rangle_A N_{\rm n} N_A$
  consequence: there is only 1 stable nucleus to be considered for a given mass number A
  e.g.: in the above dN_{A+1}/dt, N_{A+1} is the abundance of $(Z+1, A+1)$!

  $\Rightarrow$ at each A in the s-process path:

$$\boxed{\frac{dN_A}{dt} = -\langle \sigma v \rangle_A N_{\rm n} N_A + \langle \sigma v \rangle_{A-1} N_{\rm n} N_{A-1}}$$

- as $\langle \sigma v \rangle \simeq \langle \sigma \rangle v_T \simeq \sigma v_T$ $\quad\Rightarrow\quad \dfrac{dN_A}{dt} = v_T N_{\rm n} (-\sigma_A N_A + \sigma_{A-1} N_{A-1})$
  note that $N_{\rm n} = N_{\rm n}(t)$
  define: ${\rm d}\tau = v_T \cdot N_{\rm n}(t) dt$ $\quad\rightarrow\quad \tau = v_T \int N_{\rm n}(t) dt$ $\quad$("neutron exposure")

$\rightarrow$ $\boxed{\dfrac{dN_A}{d\tau} = \sigma_A N_A + \sigma_{A-1} N_{A-1}}$

Initial conditions:

^{56}Fe has a strong abundance peak ($\rightarrow$ solar system abundances)
$\sigma \uparrow$ for larger A
$\Rightarrow$ at $t = 0 : N_A(0) = \begin{cases} N_{56}(0) & A = 56 \\ 0 & A > 56 \end{cases}$

$\rightsquigarrow$ solve ~ 150 coupled differential equations; possible to do this analytically
(cf. Clayton p. 562)

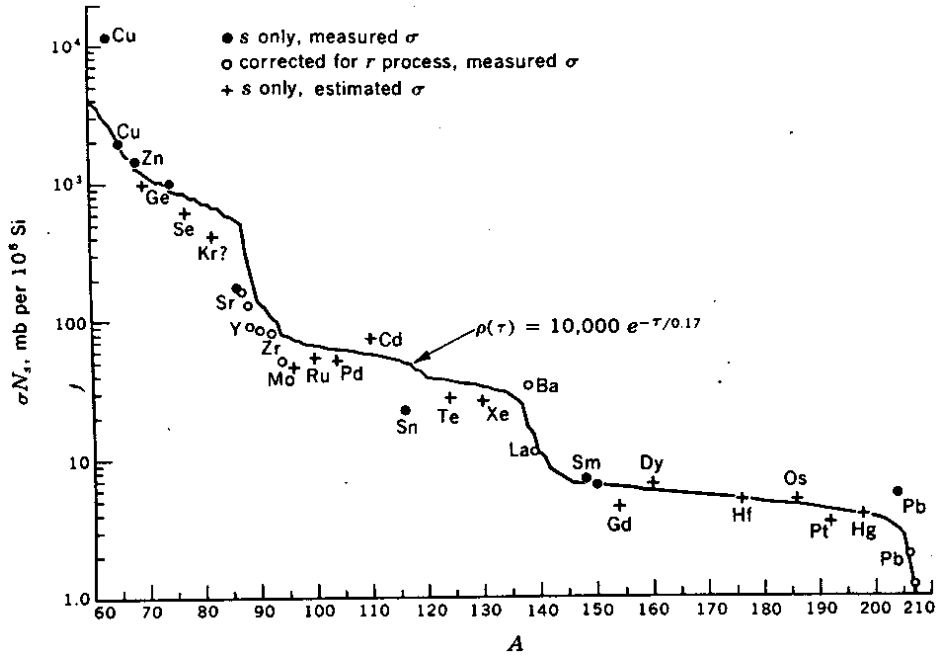

Figure 5.2: The σN-curve for solar system s-process material. The product of n-capture cross section σ times the abundance per 10^6 Si atoms is plotted against mass number A. The solid curve is the calculated result of an exponential distribution of neutron exposures. Figure from CLAYTON. Compare this figure to Fig. 5.13 for r-process elements.

• properties of the solution:

differential equation: self-regulation!

$$\text{if } N_A > \frac{\sigma_{A-1}}{\sigma_A} N_{A-1} \Rightarrow \frac{dN_A}{dt} < 0$$

$$\text{if } N_A < \frac{\sigma_{A-1}}{\sigma_A} N_{A-1} \Rightarrow \frac{dN_A}{dt} > 0$$

$$\Rightarrow \boxed{\sigma_A N_A \simeq \sigma_{A-1} N_{A-1}} \quad \text{(for } A \text{ non-magic!)}$$

$\rightsquigarrow$ testable without astrophysical knowledge $\rightarrow \sigma N$-curve (Fig. 5.2)

note: only "pure s-nuclei" should be considered (see below)

• Average number of neutrons captured:

$$n_c := \sum_{A=57}^{209} (A - 56) \frac{N_A - N_{A,i}}{N_{56,i}}$$

NB: the index i refers to: initial value

$\Rightarrow$ find abundance distribution as $f(n_c)$
(i.e. as function of number of available neutrons; e.g. Fig. 5.5)

• s-process path in the (N, Z) diagram (Fig. 5.3):

$\rightsquigarrow$ leaves out some n-rich isotopes: define them as **pure r-process** nuclei
$\rightsquigarrow$ leaves out some p-rich isotopes: define them as **pure p-process** nuclei
$\rightsquigarrow$ define **pure s-process** nuclei such that
a) they lie on the s-process path
b) they can not form from β^--decays of nuclei far from the valley of stability

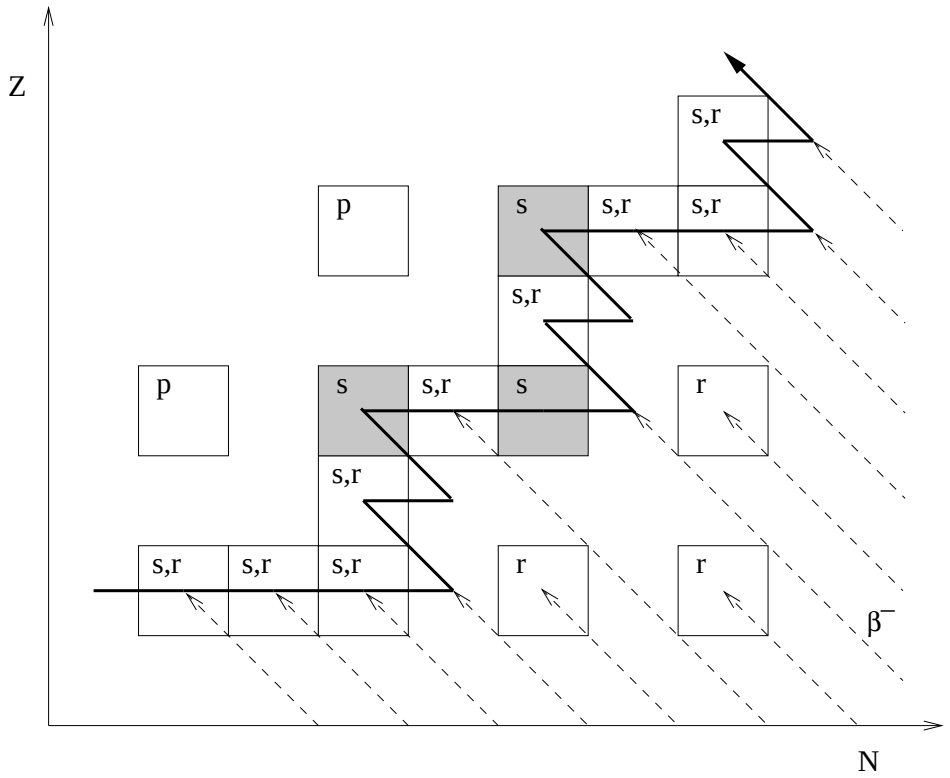

Figure 5.3: Schematic section of the nuclide chart, showing the s-process path as the thick solid line. Dashed lines show the β-decay paths of neutron-rich nuclei produced by the r-process. Shaded boxes show nuclei that are shielded from the r-process.

B. s-process components

- branchings on s-process path

  if $\tau_{\beta^-} \simeq \tau_{\mathrm{s-process}} = \tau_{\mathrm{n-capture}}$ at a given β^- unstable nucleus:

  $\Rightarrow$ - for "small" n-density $\rightsquigarrow$ s-process avoids path through β-unstable nucleus
  - for "large" n-density $\rightsquigarrow$ s-process path goes mainly through this β-unstable nucleus

  $\Rightarrow$ abundance ratios in the split part of the s-process path just after a branching depend on n-density!

  $\Rightarrow$ analysis of $\odot$ abundances at branching $\rightsquigarrow$ n-density!

- for some β-unstable nuclei, τ_{β^-} depends on temperature T

  Once we **know** the n-density (from T-insensitive branchings)

  $\Rightarrow$ analysis of $\odot$ abundances at T-sensitive branching $\rightsquigarrow$ temperature!

Result: $\exists$ two distinctly different s-process components

a) the **main component** ($A \gtrsim 90$): $N_{\mathrm{n}} \simeq 2 \cdot 10^8$ cm^{-3}, $kT \simeq 25$ keV

b) the **weak component** ($56 \leq A \leq 90$): $N_{\mathrm{n}} \simeq 7 \cdot 10^7$ cm^{-3}, $kT \simeq 40$ keV

- Absolute abundances in $\odot$

  $\Rightarrow$ weak component requires $n_c \simeq 20$
  main component requires $n_c \simeq 50$

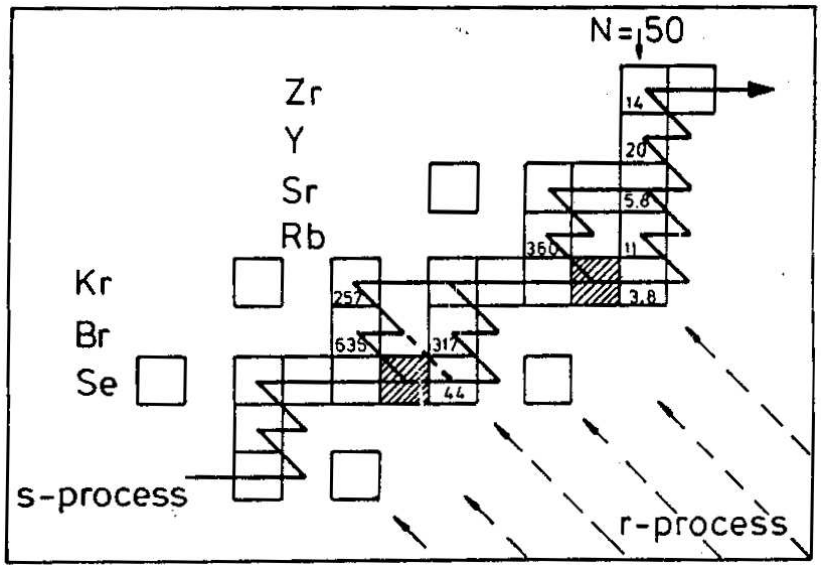

Figure 5.4: Scheme of some branching ratios for the s-process, allowing to determine the neutron densities responsible for the s-process.

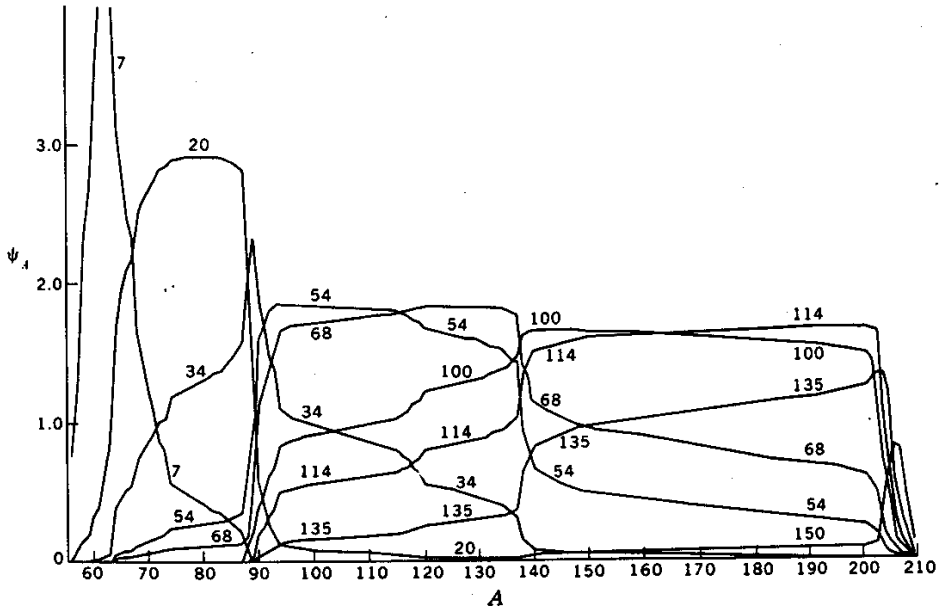

Figure 5.5: Theoretical distributions of $\psi_A = \sigma_A N_A$ versus mass number, for different levels of neutron irradiation as measured by the parameter n_c, the average number of neutrons captured per initial iron seed nucleus. Figure from CLAYTON.

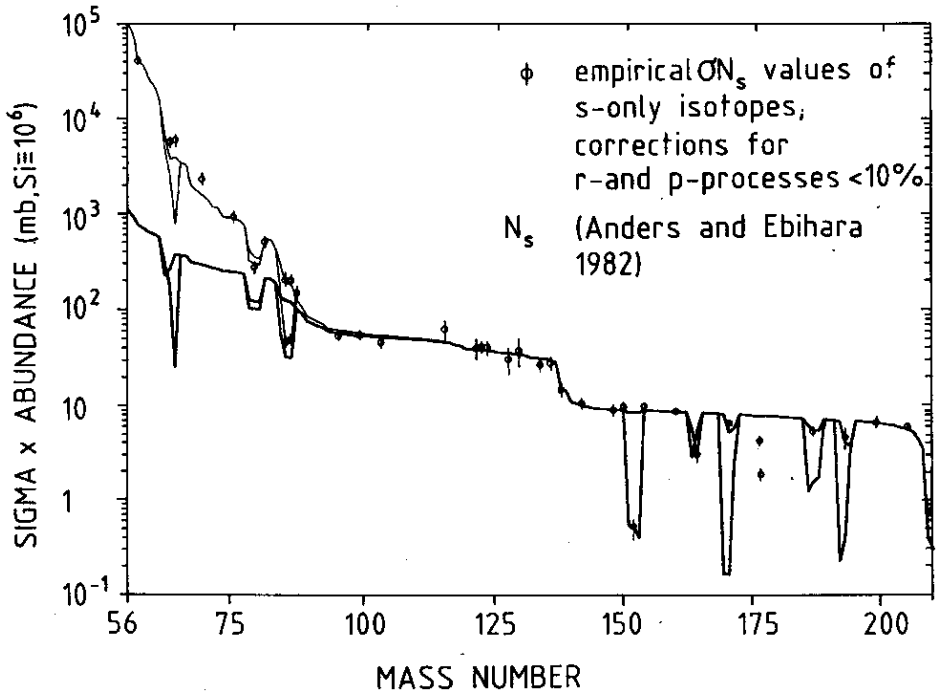

Figure 5.6: As Fig. 5.2, but now showing as the thick solid line the contribution of the main s-process component (due to relatively strong neutron irradiation) responsible for s-process elements with $A > 90$. The thin line shows the weak s-process component (due to weak neutron irradiation on many more Fe seed nuclei) which accounts for the formation of $A < 90$ s-process elements. Figure from Käppeler et al. (1989).

C. Where does the s-process occur?

Only two efficient n-sources in hydrostatic stellar evolution:

1) $^{22}\mathrm{Ne}(\alpha,\mathrm{n})^{25}\mathrm{Mg}$

2) $^{13}\mathrm{C}(\alpha,\mathrm{n})^{16}\mathrm{O}$

- Process 1) occurs naturally during the late helium burning of **massive stars**
  $\rightarrow T \gtrsim 4 \cdot 10^8$ K
  $\rightarrow$ provides right T, N_n for **weak component** (Fig. 5.7)
- Process 2) occurs at the right **temperature** to produce the main component ($2 \cdot 10^8$ K)
  However: the ^{13}C-abundance after hydrogen burning is **insufficient**

  Need: mixing of protons into helium-burning layers $\rightarrow$ $^{12}\mathrm{C}(\mathrm{p},\gamma)^{13}\mathrm{N}(\beta^+\nu)^{13}\mathrm{C}(\alpha,\mathrm{n})$
  $\rightsquigarrow$ requires non-standard mixing process in stars

  Site: thermally pulsing AGB stars (see Fig. 5.8)
  $\rightsquigarrow$ dredge-up of carbon (^{12}C!)
  observational evidence: carbon stars
  $\Rightarrow$ at base of the envelope, p-rich and ^{12}C-rich layers are in contact

  Obs. proof for s-process in AGB stars: spectral lines of Tc have been found!
  Tc: **no** stable isotopes
  ^{99}Tc is on s-process path: $\tau_{1/2} \simeq 10^5$ yr

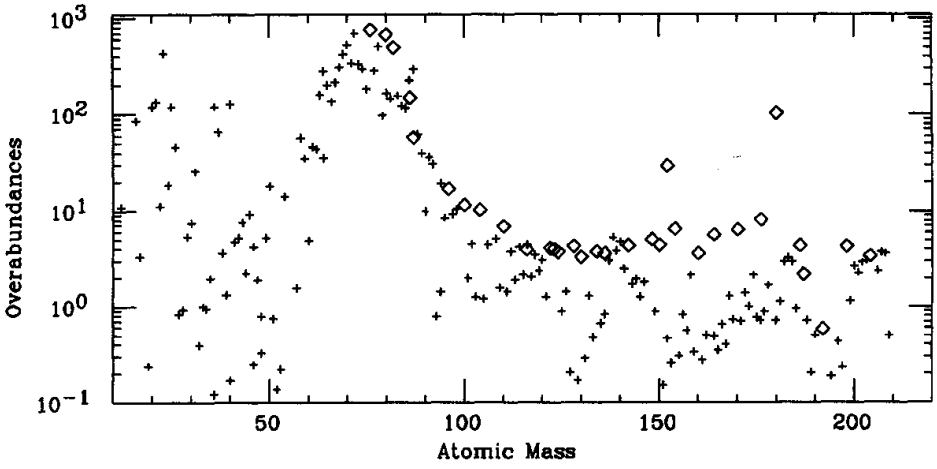

Figure 5.7: Overabundances of isotopes after He burning in a $25\,\mathrm{M}_\odot$star. The s-only isotopes are shown as diamonds. The peak at $A \approx 70$ shows that the weak component of the s-process is produced here. Figure from Raiteri et al. (1991).

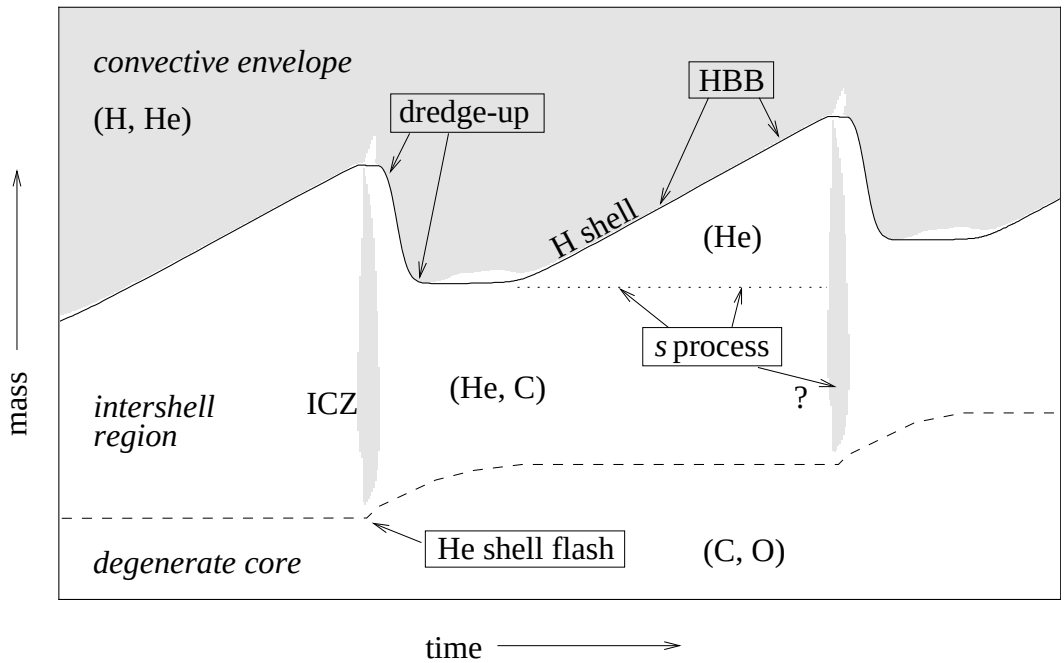

Figure 5.8: Schematic evolution of an AGB star through two thermal-pulse cycles. Convective regions are shown as shaded areas, where "ICZ" stands for the intershell convection zone driven by the He-shell flash. The H-exhausted core mass is shown as a solid line and the He-exhausted core mass as a dashed line. Only the region around the two burning shells is shown, comprising $\sim 0.01\,\mathrm{M}_\odot$. The time axis is highly non-linear: the He shell-flash and dredge-up phases (lasting ~ 100 years) are expanded relative to the interpulse phase ($10^4 - 10^5$ years). Following the dredge-up, a thin "pocket" of ^{13}C forms at the interface between the H-rich envelope and the C-rich intershell region. The location of this ^{13}C pocket is shown as the dotted line. When the temperature reaches 10^8 K, neutrons are released by $^{13}\mathrm{C}(\alpha,\mathrm{n})^{16}\mathrm{O}$ which are captured by the Fe seeds inside the pocket. The s-enriched pocket is ingested into the ICZ during the next pulse, and mixed throughout the intershell region. Some additional s-processing may take place during the He-shell flash due to neutrons released by $^{22}\mathrm{Ne}(\alpha,\mathrm{n})^{25}\mathrm{Mg}$. The s-process material from the intershell region is subsequently mixed to the surface (together with carbon) in the next dregde-up phase.

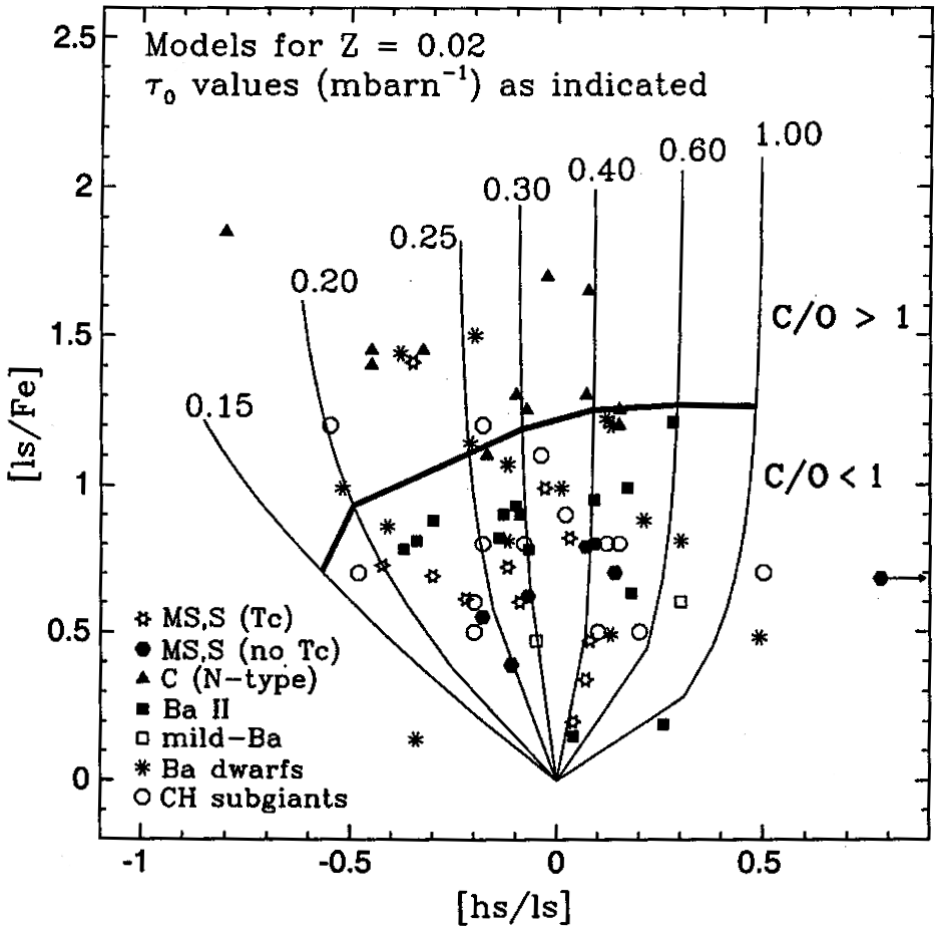

Figure 5.9: Observations of logarithmic ratios [ls/Fe] versus [hs/ls] relative to the Sun, where "ls" stands for light s-process elements (Y, Zr) and "hs" for heavy s-elements (Ba, La, Nd, Sm). The symbols refer to different types of s-enriched stars. Note that carbon stars (stars with C/O > 1; solid triangles) tend to have the highest s-process overabundances. This is in reasonable agreement with theoretical models for nucleosynthesis in AGB stars, shown as solid lines for different values of the mean neutron exposure τ_0. Each curve represents the evolution of envelope composition, for increasing dredge-up of processed material. The points on each curve where the model stars turn into carbon stars are connected by the thick line. Note that individual stars have different mean neutron exposures, but the average of the population corresponds roughly to the value $\tau_0 = 0.28\,\mathrm{mbarn}^{-1}$ that is required to explain the solar system main s-process component. Figure from Busso et al. (1999).

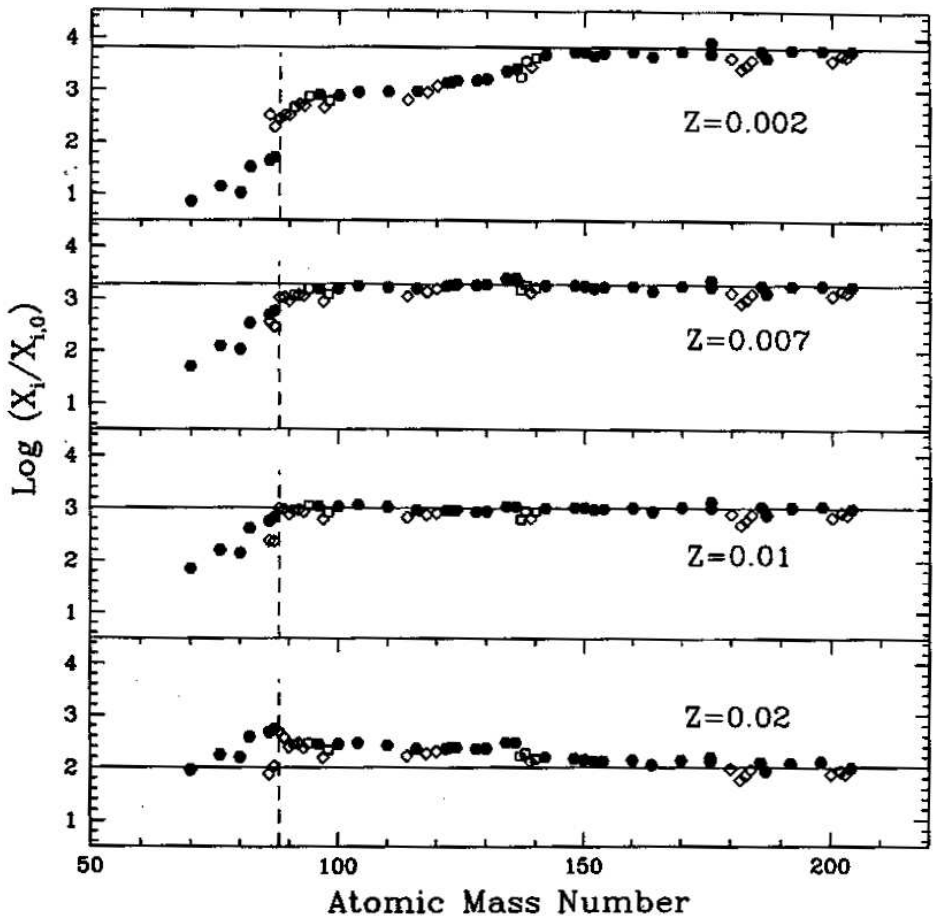

Figure 5.10: Distributions of enhancement factors of s-process isotopes, compared with the initial composition for different Z values in the material cumulatively mixed to the surface of thermally pulsing AGB stars. The models are for a $2\,M_\odot$ star at different metallicities, with the same size of the (artificial) ^{13}C pocket. Solid dots are s-only nuclei. Models with $Z \approx 0.01$ have a flat distribution for $A > 90$, and provide a good approximation to the solar system main s-component; while lower-Z models produce relatively more heavy s-elements ($A > 140$). However, this result depends on the assumed size of the ^{13}C pocket. Compare this to Fig 5.7 for the weak component. Figure from Busso et al. (1999).

Suggestions for further reading

– Chapter 6 of Pagel.
– Chapter 7.3 of Clayton provides a lucid discussion of the phenomenology of neutron-capture nucleosynthesis.
– For an overview of current ideas about the operation of the s-process in AGB stars: Busso, Gallino & Wasserburg (1999), *Nucleosynthesis in Asymptotic Giant Branch Stars*, ARA&A, 37, 219.

Exercises

5.1 Most neutron captures produce energy: $(Z, A) + \mathrm{n} \rightarrow (Z, A+1) + \gamma$.
Why can stars nevertheless not produce significant amounts of energy by n-capture?

5.2 Compare the thermal neutron capture cross section of heavy elements with their geometrical cross sections.
Examples: $\sigma_{\mathrm{n}}(^{88}\mathrm{Sr}) = 5.8\,\mathrm{mb}$, $\sigma_{\mathrm{n}}(^{100}\mathrm{Ru}) = 5.8\,\mathrm{b}$ (for $T \simeq 10^8\,\mathrm{K}$)

5.3 Can $^{22}\mathrm{Ne}(\alpha, \mathrm{n})$ provide enough neutrons to explain the weak component of the s-process? Hint: use the result of exercise 4.13 for the ^{22}Ne abundance. $X(^{56}\mathrm{Fe}) = 1.2 \times 10^{-3}$.

5.4 The following figure is a section of the nuclide chart, showing the s-process path:

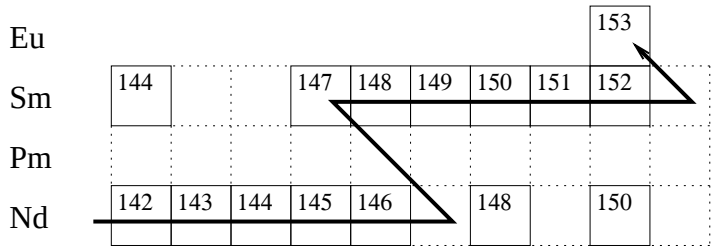

Table 5.1: Samarium isotopes at 30keV

A	N_A,%	σ, millibarns
144	2.87	119 ± 55
147	14.94	1173 ± 192
148	11.24	258 ± 48
149	13.85	1622 ± 279
150	7.36	370 ± 72
152	26.90	411 ± 71
154	22.84	325 ± 61

(a) Identify two pure r-process nuclei, two pure s-nuclei and a pure p-nucleus in the diagram.

(b) Using the pure s-isotopes of Sm, and the data in the Table 5.1, verify the local approximation to the s-process (i.e., $\sigma N \approx$ constant).

(c) Estimate the contribution of the r-process to the abundances of ^{147}Sm and ^{149}Sm.

5.5 Assume $n_c \simeq 20$ for the weak s-process component. By which factor will the weak s-process elements be overproduced in the He-burning layer (i.e., estimate $N_{\mathrm{final}}/N_{\mathrm{initial}}$ for a typical weak s-element in the helium burning zone)?

5.6 Using the result of the previous exercise, estimate the amount of s-process enriched matter which a typical massive star ejects into the interstellar medium. Compare to oxygen.

5.2 The r- and p-process: explosive production

A. How to produce a core-collapse supernova

• $M_{\rm core} \geq M_{\rm Chandrasekhar}$ → all burning stages achieved
→ "Fe"-core
→ end of thermonuclear energy production

• Fe-core loses energy (mostly due to ν-emission)
→ contraction → $T, \rho \uparrow$

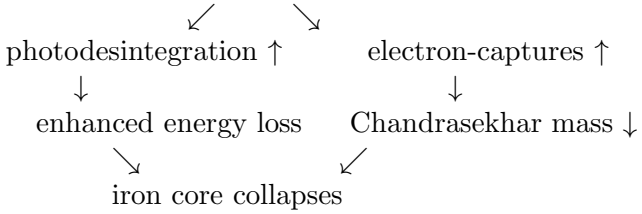

• Fe-core collapse (time scale $\sim$ 1 ms): $T, \rho \uparrow\uparrow$
$\rightsquigarrow$ co-existence of heavy nuclei, $\alpha, \mathrm{p}, \mathrm{n}, \mathrm{e}^-, \nu$
note: $\boxed{\mathrm{p} + \mathrm{e}^- \rightarrow \mathrm{n} + \nu}$ leads to n-rich matter

• central part of Fe-core: bounce at $\rho \simeq \rho_{\rm nucleon} \simeq 10^{14}$ g cm^{-3}
rebounce + ν-momentum deposition
$\Rightarrow$ shock wave forms in former Fe-core, travels outwards, explodes the "envelope"

• conditions close to, but above, the "mass cut" (the separation between proto-neutron star and supernova ejecta):
- n-rich environment
- heavy particles + $\alpha, \mathrm{p}, \mathrm{n}$
- for $T \gtrsim 5 \cdot 10^9$ K: charged particle reactions still possible
however: $T \downarrow$
- for $T \lesssim 5 \cdot 10^9$ K: • charged particle reactions "freeze out"
• $(\mathrm{n}, \gamma), (\gamma, \mathrm{n})$ reactions still possible
• time scale $\sim$ 1 s

B. The static r-process

Assumptions: 1) $T, \rho, N_{\rm n} \equiv$ constant for period $\tau_{\rm r}$
2) start from seed nucleus (e.g. Fe, but can be lighter elements)
3) consider only $(\mathrm{n}, \gamma), (\gamma, \mathrm{n})$ reactions

extremely simplified, but can reproduce main features

• stable seed nucleus (A, Z), N_{n} high, T high

$\Rightarrow (A, Z) + \mathrm{n} \rightarrow (A+1, Z) + \mathrm{n} \rightarrow (A+2, Z) \ldots$

but: the more n-rich the nuclei become

$\rightarrow$ 1) (n, γ) cross sections become smaller

2) (γ, n) cross sections become larger

$\Rightarrow (A, Z) + \mathrm{n} \rightarrow (A+1, Z) + \mathrm{n} \ldots \leftrightarrow (A+i, Z)$

stops at nucleus $(A+i, Z)$, for which the (n, γ)-rate = (γ, n) rate

$\rightarrow$ $\boxed{(\mathrm{n}, \gamma) - (\gamma, \mathrm{n})\text{- equilibrium}}$

• Once $(\mathrm{n}, \gamma) - (\gamma, \mathrm{n})$-equilibrium is reached: wait for β^--decay!

$\rightarrow$ nuclei with $Z+1$ are formed

$\rightarrow$ nuclei with $Z+1$ reach $(\mathrm{n}, \gamma) - (\gamma, \mathrm{n})$-equilibrium

$\rightarrow$ and so on... $\Rightarrow$ r-process path in (N,Z)-plane

• features of r-process path:

- r-process flow is dammed up at magic n-numbers:

(γ, n)-cross section just past a magic n-number is particularly large!

$\rightsquigarrow$ pile-up of nuclei at magic n-number

$\rightsquigarrow$ r-process path proceeds at constant N for a while

- flow stops at high Z due to n-induced fission $\rightarrow$ cycling back to lower Z values

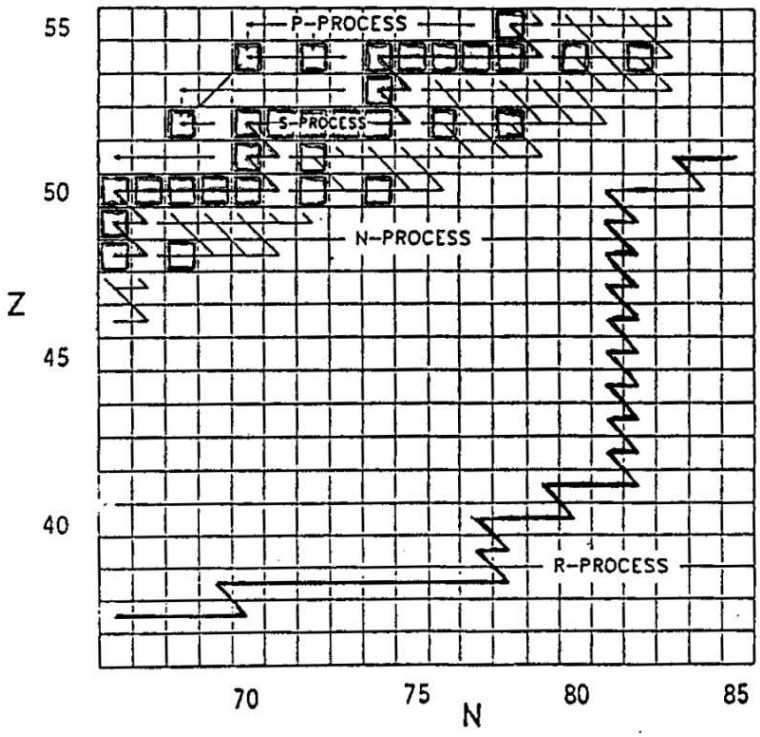

Figure 5.11: Part of the nuclear chart, showing the s-process path through the valley of stability, and the r-process path far from the valley. Note the extended vertical part of the r-process path at the magic neutron number $N = 82$.

- after the period τ_{r}: n-flow assumed to stop
  - $\rightarrow$ nuclei decay towards valley of stability
    - mostly β^--decays
    - α-decays for $A \gtrsim 210$
    - (β-delayed fission, β-delayed n-emission)
  - $\Rightarrow$ abundance peaks at magic n-number **during** r-process $\rightsquigarrow$ abundance peaks to left of the s-process peaks **after** r-process (in solar system abundances)
- distance of r- and s-peaks in solar system abundances
  - $\rightarrow$ distance of the r-process path from valley of stability (at closed n-shells)
  - $\rightarrow$ order of magnitude of $N_{\mathrm{n}} : N_{\mathrm{n}} \simeq 10^{20}$ cm^{-3}

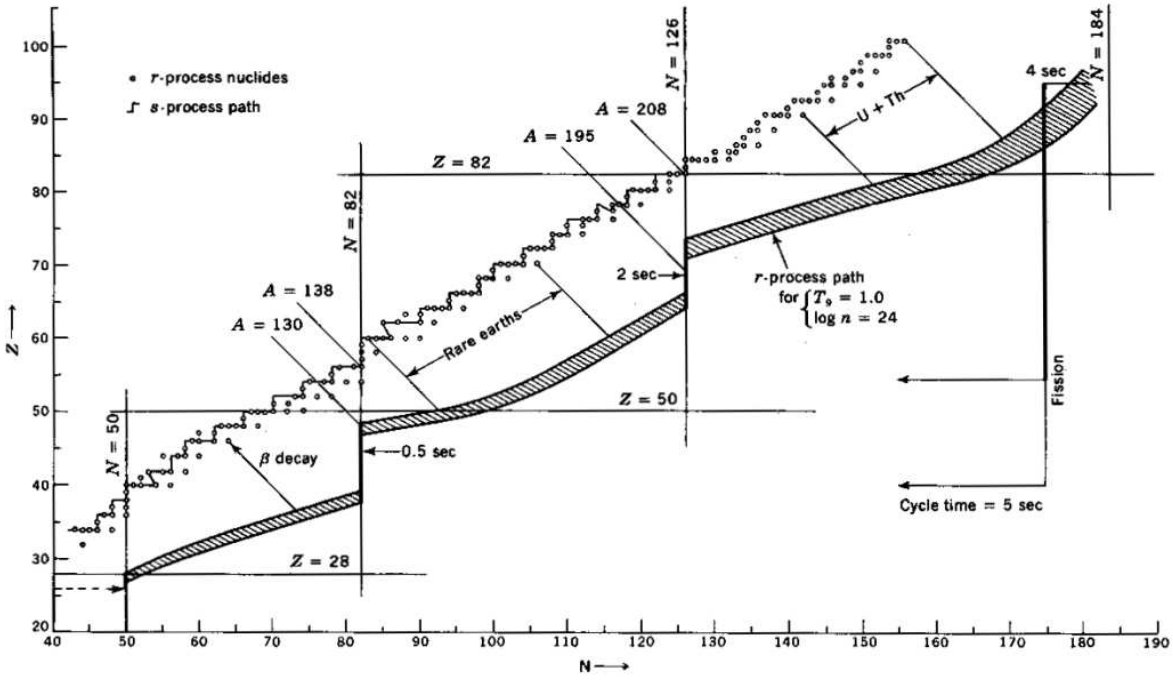

Figure 5.12: Neutron-capture path for the r-process compared to the s-process. The r-process path was calculated for $T = 10^9$ K and a neutron density $n_{\mathrm{n}} = 10^{24}$ cm^{-3}. Neutron capture flows upward along the shaded band until neutron-induced fission occurs at $A = 270$. Figure from Clayton.

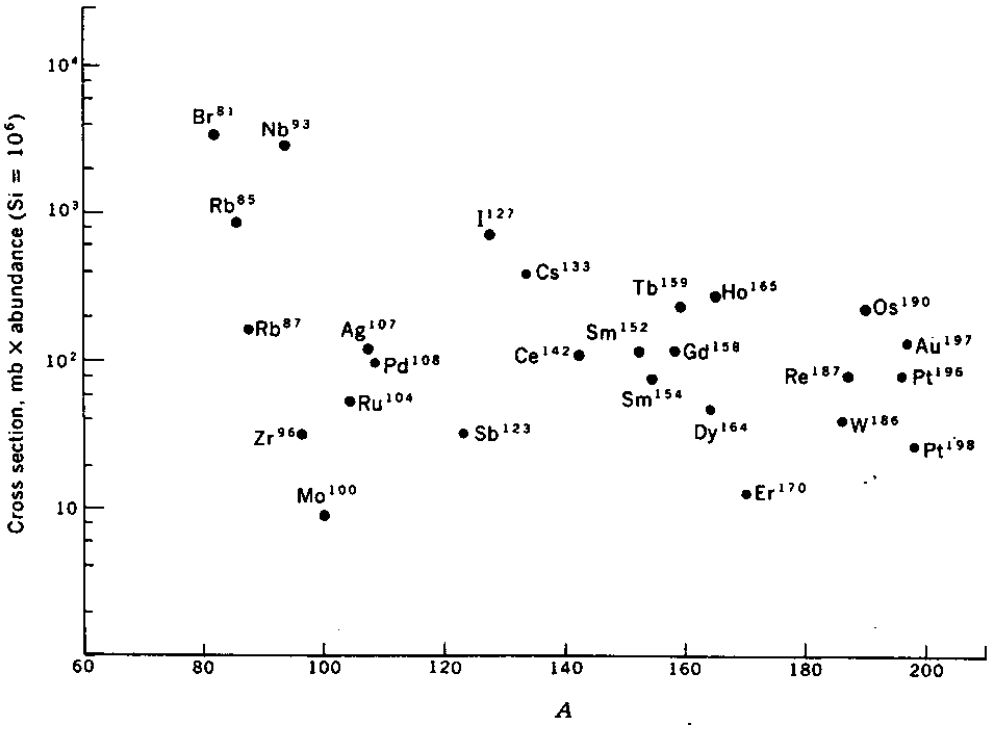

Figure 5.13: The σN-curve for solar system r-process material. Compare to Fig. 5.2 for s-process elements. Figure from CLAYTON.

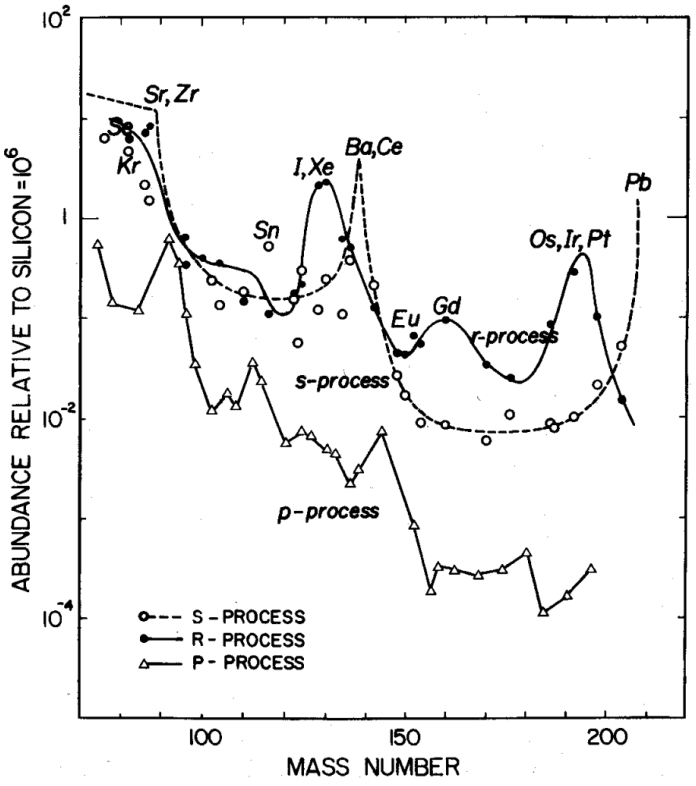

Figure 5.14: Abundance distribution in the solar system for r- and p-process (solid lines) compared to s-process (dashed curve). Figure adapted from Cameron (1982).

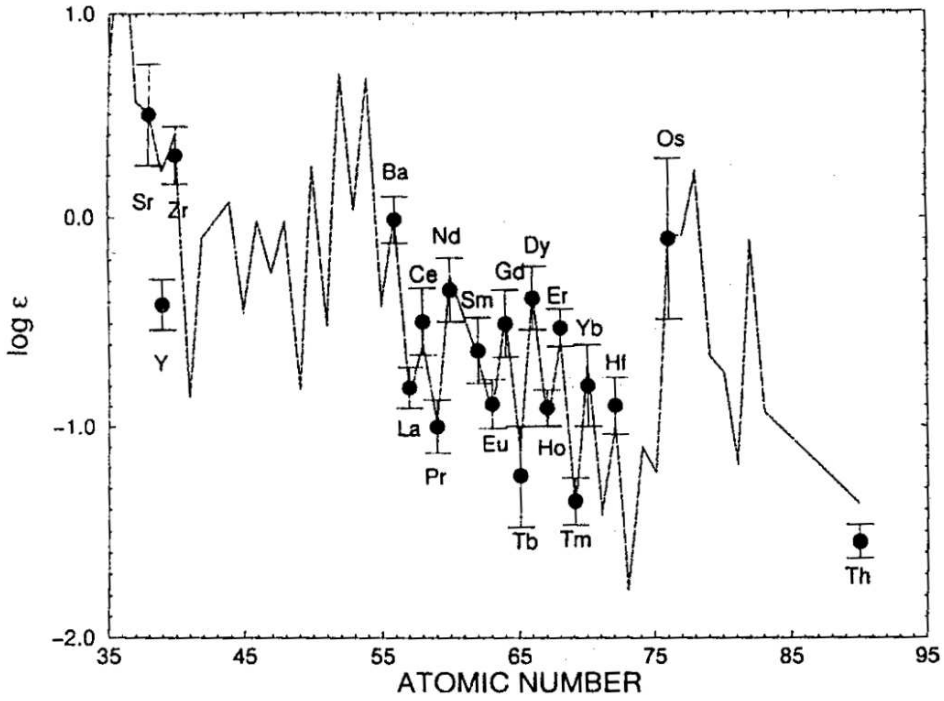

Figure 5.15: Observed abundances of heavy elements in an extremely metal-poor star (dots with error bars) superimposed on a graph showing the solar-system r-process abundances scaled down to the appropriate metallicity. The striking agreement indicates that the heavy r-elemets have been synthesized with solar proportions already early on in the chemical evolution of our Galaxy.

C. The r-process site

- conditions implied by static r-process considerations
  - $\rightsquigarrow$ time scales of **seconds**
  - $\rightsquigarrow$ explosive events
- two possibilities
  1) same environment as s-process, i.e.:
     He-burning
     $\rightsquigarrow$ He-burning shell (only He-burning site in a pre-supernova star)
     but liberation of neutrons on explosive time scale
     $\rightsquigarrow$ supernova shock wave travelling through He-layer
     Problem: two possible neutron sources:
     $^{13}\mathrm{C}(\alpha,\mathrm{n})^{16}\mathrm{O}$ and $^{22}\mathrm{Ne}(\alpha,\mathrm{n})^{25}\mathrm{Mg}$
     neither ^{13}C nor ^{22}Ne is expected to be abundant enough to produce enough neutrons
     $\rightsquigarrow$ need of mixing process which brings protons into He-shell **before** supernova explosion
     $\rightsquigarrow$ $^{12}\mathrm{C}(\mathrm{p},\gamma)^{13}\mathrm{N}(\mathrm{e}^{+}\nu)^{13}\mathrm{C}$ (analogous to s-process in AGB stars)

2) close to "mass-cut" in core collapse supernova (cf. **A**)
$\rightsquigarrow$ r-process here **not** describable by steady neutron flow
instead: $\rho \uparrow\uparrow$ $\rightsquigarrow$ a) heavier nuclei form
b) electron captures $\rightarrow$ matter becomes neutron rich

Problem: current models of core collapse supernovae do not obtain solar system abundance pattern!

- in particular, nuclei with $A \lesssim 110$ are **not** abundantly formed in supernova models.

- open questions:
  - are there several r-process components? (note: there are several s-process components!)
  - why are s- and r-abundance peaks equally high in the solar system abundance curve?
- observational facts:
  - r-process is **primary**: very metal poor stars show enrichment in pure r-nuclei
  - for high A ($\gtrsim 150$), the r-process pattern seems unique: very metal poor stars ($Z \lesssim 10^{-4} Z_\odot$) show exactly the same abundance pattern as the Sun!

D. The p-process

- p-process nuclei are: a) n-poor
  b) 10 ... 100 times rarer than s/r-nuclei

  $\rightsquigarrow$ nuclei are made out of s/r-nuclei
  $\rightsquigarrow$ as (p,γ)-reactions are prohibited by huge Coulomb-barrier $\Rightarrow (\gamma,\mathrm{n})$ reactions!
- for (γ,n) to be important
  $\rightsquigarrow$ 1) high temperature (need photons of some MeV energy!)
  2) "low" density to suppress immediately (n,γ)
  3) pre-enriched s-process
  $\Downarrow$
  explosive C, O-burning in very massive stars
- realistic detailed stellar models (cf. Rayet et al 1995)
  $\Rightarrow$ a) p-nuclei in the whole mass range $74 \lesssim A \lesssim 200$ can be produced when the supernova shock travels through the C/O-layers in stars of 12...25 $M_\odot$
  b) no strong trends with initial mass are found
  c) the pre-enrichment of s-nuclei is essential

however

d) only 60% of the p-nuclei are co-produced. In particular, Mo and Ru p-isotopes, but also others, are underproduced (i.e. **destroyed**!)

e) the p-isotopes which are produced are produced by a factor of 3 ... 4 only, i.e. clearly less than oxygen (factor ~ 10).

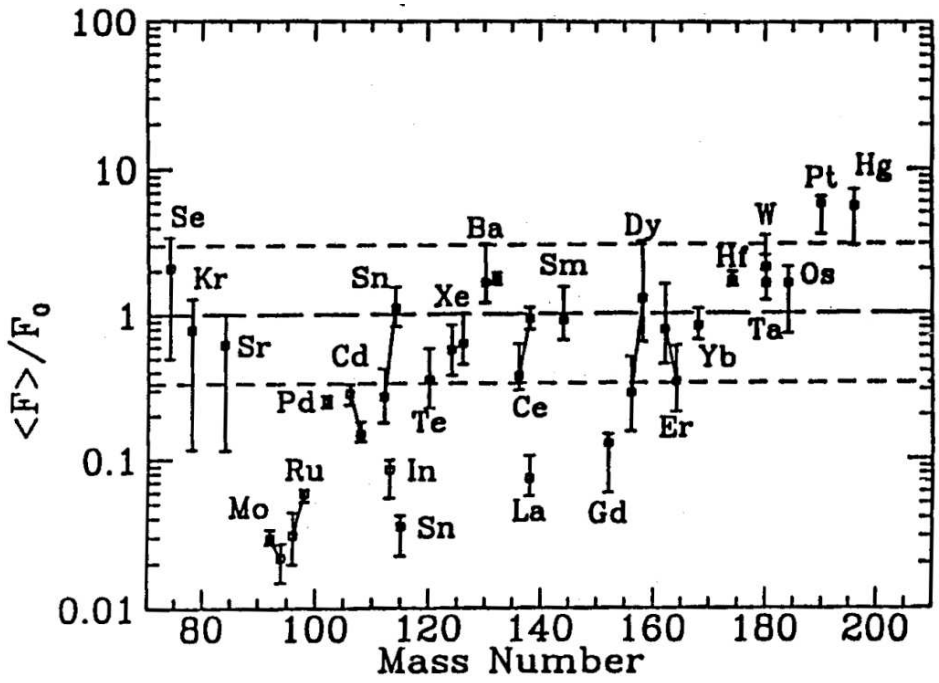

Figure 5.16: Production factors of p-nuclei in the C/O-rich layers of a very massive star after the supernova explosion. Note that especially the heavy p-nuclei are nicely produced. From Rayet et al. (1995).

Exercises

5.7 Identify 2 pure r, s and p nuclei. Chose the 2 pure s-nuclei such that you can predict the ratio of their abundances in the universe.

5.8 Discuss for s-, r- and p-process, whether they are primary or secondary.

5.9 In an extremely metal-deficient star, thorium is found to be less abundant by 0.2 dex than it would be if the solar-system r-process pattern could be extrapolated to thorium. Does this constrain the age of the universe? (N.B. The half-life of thorium is 14 Gyr; the age of the solar system is 4.6 Gyr.)

5.10 It is (almost) impossible, to measure *isotopic* abundances of the heavy elements ($A \gtrsim 56$) in stars. Which *elements* can one investigate in order to learn something about r- and s-process abundances in stars of various metallicities?

Chapter 6

Thermonuclear supernovae

A. Thermonuclear runaway

white dwarf:

$P = K\rho^{5/3}$ ($\rightsquigarrow T \downarrow$ with time in white dwarfs!)

$\rightarrow P \neq f(T)$

Assume $\epsilon_{\rm nuc} \uparrow$ in **normal** star (ideal gas)
$\rightarrow T \uparrow$
$\rightarrow P = \frac{\Re}{\mu}\rho T \quad \uparrow$
$\rightarrow$ Expansion
$\rightsquigarrow \rho \downarrow, \quad P, T \downarrow, \quad \epsilon_{\rm nuc} \downarrow$
$\rightarrow$ self-regulation

Assume $\epsilon_{\rm nuc} \uparrow$ in degenerate star
$\rightarrow T \uparrow$
$\rightarrow P$ remains unchanged !
$\rightarrow \epsilon_{\rm nuc} \uparrow\uparrow$
$\rightarrow T \uparrow\uparrow$
$\rightarrow$ thermonuclear runaway

B. Nuclear statistical equilibrium (NSE)

NSE defined by: all strong and electromagnetic interactions are exactly balanced by their reverse interactions

i.e. (p, γ) reactions are exactly balanced by (γ, p)
(n, γ) reactions are exactly balanced by (γ, n)
etc.

- for $T \lesssim 5 \cdot 10^9$ K: no NSE, but build-up of heavier nuclei from lighter ones
- for higher temperatures: NSE possible (depending also on density, time scale involved)

NSE: abundances **not** determined any more by reaction rates, but by **binding energies**

i.e. $$\frac{N(A-1,Z)N_{\rm n}}{N(A,Z)} = \Theta \cdot \exp\left(-\frac{Q_{\rm n}}{kT}\right)$$

with $$\Theta = \frac{2G(A-1,Z)}{G(A,Z)} \cdot \left(\frac{2\pi\mu kT}{h^3}\right)^{2/3}$$

and $Q_{\rm n}$ = neutron binding energy in nucleus (A,Z).

and $$\frac{N(A-1,Z-1)N_{\rm p}}{N(A,Z)} = \Theta' \cdot \exp\left(-\frac{Q_{\rm p}}{kT}\right)$$

- Such equations can be written down for all nuclei

  $\rightarrow$ all abundances can be determined by specifying $\boxed{\mathrm{T},\ \rho, \overline{Z/N}}$

- Timescales are usually so short that β-decays can be **neglected** (i.e. $\overline{Z/N}$ = const.).

- Exploding white dwarfs:

  initial composition: ^{12}C, ^{16}O, $\overline{Z}/\overline{N} = 1$

$$\boxed{\text{NSE} \Rightarrow {}^{56}\text{Ni}}$$

Exercises:

6.1 Assume a Chandrasekhar-mass white dwarf is completely incinerated by a carbon detonation. Assume further that the detonation energy is completely transformed into kinetic energy. What is the average expansion velocity of the corresponding supernova? (Hint: use binding energies as given in Table 2.1.)

Compare the energy release by the detonation with the energy released by a core-collapse supernova. ($R_{\rm neutron-star} \simeq 10$ km, $R_{\rm WD} \simeq 0.01 R_\odot$)

6.2 Assume the light curve of thermonuclear supernovae is dominated by the release of energy in the radioactive decay: $^{56}\text{Ni} \xrightarrow{6\,\text{d}} {}^{56}\text{Co} \xrightarrow{77\,\text{d}} {}^{56}\text{Fe}$. How bright is the supernova initially, how bright after 390 days?

(NB: $\sim 0.6 M_\odot$ of Ni is produced per supernova. Decay energies: ^{56}Ni: 1.72 MeV, ^{56}Co: 3.59 MeV per decay.)

6.3 What can one conclude from the occurence of Type Ia supernovae in elliptical galaxies? Are there implications for the [O/Fe] vs. [Fe/H] diagram for stars in our galaxy?

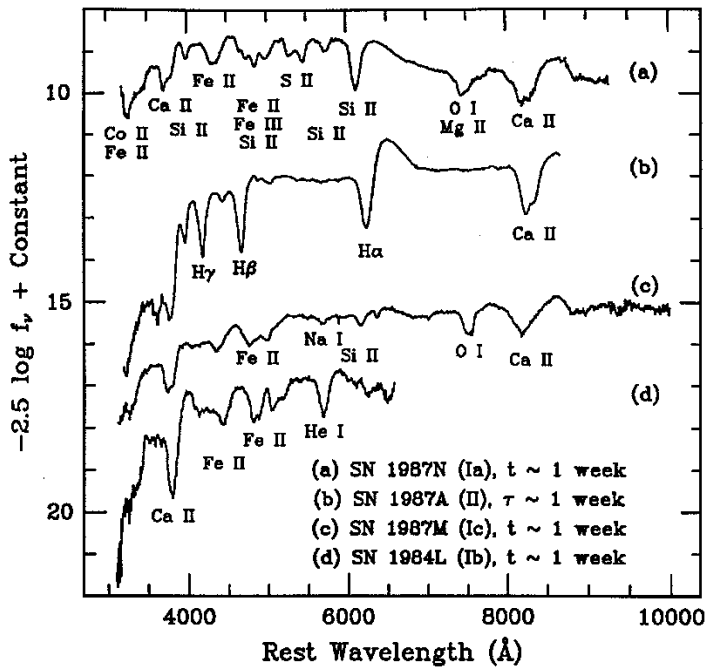

Figure 6.1: Spectra of supernovae about one week after maximum light, showing the distinctions between the different (sub)types. Note the absence of hydrogen in the SN Ia spectrum (upper curve) and the presence of Si, Ca, Fe and O. Figure from Filippenko (1997).

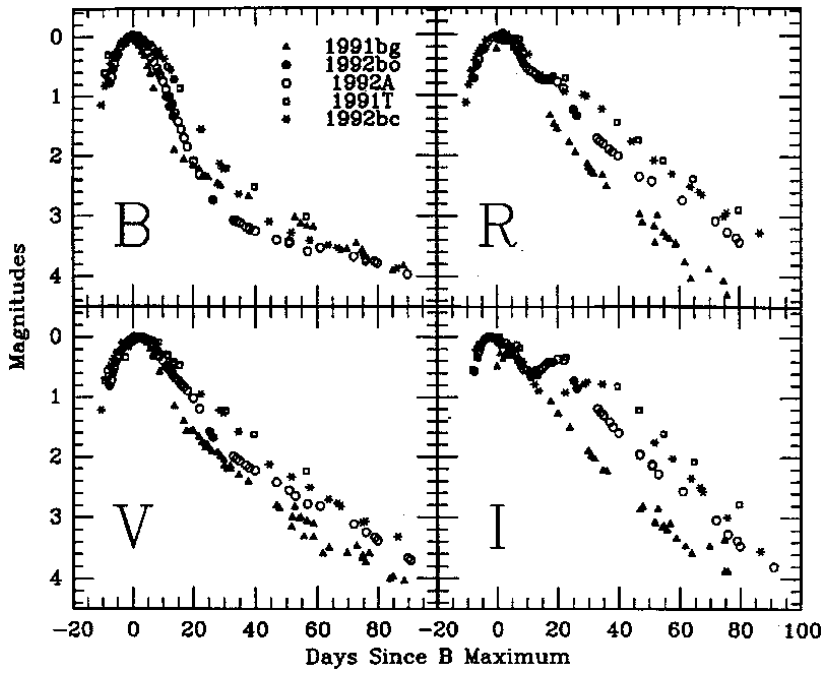

Figure 6.2: Lightcurves of several bright Type Ia supernovae. Notice the change in slope after ≈ 20 days, in particular in the B-band lightcurve, due to the transition from ^{56}Ni decay ($\tau = 6\,\mathrm{d}$) to ^{56}Co decay ($\tau = 77\,\mathrm{d}$). Figure from Filippenko (1997).

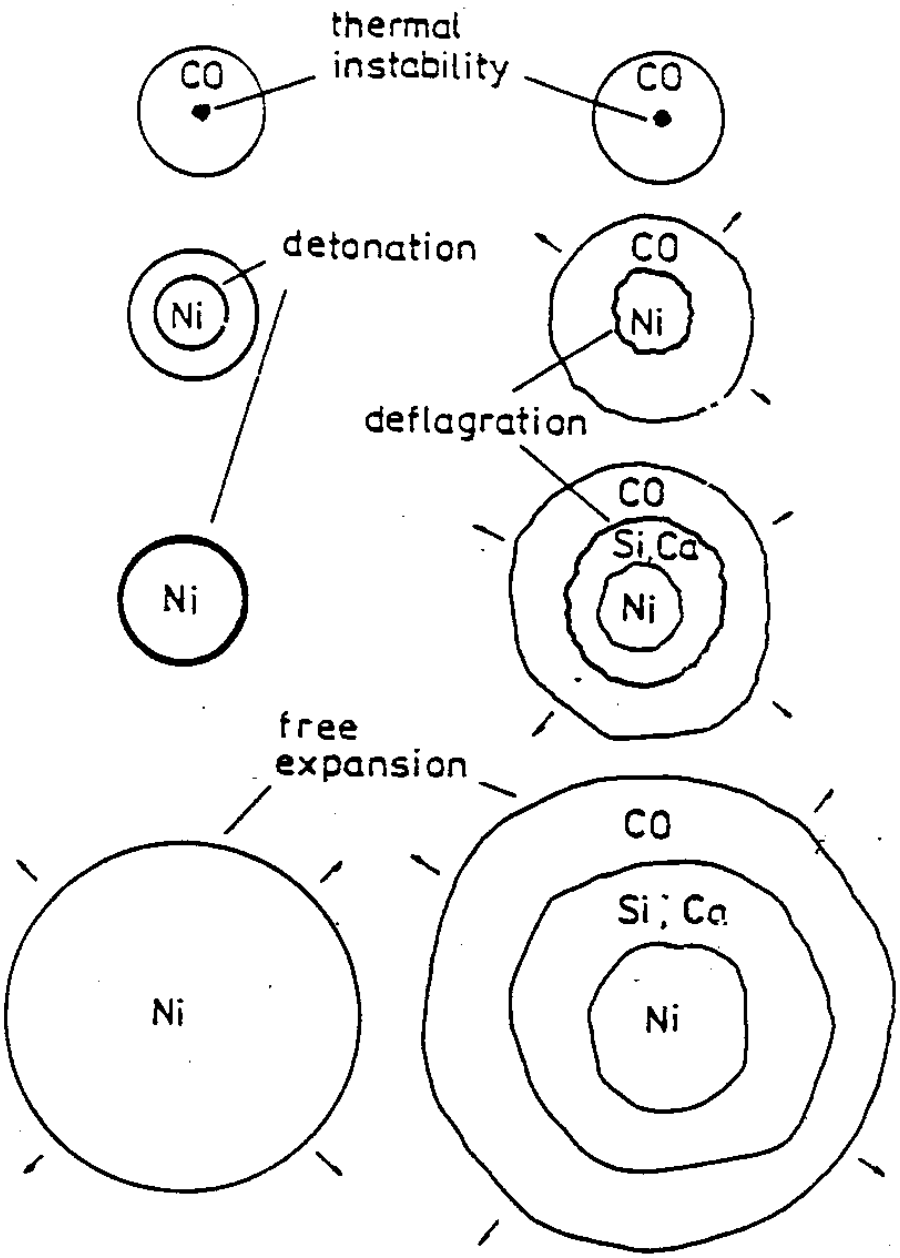

Figure 6.3: Schematic comparison of the two ways a Chandrasekhar mass C/O white dwarf can explode. In a *detonation (left)*, the supersonic burning front incinerates the whole white dwarf before degeneracy is lifted and pressure forces can explode the star. In a *deflagration (right)*, the sub-sonic burning front leaves the white dwarf time to expand *during* the passage of the burning front through the star. As a result, the outer layers of the white dwarf are not burnt. The deflagration seems to be favoured in nature, because Si, Ca, O and C are observed in Type Ia supernovae.

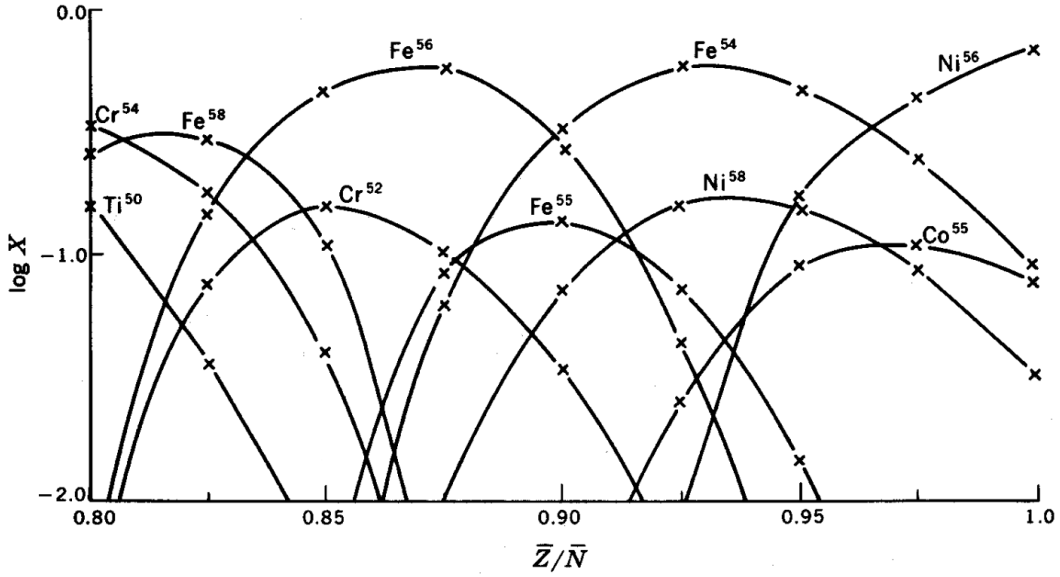

Figure 6.4: Nuclear statistical equilibrium abundances for $T = 4\times10^9$ K and $rho = 10^6$ g/cm^3 as a function of the average proton-to-neutron ratio. The right part of the diagram applies to exploding C/O layers. Figure from Clayton.

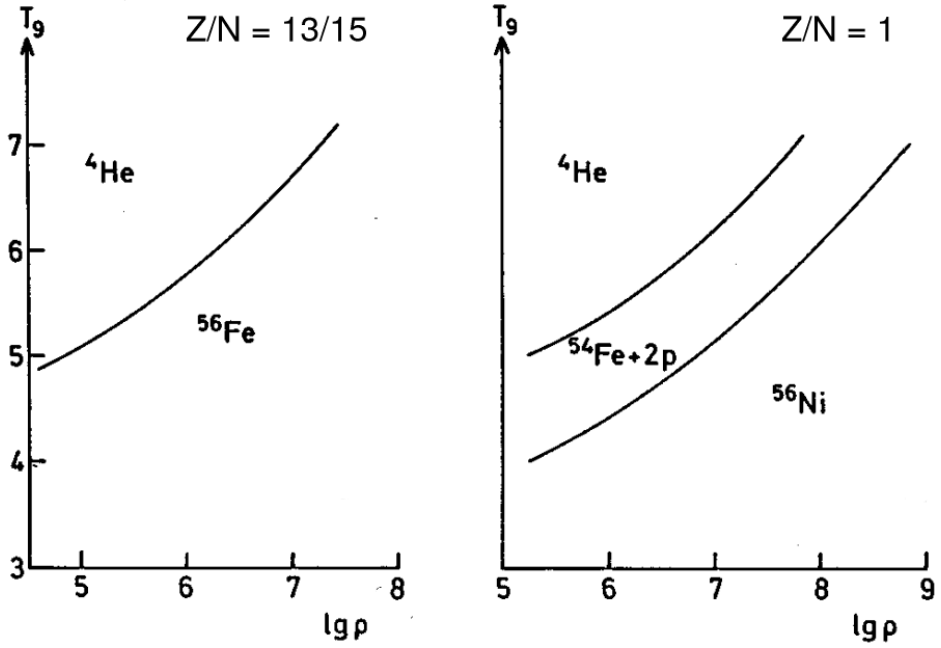

Figure 6.5: The dominant nucleus for NSE abundances in the $T-\rho$ diagram, for two average neutron-to-proton ratios as indicated. Figure from Kippenhahn & Weigert (1990).

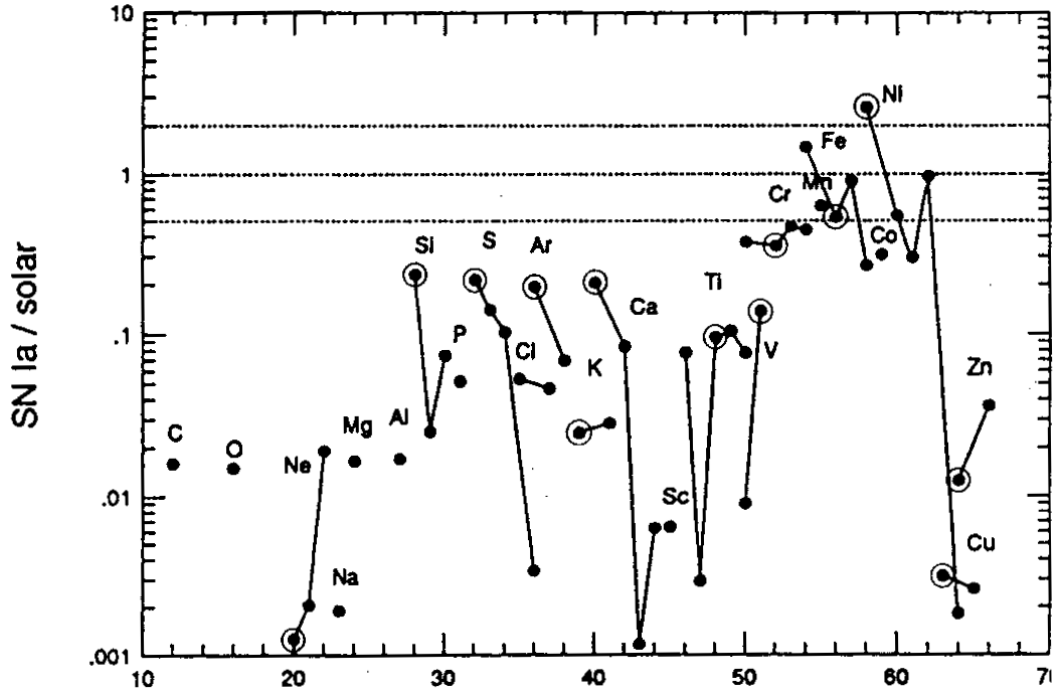

Figure 6.6: Production factors in a typical carbon-deflagration supernova. The abundances are shown relative to their solar values, with the ratio normalized to 1 for ^{56}Fe. The Fe and Ni isotopes are the most over-abundant. Compare with Fig. 4.24, and notice how nicely Type Ia and Type II supernovae complement each other.

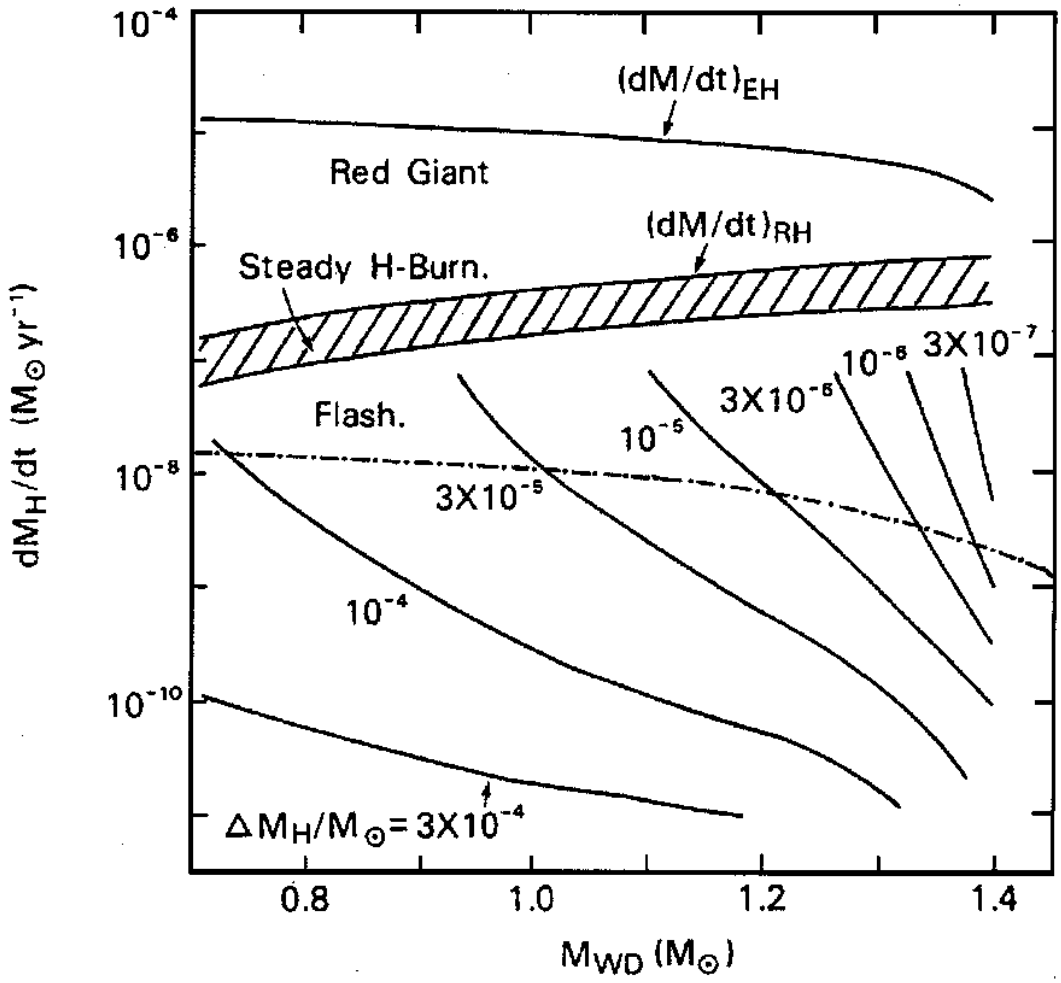

Figure 6.7: Critical mass transfer rates for hydrogen-accreting white dwarfs, as a function of the WD mass. Only for a small range of mass transfer rates (hatched area) can the material quietly burn on the WD surface, and thus lead to a growth of the WD mass towards the Chandrasekhar mass. Figure from Kahabka & van den Heuvel (1997).

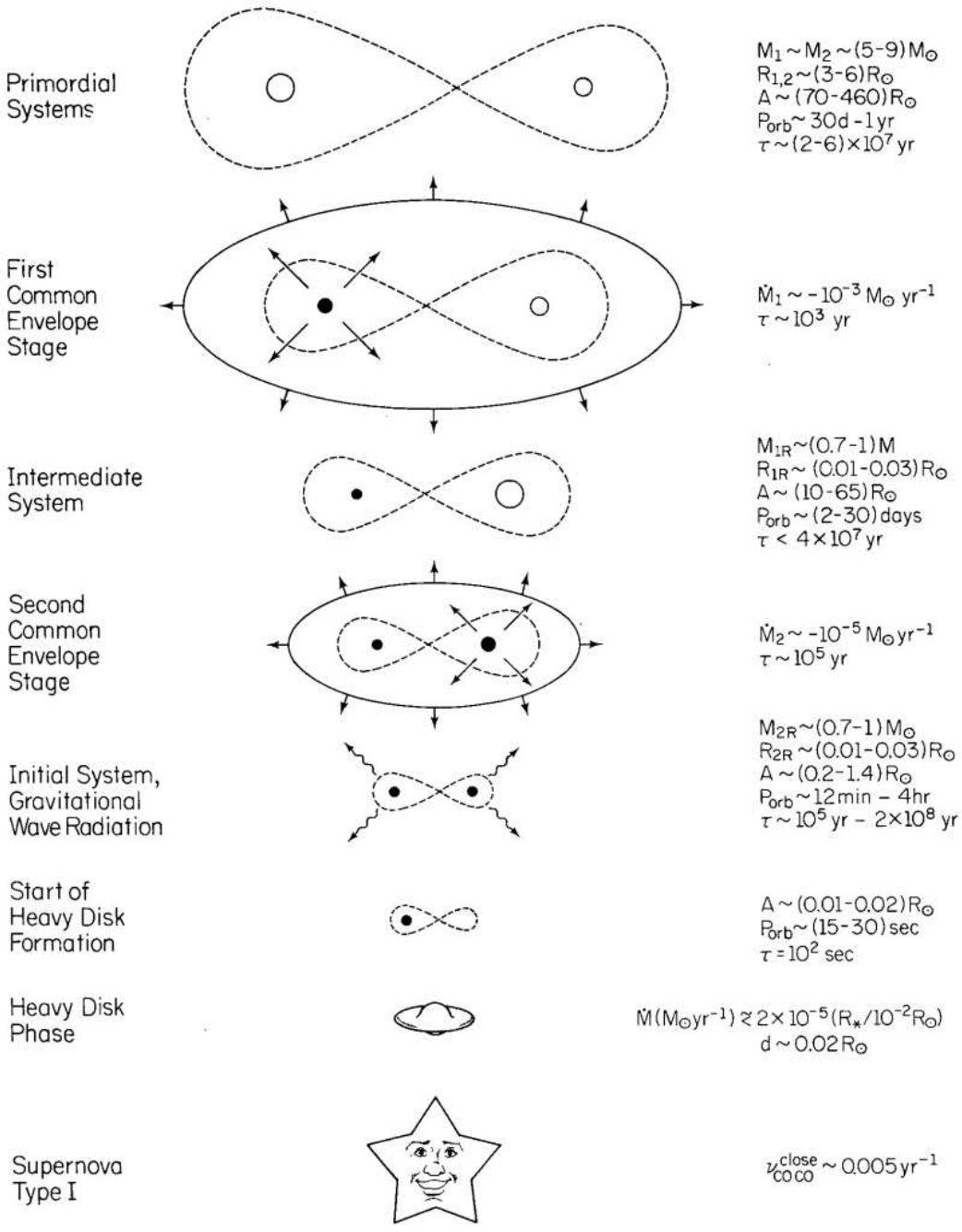

Figure 6.8: Double-degenerate scenario for Type Ia supernovae, according to which such an explosion is due to the merging of two C/O white dwarfs with a total mass above the Chandrasekhar mass. Figure from Iben & Tutukov (1984). This scenario is controversial at present.

Chapter 7

The origin of Li, Be and B

A. The problem

• previous chapters: big bang + stellar nucleosynthesis
⇒ abundances of **almost** all nuclei

clearest exception: ^{6}Li, ^{9}Be, ^{10,11}B
(reminder: ^{7}Li **was** produced in the big bang; cf. Chapter 3)

reason: stability gaps at mass number 5 and 8
⇝ pp-chain produces mainly ^{4}He,
He-burning bypasses Li Be B-region ⇝ ^{12}C
even if LiBeB were produced, they would be completely destroyed in the stellar interior due to proton-capture reactions

⇒ LiBeB-abundances expected from stellar models are many orders of magnitude smaller than **observed** LiBeB-abundances, in the solar system and elsewhere.

⇒ LiBeB cannot be of stellar origin

• Since ^{6}Li, ^{9}Be, ^{10,11}B are also **not** produced in the big bang
⇝ postulation of an "l-process" (l for light elements) **outside stars**
(Burbidge et al, ∼ 1960)

• clearly: l-process requires low temperature environment ($T \lesssim 10^6$ K)
such that LiBeB are not immediately destroyed

B. Galactic Cosmic Rays

∼ 1970: it was found that LiBeB are ∼ $10^6\times$ more abundant in cosmic rays than in solar system!

What are Galactic Cosmic Rays?
GCR: highly energetic particles

- mostly p, α; 1% heavier nuclei
- stripped of their electrons

- continuous energy distribution : $\Phi(E) \sim E^{-x}$
  $x \simeq 2.5 \ldots 2.7$
- most measured particles have $E = 100 \ldots 3000$ MeV
- measurable only above the Earth atmosphere
- $E \lesssim 10^9$ MeV $\Rightarrow$ **galactic origin**
- $E \lesssim 10^9$ MeV: particles confined in Galaxy due to magnetic field for $\tau \simeq 10^7$ yr

• Origin of GCR:
still uncertain, but likely:
particles accelerated in magnetic shock fronts of supernova remnants (Fermi-processes)

• Abundance distribution: "similar" to solar system abundances but large **overabundance of LiBeB** (Fig. 7.1)

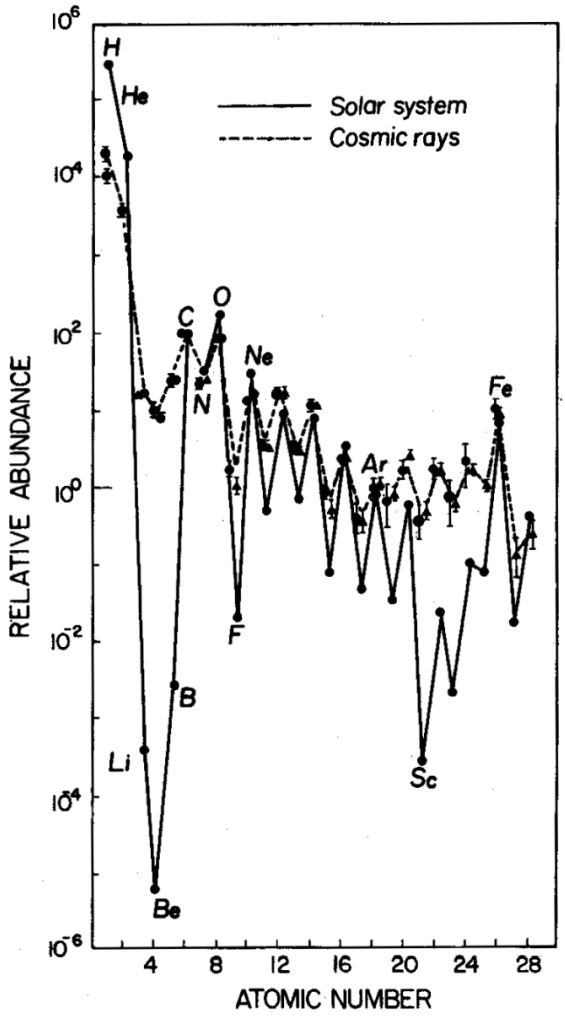

Figure 7.1: Comparison of the elemental abundance distribution in cosmic rays measured in earth orbit (dashed line) and solar system material (solid line). Note the rather good agreement of both compositions, except for the extreme overabundance of Li, Be, B in cosmic rays, by six orders of magnitude. Figure from Rolfs & Rodney (1988).

C. Production of Li, Be, B via spallation

1) Cosmic ray source $\rightsquigarrow$ "original" cosmic ray particles

2) Original cosmic ray particles interact with ISM particles

3) Formation of "additional" cosmic ray particles of different kinds

- This "interaction" is typically a spallation reaction
  := reaction with several particles in the exit channel.
  i.e., heavier nuclei are literally **broken up into pieces**.

Example: $^{12}\mathrm{C} + \mathrm{p}$ reaction with relative kinetic energy of 1 GeV:

$^{12}\mathrm{C} + \mathrm{p} \rightarrow {}^{11}\mathrm{B} + 2\mathrm{p}$	$\mathrm{Q} = -16.0$ MeV
$\rightarrow {}^{10}\mathrm{B} + 2\mathrm{p} + \mathrm{n}$	-27.4
$\rightarrow {}^{10}\mathrm{B} + {}^{3}\mathrm{He}$	-19.7
$\rightarrow {}^{9}\mathrm{Be} + 3\mathrm{p} + \mathrm{n}$	-34.0
$\rightarrow {}^{9}\mathrm{Be} + {}^{3}\mathrm{He} + \mathrm{p}$	-26.3
$\rightarrow {}^{7}\mathrm{Li} + 4\mathrm{p} + 2\mathrm{n}$	-52.9
$\rightarrow {}^{7}\mathrm{Li} + {}^{4}\mathrm{He} + 2\mathrm{p}$	-24.6
$\rightarrow {}^{6}\mathrm{Li} + 4\mathrm{p} + 3\mathrm{n}$	-60.2
$\rightarrow {}^{6}\mathrm{Li} + {}^{4}\mathrm{He} + 2\mathrm{p} + \mathrm{n}$	-31.9
$\rightarrow {}^{6}\mathrm{Li} + {}^{4}\mathrm{He} + {}^{3}\mathrm{He}$	-24.2

- high negative Q-values hardly matter for energy balance
- LiBeB particles created this way have high chance to **survive**
- LiBeB particles will thermalise and become part of normal ISM

- Quantitative estimate for change of abundance of product nucleus i in the ISM:

$$\frac{dN_i}{dt} = \sum_{P,T} N_T N_P \int_0^\infty \Phi(E)\sigma^i_{P,T}(E)dE - \left(\frac{dN_i}{dt}\right)_{\text{stars}}$$

with the energy distribution of cosmic rays $\Phi(E)$, the nuclear cross section for interaction of projectil (GCR) nucleus P with target (ISM) nucleus T with the result i, and N_T, N_P being the abundance of target and projectile. The term $(dN_i/dt)_{\text{stars}}$ takes into account that some of the particles i are incorporated into stars and are lost that way. The summation has to go over all possible target and projectile nuclei.

- Terms in the above summation are largest for large products $N_T \cdot N_P$

  $\Rightarrow$ by far most important are CNO + proton - reactions

• **Assume:** C, O are targets (ISM), p projectile (GCR); [however, see below]

$\sigma(E)$ **not** strongly E-dependent, $\int \Phi(E)dE = F$, $\left(\frac{dN_i}{dt}\right)_{\text{stars}} \simeq 0$

$$\Rightarrow \frac{dN_i}{dt} \simeq \left[N_{\rm C}\sigma^i_{\rm pC} + N_{\rm O}\sigma^i_{\rm pO}\right] F$$

$$\rightsquigarrow \frac{N_i}{\rm H} \simeq \left[\frac{N_{\rm C}}{\rm H}\sigma^i_{\rm pC} + \frac{N_{\rm O}}{\rm H}\sigma^i_{\rm pO}\right] \cdot F \cdot \tau_{\rm galaxy}$$

With $F = 8.3$ cm^{-2} s^{-1}
$N_{\rm C}/{\rm H} \simeq 0.00048$
$N_{\rm O}/{\rm H} \simeq 0.00085$ $\Rightarrow$ (Austin 1981):

	$\sigma^i_{\rm pC}$ (mb)	$\sigma^i_{\rm pO}$ (mb)	$(N_i/{\rm H})_{\rm theo}$ ($\times 10^{-12}$)	$(N_i/{\rm H})_{\rm obs}$ ($\times 10^{-12}$)	$(N_i/{\rm H})_{\rm theo}/(N_i/{\rm H})_{\rm obs}$
^{6}Li	14.8	13.9	45	70	0.64
^{7}Li	20.5	21.2	6.6	90	0.07
^{9}Be	6.2	4.4	16	14	1.14
^{10}B	22.7	12.7	51	30	1.70
^{11}B	57.0	26.5	118	120	0.98

$\Rightarrow$ rather good agreement, except for ^{7}Li
($\rightsquigarrow$ this confirms that ^{7}Li is produced in the Big Bang!)

However: C, O targets, p projectile $\rightarrow$ LiBeB are **secondary** nuclei!
(The **first** supernova remnants could not produce LiBeB)

• recent observational evidence: at least Be seems **primary**
$\rightsquigarrow$ protons are target, C and O projectiles?
problem: resulting LiBeB-particles are very **energetic**
$\rightsquigarrow$ likely destroyed further

$\rightsquigarrow$ Open question...

Suggestion for further reading

– Chapter 9 of Pagel.

Chapter 8

Galactic chemical evolution

A. Ingredients of galactic chemical evolution (GCE) models

Compare to the scheme for 'cosmic recycling', Fig. 1.4:

- **Initial conditions**
  – usually: primordial (Big Bang) abundances
  – all the mass in a galaxy in the from of gas (including dust)

- **Star formation rate**
  How much gas is converted into stars per year (in $M_\odot$/year)?
  SFR $= f(t, M_{\rm gas}, \rho_{\rm gas}, \ldots)$

  $\rightsquigarrow$ complicated, no simple dependence

  depends on *type of galaxy* and on the *stellar population* (e.g. see Fig. 8.1):
  – Galactic disk: SFR $\approx$ constant over time, or slowly declining
  – Galactic halo: SFR $= 0$ for past $8 - 10$ Gyr
  – starburst galaxies: strong spike of star formation, SFR $= \delta(t)$
  – dwarf galaxies: irregular SFR(t)

- **Initial mass function (IMF)**
  IMF = relative birth rate of stars with different initial masses (Fig. 8.2)
  For $m > 1$ (m is initial stellar mass in $M_\odot$) the IMF is approximately a power law:

$$\phi(m) := \frac{dN}{dm} = m^{-(1+x)} \qquad \text{or} \qquad \xi(m) := \frac{dN}{d\ln m} = m^{-x}$$

  The above equations define $x \rightarrow$ observations give $x \sim 1.3 \ldots 1.7$.

- **Products of stellar evolution**
  For a star of given initial mass and metallicity:
  – how much mass is ejected into the ISM at the end of their evolution?
  – in the form of which elements/isotopes? (e.g. see Fig. 3.32)
  – after how much time?

Three classes of stars:

1. massive stars ($m \gtrsim 8$): lifetime $\tau < 10^8$ Gyr
   $\Rightarrow$ compared to galactic timescale, *instantaneously* recycle their ejecta (SNe, stellar winds) after they form
2. intermediate-mass stars ($1 \lesssim m \lesssim 8$): $10^8 < \tau < 10^{10}$ Gyr
   $\Rightarrow$ significant delay in recycling their ejecta
3. low-mass stars ($m \lesssim 1$): $\tau > 10^{10}$ Gyr
   $\Rightarrow$ do not evolve and recycle, only serve to lock up gas (*but* act as important tracers of the chemical history of the Galaxy)

- **Galaxy-evolution processes**
  Chemical evolution of galaxies has to be considered in conjunction with their *dynamical* evolution (of the stars and the gas), as well as the *thermal* evolution of the gas.

  $\rightsquigarrow$ introduces many uncertainties...

  Important issues:

  – can a galaxy be considered as a closed system ('closed box'), or are *inflows* (accretion of gas) and/or *outflows* (e.g. galactic winds) important?
  – are the outflows metal-enhanced (e.g. if galactic winds are primarily due to supernovae)?
  – are the stellar ejecta well mixed through the ISM, or are there significant inhomogeneities?

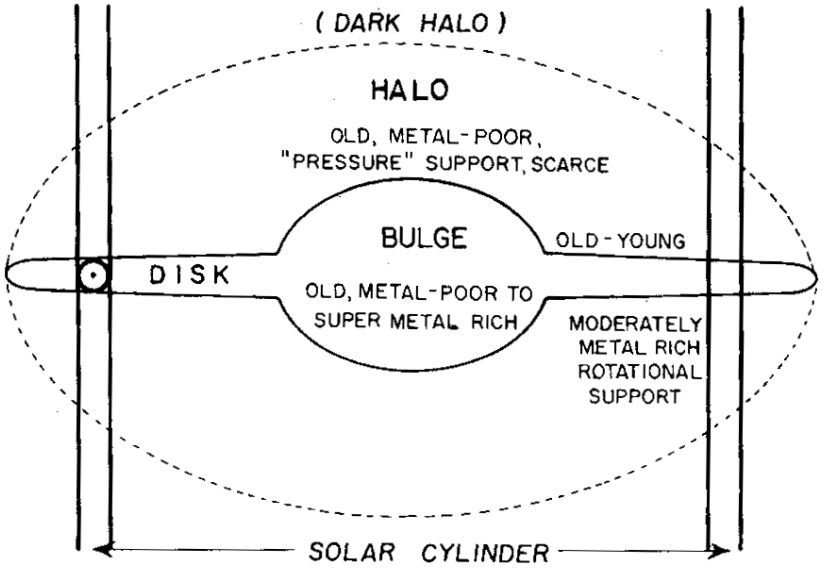

Figure 8.1: Schematic cross-section through the Galaxy, showing the different galactic stellar populations. Figure from Pagel.

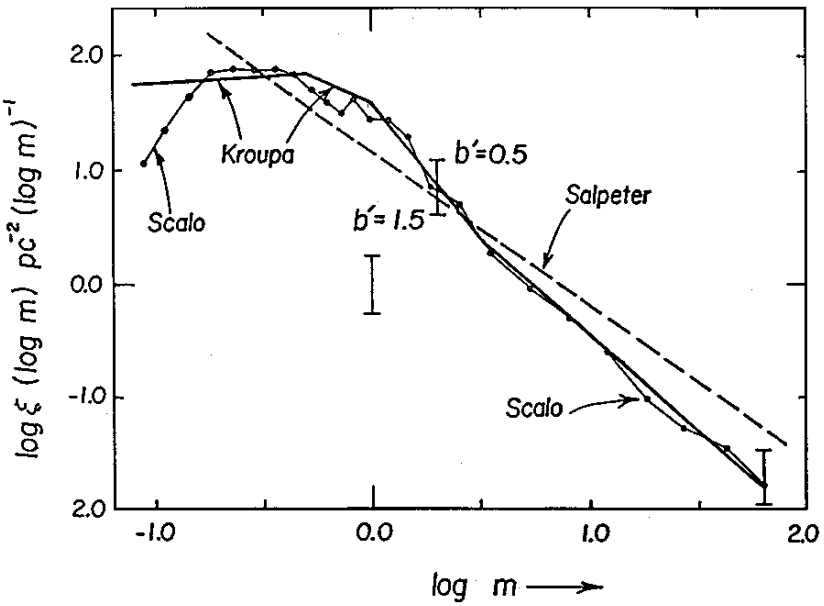

Figure 8.2: The initial mass function (IMF) derived for the solar neighbourhood by Salpeter (1955; dashed line), by Scalo (1986; points connected by thin lines) and by Kroupa et al. (1991; think line). Figure from Pagel.

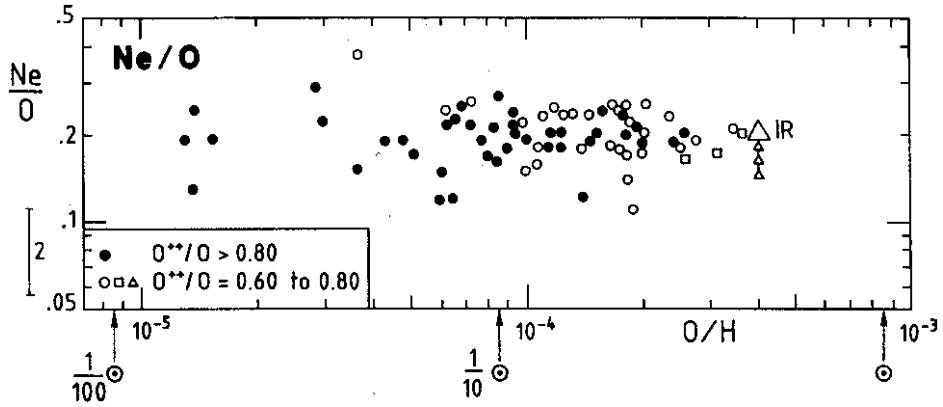

Figure 8.3: The neon-to-oxygen ratio versus the oxygen-to-hydrogen ratio, derived from galactic and extragalactic emission-line nebulae. Both O and Ne are primary elements, produced mainly by Type II supernovae. As expected, their ratio does not change with metallicity. Figure from Pagel.

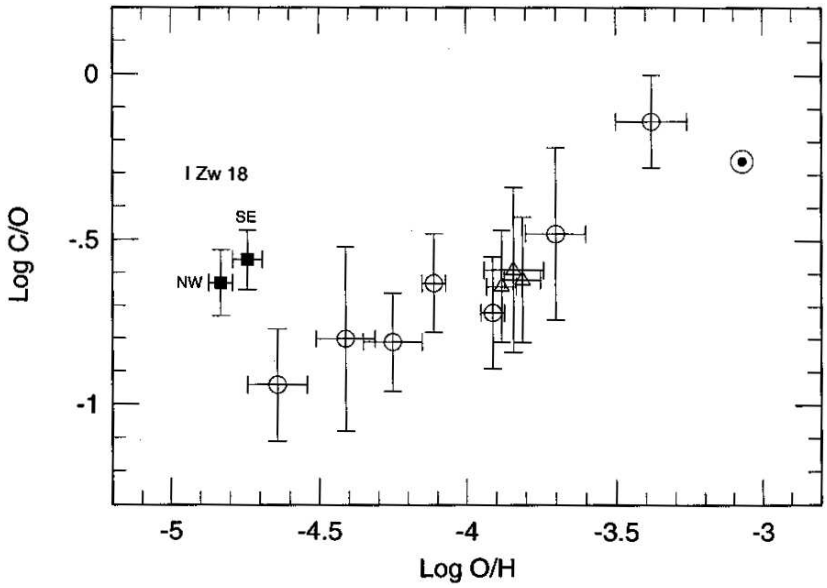

Figure 8.4: The C/O ratio versus O/H, derived from galactic and extragalactic emission-line nebulae like in Fig. 8.3. Although carbon is also a (mainly) primary element, the C/O ratio increases with metallicity. This is probably caused by two effects: (1) a substantial part of carbon comes from massive Wolf-Rayet stars, which lose more mass and therefore produce more carbon at high metallicity; (2) another substantial part of carbon comes from intermediate-mass AGB stars which live relatively long, so that their contribution to carbon enrichment is delayed with respect to that of massive stars. (N.B.: the C/O ratio derived for *stars* in the Galaxy shows a very similar trend to that shown here.) Figure from Pagel.

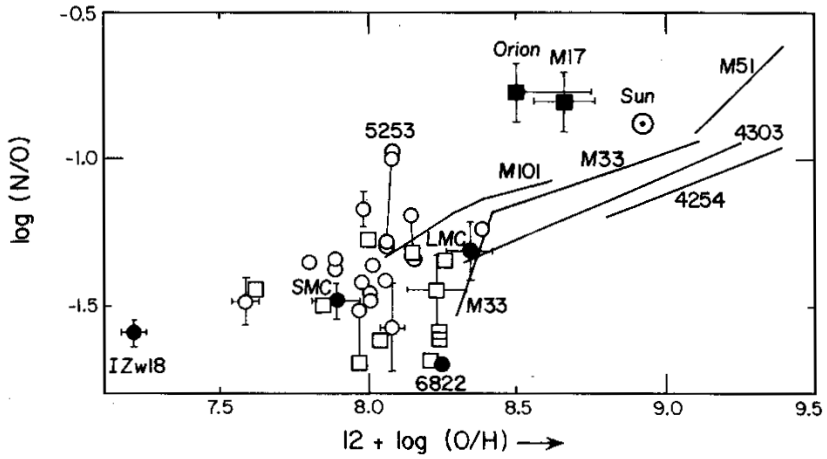

Figure 8.5: The N/O ratio versus O/H, derived from galactic and extragalactic emission-line nebulae. Since nitrogen is a secondary element (produced by CNO-cycling of already present carbon and oxygen), one would expect a linear increase of N/O with the O abundance (slope = 1 in a log-log plot). Instead, the slope is shallower, which suggests that there must be a primary component to the production of nitrogen at low metallicity. Figure from Pagel.

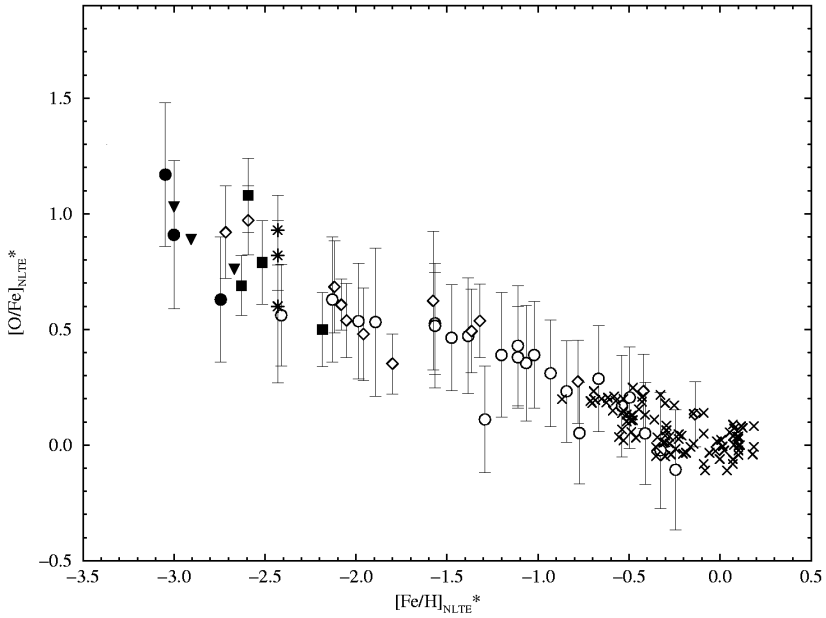

Figure 8.6: Oxygen-to-iron ratio (normalised to the solar ratio: $[\mathrm{O/Fe}] = \log \frac{\mathrm{O/Fe}}{(\mathrm{O/Fe})_\odot}$, etc.) for unevolved galactic stars of various metallicities. Note the steady increase of O/Fe with decreasing Fe/H, showing that the production of Fe (mainly from Type Ia supernovae) is delayed with respect to the production of O (from Type II SNe, which is almost immediate). The fact that the O/Fe ratio continues to increase even at small metallicities ([Fe/H] < -2), suggests that Type II SNe may have produced relatively more oxygen at very early epochs (very low metallicities) than later on. Figure from Israelian et al. (2001).

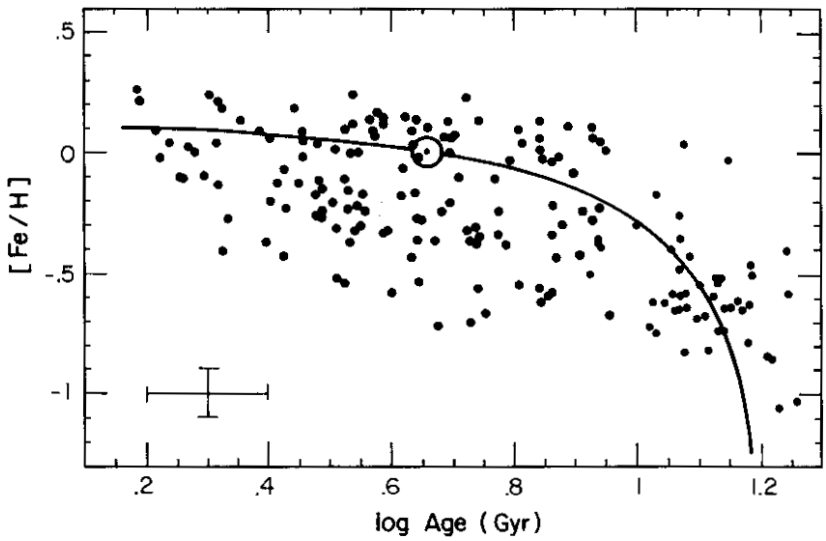

Figure 8.7: Relation between metallicity and age for stars in the solar neighborhood, from Edvardsson et al. (1993). The line going through the relevant data point for the Sun ($\odot$) assumes a linear increase of metallicity with age. This reproduces the overall trend, but the scatter is much larger than the measurement errors (shown in the lower left corner). This scatter is probably due to inhomogeneous mixing of stellar ejecta through the interstellar medium.

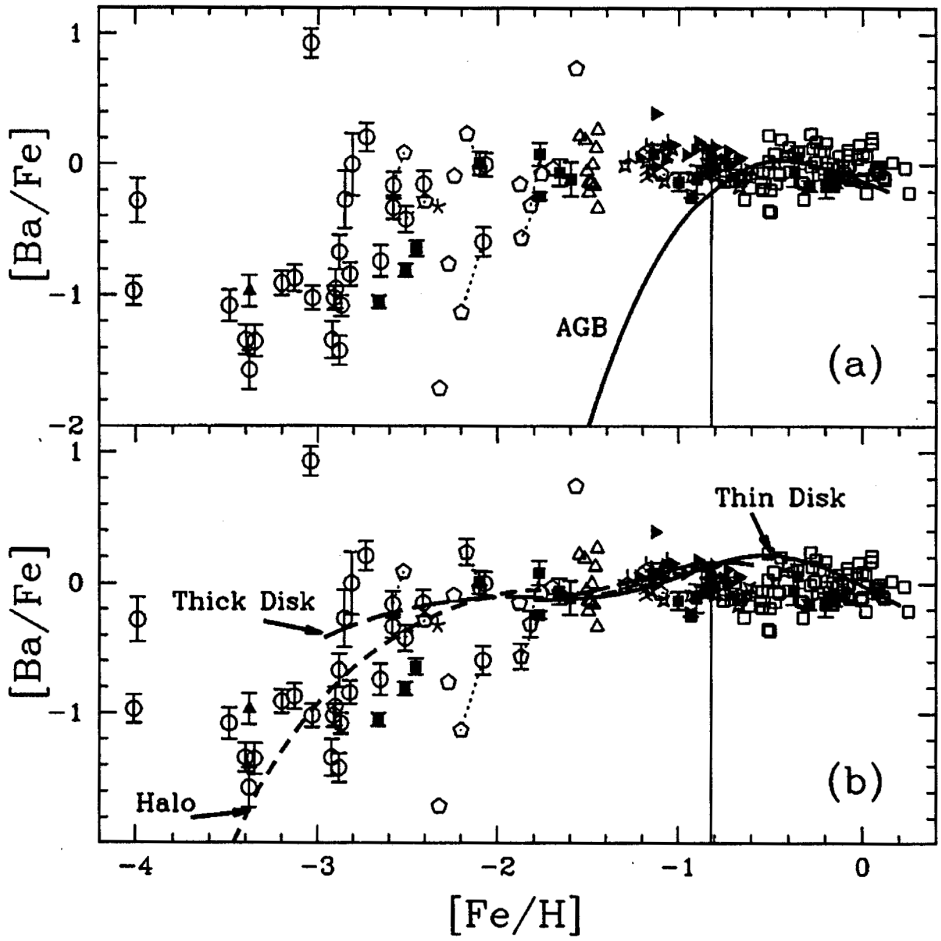

Figure 8.8: Barium-to-iron ratio (normalised to solar ratio) for unevolved galactic stars of various metallicities. Note that barium is an s-process indicator. The line in panel (a) shows a galactic chemical evolution model for the s-process component of Ba produced by AGB stars. This reproduces the observations well for [Fe/H] > -1, but decreases much too fast at lower metallicities - not unexpected given the secondary nature of the s-process, and the time-delay involved in AGB evolution. Panel (b) shows the same data with a model including a (primary) r-process component from Type II supernovae. This reproduces the overall trend at low metallicities much better. Figure from Busso et al. (1999).

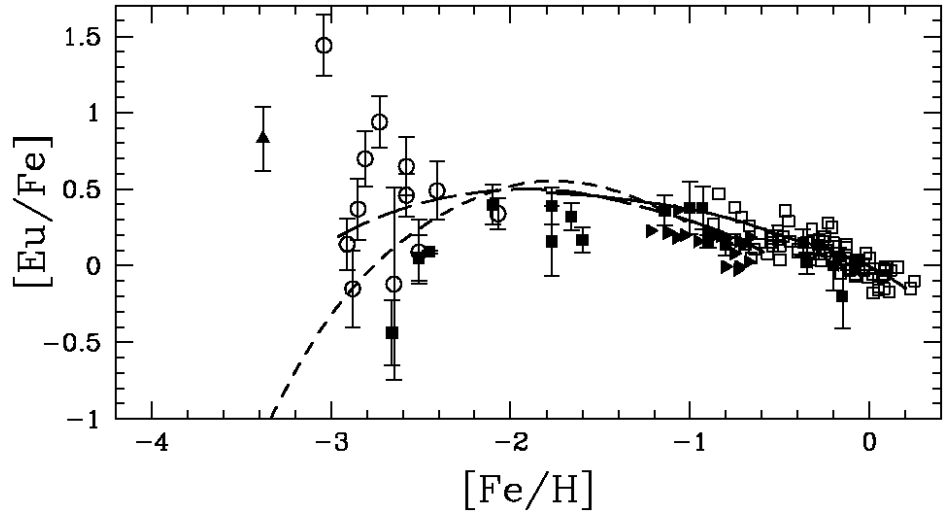

Figure 8.9: Same as Fig. 8.8, but showing europium (an r-process indicator) instead of barium. Here, no decrease as in the case of barium occurs for very low metallicity, indicating the primary nature of europium. The galactic chemical evolution model is the same as in Fig. 8.8b. As is also the case for Ba, the large increase of scatter for lower metallicities is real and is interpreted as the signature of individual nucleosynthesis events, which is averaged out at higher metallicity. Figure from Travaglio et al. (1999).

Suggestions for further reading

– Chapters 7 and 8 of Pagel.

Exercises:

8.1 The Initial Mass Function (IMF) is given by

$$\frac{dN}{dm} := \phi(m) = \begin{cases} 0.291\ m^{-1.3} & 0.1 \leq m < 0.5 \\ 0.155\ m^{-2.2} & 0.5 \leq m \leq 1.0 \\ 0.155\ m^{-2.7} & 1.0 \leq m \leq 100 \end{cases}$$

where m is mass in solar units. It is normalized such that $\int_{0.1}^{100} \phi(m) dm = 1$.

(a) What is the average initial stellar mass of one generation?

(b) Which fraction of stars undergo a Type II SN explosion, if all stars between 10 and 100 $M_\odot$ do so?

(c) If the star formation rate in the Galaxy is about 5 $M_\odot$/yr, then calculate the SN II rate (number of SNe per year) using the answers of (a) and (b).

8.2 The mass of oxygen produced in a star of mass m (in $M_\odot$) can be approximated by

$$M_{\rm O}(m) = \begin{cases} 2.4(m/25)^3 & 10 \leq m \leq 25 \\ 2.4(m/25)^2 & 25 \leq m \leq 100 \end{cases}$$

(a) Using the results from the previous exercise, show that the average SN II ejects $\approx$ 2 $M_\odot$ of oxygen.

(b) Given that each SN II produces ≈ 0.08 $M_\odot$ of ^{56}Fe, while each SN Ia produces $\approx$ 0.7 $M_\odot$ of ^{56}Fe, estimate the relative rate of SN Ia to SN II required to reproduce the solor O to Fe ratio. ($X_\odot({\rm O}) = 9.6 \times 10^{-3}$, $X_\odot({\rm Fe}) = 1.2 \times 10^{-3}$)

(c) How does this compare to the observed SN Ia rate of $4 \pm 1 \times 10^{-3}\,{\rm yr}^{-1}$?

References

Angulo C., Arnould M., Rayet M., et al., 1999, Nucl. Phys A, 656, 3

Arnould M., Mowlavi N., 1993, in *Inside the Stars*, IAU Coll. 137, eds. W.W. Weiss & A. Baglin, ASP Conf. Series, 40, 310

Bahcall J.N., 1989, *Neutrino Astrophysics*, Cambridge University Press

Berheide M., et al., 1992, preprint

Burles S., Nollett K.M., Turner M.S., 1999, astro-ph/9903300

Busso M., Gallino R., Wasserburg G.J., 1999, ARA&A, 37, 239

Cameron A.G.W., 1982, in *Essays in Nuclear Astrophysics*, eds. C.A. Barnes et al., Cambridge University Press

Clayton D.D., 1968, *Principles of Stellar Evolution and Nucleosynthesis*, University of Chicago Press

Coc A., Vangioni-Flam E., Descouvemont P., Adahchour A., Angulo C., 2004, ApJ, 600, 544

Edvardsson B., Andersen J., Gustafsson B., Lambert D.L., Nissen P.E., Tomkin J., 1993, A&A, 275, 101

Fields B.D., Olive K.A., 1998, ApJ, 506, 177

Filippenko A.V., 1997, ARA&A, 35, 309

Iben I., 1991, ApJS, 76, 55

Iben I., Tutukov A.V., 1984, ApJS, 54, 335

Israelian G., Rebolo R., Garcıa López R.J., et al., 2001, ApJ, 551, 833

Kahabka P., van den Heuvel E.P.J., 1997, ARA&A, 35, 69

Kappeler F., Beer H., Wisshak K., 1989, Rep. Prog. Ph., 52, 945

Kippenhahn R., Weigert A., 1990, *Stellar Structure and Evolution*, Springer-Verlag

Kroupa P., Tout C.A., Gilmore G., 1991, MNRAS, 251, 193

Landré V., Prantzos N., Aguer P., et al., 1990, A&A, 240, 85

Pagel B.E.J., 1997, *Nucleosynthesis and Chemical Evolution of Galaxies*, Cambridge University Press

Raiteri C.M., Busso M., Picchio G., Gallino R., 1991, ApJ, 371, 665

Rayet M., Arnould M., Hashimoto M., Prantzos N., Nomoto K., 1995, A&A, 298, 517

Riess A.G., Filippenko A.V., Challis P., et al., 1998, AJ, 116, 1009

Rolfs C.E., Rodney W.S., 1988, *Cauldrons in the Cosmos*, University of Chicago Press

Salpeter E.E., 1955, ApJ, 121, 161

Scalo J.M., 1986, Fund. Cosmic Ph., 11, 1

Spergel D.N., Verde L., Peiris H.V., et al., 2003, ApJS, 148, 175

Tegmark M., Strauss M.A., Blanton M.R., et al., 2004, to appear in PhRvD (astro-ph/0310723)

Travaglio C., Galli D., Gallino R., Busso M., Ferrini F., Straniero O., 1999, ApJ, 521, 691
Weaver T.A., Woosley S.E., 1993, Phys. Rep., 227, 65
Woosley S.E., Heger A., Weaver T.A., 2002, Rev. Mod. Ph., 74, 1015